UNIVERSITAT DE BARCELONA

Molecular mechanisms of apoptosis induction by AICAR and the new prohibitin-binding compound fluorizoline

Cristina Moncunill Massaguer

Universitat de Barcelona

DOCTORAL PROGRAM IN BIOMEDICINE

MOLECULAR MECHANISMS OF APOPTOSIS INDUCTION BY AICAR AND THE NEW PROHIBITIN-BINDING COMPOUND FLUORIZOLINE

This thesis has been conducted under the guidance of Dr. Joan Gil Santano and Dr. Daniel Iglesias i Serret in the Biochemistry Unit of Physiological Sciences II Department at the Universitat de Barcelona

Cristina Moncunill Massaguer Dr. Joan Gil Santano Dr. Daniel Iglesias i Serret

Doctoral thesis submitted by Cristina Moncunill Massaguer to obtain the PhD Degree by the Universitat de Barcelona

#107. Smile a lot. It costs nothing and is beyond price.
#273. Remember that overnight success usually takes about fifteen years.
#399. Focus on making things better, not bigger.
#511. Call your mother.

Life's Little Instructions Book, by H. Jackson Brown, Jr.

INDEX

ABBREVIATIONS

A1: BCL-2 related gene A1
ABB: annexin binding buffer
ACC: acetyl-CoA carboxylase
ActD: actinomycin D
AICAR: 5-aminoimidazole-4-carboxamide riboside
AK: adenosine kinase
AMPK: AMP-activated protein kinase
APAF-1: apoptotic protease-activating factor-1
APC: allophycocyanin
ATIC: AICAR transformylase IMP cyclohydrolase
ATM: ataxia telangiectasia-mutated
BAD: BCL-2 antagonist of cell death
BAK: BCL-2-antagonist/killer-1
BAP-37: B-cell-receptor-associated protein 37
BAX: BCL-2-associated X protein
BCA: bicinchoninic acid
BCL-2: B-cell lymphoma-2
BCL-X_L: BCL-2-related gene, long isoform
BCR: B-cell receptor
BH: BCL-2 homology
BID: BH3-interacting domain death agonist
BIK: BCL-2 interacting killer
BIM: BCL-2-like-11
BIR: baculovirus IAP repeat
BMF: BCL-2-modifying factor
BN-PAGE: blue native-polyacrylamide gel electrophoresis
BOK: BCL-2-related ovarian killer
BTK: Bruton tyrosine kinase
CAMKKβ: Ca^{2+}/calmodulin-activated protein kinase kinases β
Carbamoyl-Asp: carbamoyl-aspartate
Carbamoyl-P: carbamoyl-phosphate
CARD: caspase recruitment domain
Caspases: cysteine-dependent aspartate-directed proteases
CBB: Coomassie Brilliant Blue
CDP-DAG: cytidine diphosphate
CICD: caspase-independent cell death
CL: cardiolipin
CLL: chronic lymphocytic leukemia
CML: chronic myelogenous leukemia
CMP: cytidine monophosphate
CNT: concentrative nucleoside transporter
CRE: cAMP response element
DAG: diacylglycerol
DD: death domain
DED: death effector domain
Del: deletion
DHE: dihydroethidium
DISC: Death-Inducing Signaling Complex
DKO: double knockout
DR: death receptor
DTT: Dithiothreitol
ENT: equilibrative nucleoside transporter
ER: endoplasmic reticulum
ERK: extracellular signal-regulated kinase
FADD: Fas-associated death domain
FBS: fetal bovine serum
FCR: fludarabine + cyclophosphamide + rituximab
Fig: Figure
FITC: fluorescein isothiocyanate
FL: follicular lymphoma
HIF: hypoxia-inducible factor 1α
HRK: hara-kiri

HTNC: His-TAT-NLS-Cre recombinase
HtrA2: high temperature requirement protein A2/OMI
IAP: inhibitor of apoptosis
IGHV: immunoglobulin heavy chain variable region
IM: inner membrane
IMM: inner mitochondrial membrane
IMS: intermembrane space
IPTG: Isopropyl β-D-1-thiogalactopyranoside
JNK: c-Jun N-terminal kinase
KO: knockout
LB: lysogeny broth
MAPK: mitogen-activated protein kinases
MCL: mantle cell lymphoma
MCL-1: myeloid cell leukemia 1
MEFs: mouse embryonic fibroblasts
MFI: mean fluorescence intensity
MLKL: mixed lineage kinase domain-like protein
MM: multiple myeloma
MOMP: mitochondrial outer membrane permeabilization
NBTI: nitrobenzylthioinosine
NF-ϰB: nuclear factor kappa B cells
NLS: nuclear localization signal
NT: nucleoside transporter
OMM: outer mitochondrial membrane
OMP: orotidine monophosphate
OPA1: optic atrophy 1
P/S: penicillin/streptomycin
PA: phosphatidic acid
PARP: poly(ADP-ribose) polymerase 1
PBS: phosphate buffered saline
PC: phosphatidylcholine
PE: phycoerythrin
PEA: phosphatidylethanolamine
PG: phosphatidylglycerol
PGP: phosphatidylglycerol phosphate
PHB: prohibitin
PI: propidium iodide
PI3K: phosphatidylinositol-3-kinase
PIN: phosphatidylinositol
PKA: protein kinase A
PKC: protein kinase C
PMA: prohibitin/mAAA protease supercomplexes
PoS: ponceau staining
PRPP: phosphoribosyl-pyrophosphate
PS: phosphatidylserine
PUMA: p53-upregulated modulator of apoptosis
PVDF: polyvinyl difluoride
RCD: regulated cell death
REA: repressor of estrogen receptor activity
RIPK: receptor-interacting protein kinase
Roc-A: Rocaglamide-A
ROS: reactive oxygen species
RT: room temperature
RT-MLPA: retrotranscriptase multiplex ligation-dependent probe amplification
RT-qPCR: real-time quantitative polymerase chain reaction
SB: sample buffer (Laemmli)
SC: scramble
SDS: sodium dodecyl sulfate
SEM: standard error of the mean
SKO: SLP-2 knockout
SLP-2: stomatin-like protein
SMAC/DIABLO: second mitochondria-derived activator of caspases/direct IAP-binding protein with low PI

SMZL: splenic marginal zone B-cell lymphoma
SPFH: stomatin-prohibitin-flotilin-HflC/K
STS: staurosporine
Syk: Spleen tyrosine kinase
tBID: truncated BH3-interacting domain death agonist
TBS: tris-buffered saline
TBS-T: TBS-Tween
TM: transmembrane
TMP: thymidine monophosphate
TNF: tumor necrosis factor
TNFR: tumor necrosis factor receptor
TRADD: TNFR-associated death domain protein
TRAIL: TNF-related apoptosis-inducing ligand
UMP: uridine monophosphate
UMPS: UMP synthase
WT: wild-type
XO: xanthine oxidase
z-VAD.fmk: benzyloxycarbonyl-Val-Ala-Asp-fluoromethylketone

INTRODUCTION

1. APOPTOSIS AND CANCER

1.1. TYPES OF CELL DEATH

According to the Nomenclature Committee on Cell Death, cell death can be operationally categorized in two major groups: accidental and regulated. On the one hand, accidental cell death is induced upon exposure to severe insults, such as mechanical, chemical or physical stimuli, which results in immediate loss of cell structural integrity. Its commitment does not involve a specific molecular mechanism; thus accidental cell death cannot be targeted by pharmacologic or genetic interventions (Galluzzi et al. 2014).

In clear contrast, regulated cell death (RCD) is a controlled mechanism of removing superfluous or damaged cells within multicellular organisms. It requires a genetically encoded molecular machinery which can be pharmacologically or genetically modulated. Various cell death processes are included in this category, being apoptosis and regulated necrosis the most relevant ones (Galluzzi et al. 2014).

1.1.1. THE APOPTOTIC PROCESS

Apoptosis is the best-characterized type of RCD. It is highly conserved throughout evolution as it is required for embryogenesis, development of the immune system and tissue homeostasis. Within a completely physiologic context, apoptosis is generally referred to as programmed cell death. In addition, apoptosis can also be induced after perturbations of the microenvironment or the cellular homeostasis (Galluzzi et al. 2014). Aberrant regulation of apoptosis has severe clinical implications. In this sense, premature cell loss may contribute to the development of neurodegenerative disorders and immunodeficiency, whereas continuous cellular survival would promote autoimmunity and cancer (Fig. I.1) (Hotchkiss et al. 2009). Indeed, resistance to cell death was reported as one of the hallmarks of cancer development and progression (Hanahan and Weinberg 2011). Deregulation of the apoptotic pathway not only can promote tumorigenesis, but can also render cancer cells resistant to conventional anti-cancer agents (Fernald and Kurokawa 2013).

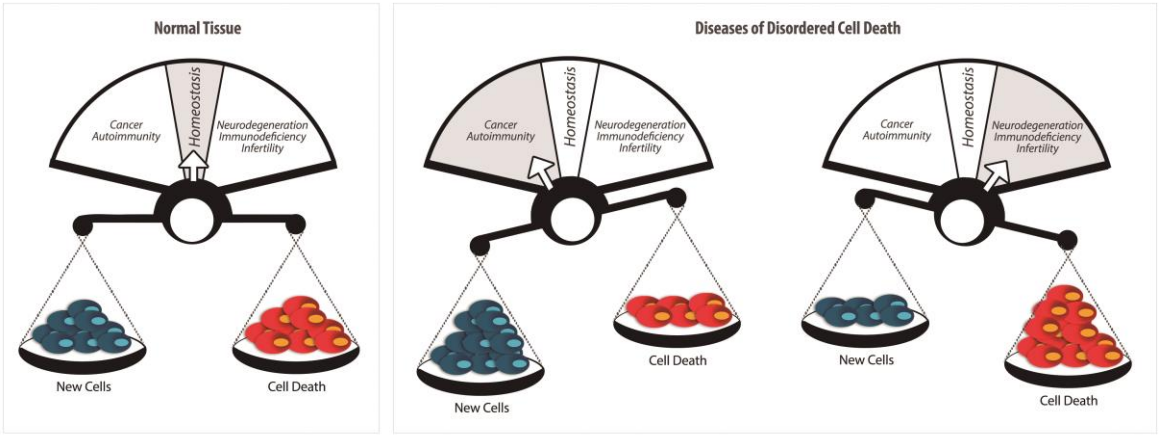

Figure I.1. Apoptosis maintains tissue homeostasis by keeping the balance between proliferation and cell death. Deregulated apoptotic machinery disrupts the balance, which may result in various diseases. Adapted from Walensky 2006 and modified in Pérez-Perarnau 2013.

Apoptotic cells can be recognized by characteristic morphological changes (Fig. I.2). Cells undergoing apoptosis first shrink, become rounded and retract from neighboring cells, which is accompanied by plasma membrane blebbing. The Golgi apparatus, endoplasmic reticulum (ER) and mitochondrial networks suffer pronounced fragmentation, and numerous proteins are released from the mitochondrial intermembrane space. The activation of proteolytic enzymes mediates the cleavage of multiple protein substrates, which usually determine the integrity and the shape of the cytoplasm or organelles. In the nucleus, the DNA is also cleaved into a ladder of fragments of 200 base pairs or multiples thereof. This pattern of fragmentation is the result of endonuclease-mediated chromatin cleavage at internucleosomal sites, and is typically accompanied by chromatin condensation. Importantly, the plasma membrane integrity is maintained during apoptosis, which avoids the release of cellular contents and minimizes tissue inflammation and damage to neighboring cells. Apoptosis frequently culminates in the fragmentation of the plasma membrane blebs into small vesicles called apoptotic bodies, which contain condensed chromatin, fragmented organelles and cytosol (Taylor et al. 2008). Phosphatidylserine (PS) is a phospholipid confined to the inner layer of the plasma membrane, but it is exposed to the outer layer during apoptosis. This becomes an *eat me* signal for macrophages, which will rapidly engulf the apoptotic bodies (Fadok and Henson 2003, Taylor et al. 2008).

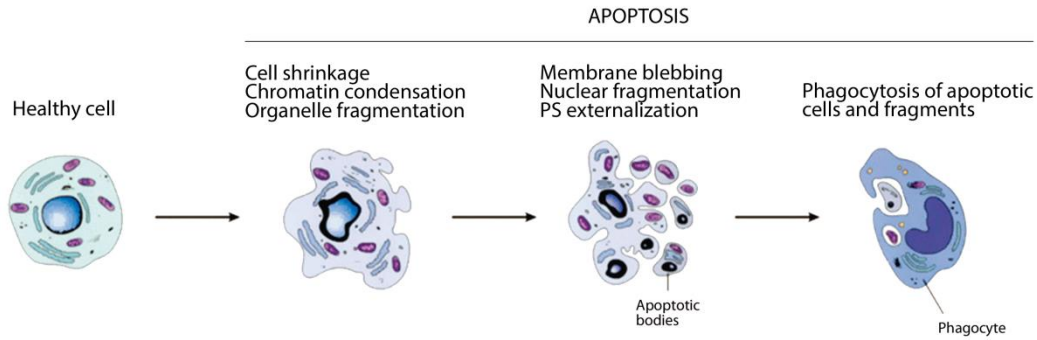

Figure I.2. Biochemical and morphological features of apoptosis. Adapted from Kumar et al. 2014.

Apoptosis can be divided into distinct phases according to these biochemical and morphological characteristics. First, pro-apoptotic stimuli trigger the activation of the central molecular machinery of apoptosis, the caspases (initiation phase). Second, during the effector phase, the molecular executioner machinery becomes fully activated. Third, the degradation phase is characterized by the loss of cellular integrity and the display of the typical biochemical and morphological changes of apoptosis (Vaux and Strasser 1996).

1.1.2. OTHER TYPES OF REGULATED CELL DEATH

Necrosis is morphologically characterized by cytoplasmic granulation and organelle swelling (oncosis), condensation of the chromatin into small and irregular patches and dilatation of the plasma membrane (Fig. I.3). Induction of the necrotic process leads to the loss of membrane integrity and the release of cellular contents into the extracellular space. Consequently, there is damage of the surrounding cells and a strong inflammatory response in the tissue.

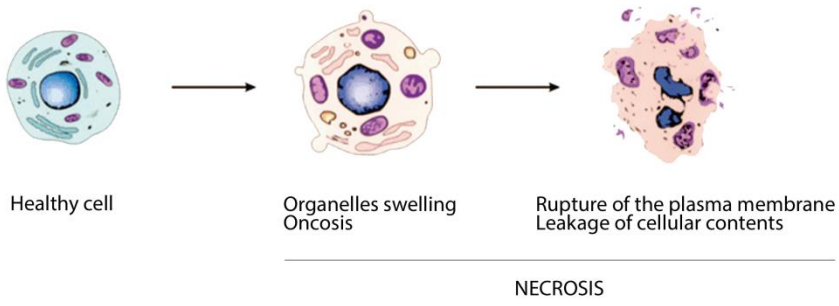

Figure I.3. Biochemical and morphological features of necrosis. Adapted from Kumar et al. 2014.

Although historically seen as an accidental cell death program, recent genetic and pharmacological evidences revealed the existence of multiple pathways of regulated necrosis (Vanden Berghe et al. 2014, Galluzzi et al. 2014). Different cell death types share the necrotic morphological features, leading to the appearance of several neologisms, such as necroptosis, ferroptosis, or pyroptosis. Each type of necrotic cell death is induced by specific stimuli, such as hyperactivation of poly(ADP-ribose) polymerase 1 (PARP1), mitochondrial permeability transition, or NADPH oxidases, and is transmitted through specific signaling pathways (Vanden Berghe et al. 2014).

One of the most studied processes of regulated necrosis is necroptosis, which is mediated by receptor-interacting protein kinase (RIPK) 3, mixed lineage kinase domain-like protein (MLKL) and, in some contexts, RIPK1. Several pro-apoptotic stimuli, under conditions of inhibition of the apoptotic machinery, can trigger necroptosis. Necrostatin-1 blocks the kinase activity of RIPK1 and thus is a potent inhibitor of necroptosis (Linkermann and Green 2014, Vanden Berghe et al. 2014).

In addition, the role of autophagy in cell death has been long debated. Autophagy is a lysosome-dependent process in which the cytosolic content is engulfed into an autophagosome, leading to the digestion of the material for its recycling. As autophagy is a pro-survival stress response, some insults that induce cell death are preceded by extensive autophagy in an attempt to face the unfavorable conditions. Thus, in most instances, autophagy only correlates, but not causes, cell death. However, in some circumstances, inhibition of autophagy blocks the onset of cell death, supporting the existence of autophagic cell death (Tait et al. 2014, Galluzzi et al. 2014).

Of note, the identification of the cell death type based on the morphology of the cell is difficult, as there are some cell death processes (such as autoschizis) that show both apoptotic and necrotic features (Vanden Berghe et al. 2014). Furthermore, the signal transduction pathways that lead to apoptosis, necroptosis and autophagic cell death are highly interconnected (Tait et al. 2014).

1.2. THE APOPTOTIC MACHINERY

1.2.1. CASPASES

Apoptosis is orchestrated by a family of cysteine-dependent aspartate-directed proteases (caspases). It is estimated that activated caspases can cleave over 700 substrates (http://bioinf.gen.tcd.ie/casbah/) to promote the morphological and biochemical features that typically occur in apoptosis. Caspases target key structural components of the cytoskeleton and nucleus, as well as numerous proteins involved in housekeeping functions within the cell. (Taylor et al. 2008). The domain structure of

caspases includes an N-terminal peptide or pro-domain, and two subunits, one large and one short, sometimes separated by a linker peptide (Fig. I.4) (Taylor et al. 2008, Shalini et al. 2014).

The caspases that are involved in apoptosis can be classified into two main groups:

1. Initiator caspases: these include caspases 2, 8, 9 and 10. They are the first to be activated after the apoptotic stimulus. Initiator caspases are characterized by the presence of a caspase-recruitment domain (CARD) or death effector domain (DED) at their N-terminus, which mediate their dimerization and/or assembling into larger complexes to promote their activation.

2. Effector or executioner caspases: these include caspases 3, 6 and 7. They are activated by the initiator caspases and are responsible for the proteolytic events that result in apoptosis.

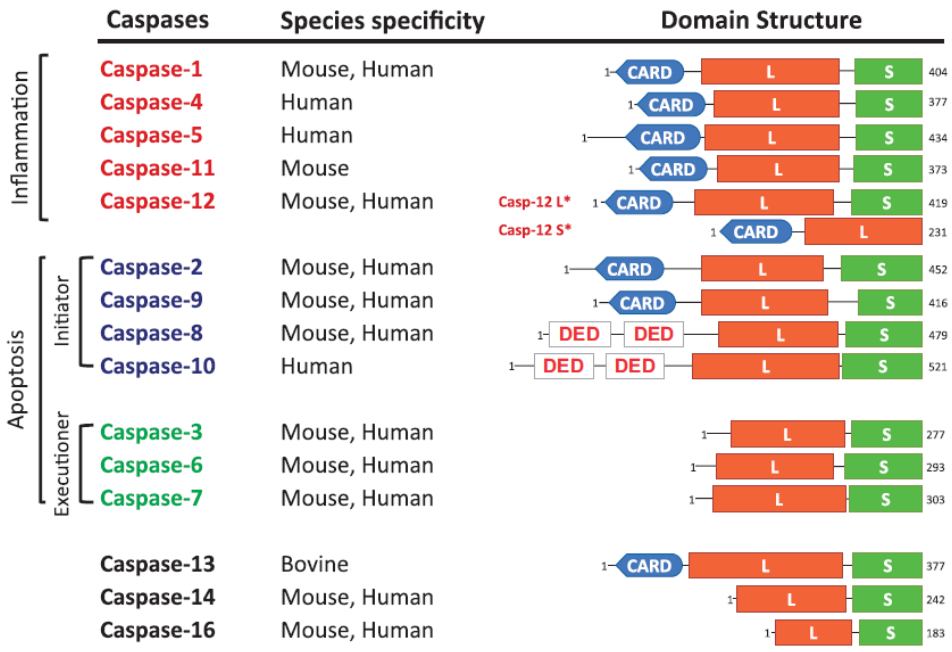

Figure I.4. Functional classification and domain structure of placental mammalian caspases. Caspases 11 and 13 are the murine and bovine orthologues of caspase 4, respectively. Caspase 16 has a similar sequence to caspase 14. CARD, caspase recruitment domain; DED, death effector domain; L, large subunit; S, small subunit; S*, short form; L*, long form. Taken from Shalini et al. 2014.

In addition to apoptosis, caspases also play a role in other processes. Caspases 1, 4, 5, 11 and 12 are called *inflammatory* caspases as they regulate the innate immune response. In addition, caspases 1 and 11 mediate inflammatory cell death by pyroptosis in response to acute viral or bacterial infection. Caspase 8 has dual role in cell death, its activation results in apoptosis but in its absence necroptosis can occur. Along the same lines, caspase 14 is only expressed in differentiating keratinocytes and

offers protection of underlying layers of the skin. Other caspase-regulated processes include tissue differentiation and regeneration, cell proliferation, autophagy inhibition, synaptic plasticity, metabolism and aging. Some of these functions involve induction of apoptosis, although some others are independent (Creagh 2014, Shalini et al. 2014).

In healthy cells, caspases are present as zymogens with little or no protease activity. Initiator caspases are present as monomers and are activated by dimerization through the pro-domains. Effector caspases exist as pre-formed dimers and are activated by the cleavage of the linker between the two subunits. Following activation, additional proteolytic events may occur to generate more mature and stable forms of the caspases (Fig. I.5) (Taylor et al. 2008, Pop and Salvesen 2009).

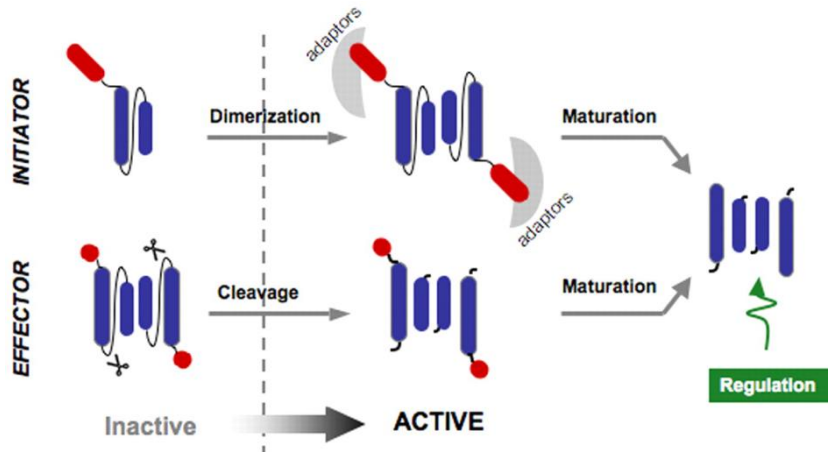

Figure I.5. Activation mechanisms of initiator and effector caspases. Taken from Pop and Salvesen 2009.

1.2.2. THE IAP FAMILY

The inhibitors of apoptosis (IAP) proteins negatively regulate caspases. IAPs comprise a family of proteins that shares the baculovirus IAP repeat (BIR) domain, a zinc-binding fold of ~70 amino acids that promotes protein-protein interactions. Some IAPs also have a carboxy-terminal RING domain, which provides them with E3 ubiquitin protein ligase activity (Fulda and Vucic 2012). In addition to apoptosis, the IAP family is also involved in cell signaling of NF-κB pathways, proliferation, mitosis and protein tagging for proteasome degradation (Gyrd-Hansen and Meier 2010).

The main members of this family are XIAP, hIAP1, hIAP2 and Survivin. XIAP is the only member that serves as a specific inhibitor of caspases 3, 7 and 9. hIAP1 and hIAP2 bind to second mitochondria-derived activator of caspases (SMAC)/direct IAP-binding protein with low PI (DIABLO) and OMI/high temperature requirement protein A2 (HtrA2). These IAP antagonists are constitutively expressed but sequestered to mitochondria. During apoptosis, they are released to the

cytosol where they bind to the BIR domain of IAPs and block their interaction with caspases, ultimately allowing caspase activation (Gyrd-Hansen and Meier 2010, Fulda and Vucic 2012).

1.3. APOPTOTIC SIGNALING PATHWAYS

In mammals, the stimuli that trigger the apoptotic process can activate different initiator caspases through distinct signaling pathways, namely the extrinsic and the intrinsic apoptotic pathways. Both converge in the activation of the executor caspases, and there might be crosstalk between the two signaling pathways in some contexts (Fig. I.6).

1.3.1. EXTRINSIC APOPTOTIC PATHWAY

The extrinsic apoptotic pathway is initiated by the binding of extracellular ligands to cell surface death receptors (DRs). DRs belong to tumor necrosis factor (TNF) receptor (TNFR) superfamily which comprises more than 20 proteins involved in various cellular functions such as regulation of cell death, survival and immunity. To date, six DRs have been identified: TNFR1 (TNFRSF1A), Fas (also known as CD95, APO-1 or TNFRSF6), DR3 (TNFRSF12), DR4 (also known as TRAILR1 or TNFRSF10A), DR5 (also known as TRAILR2 or TNFRSF10B) and DR6 (TNFRSF21). DRs specifically interact with death ligands, comprising TNF, FasL, and TRAIL to sense and transmit extracellular stress signals resulting in downstream caspase activation and apoptosis (Gonzalvez and Ashkenazi 2010). These transmembrane receptors are diverse in primary structure, but all of them contain cysteine-rich extracellular subdomains that enable to recognize their ligands with specificity. DRs also share a unique cytoplasmic domain called death domain (DD), which mediates protein-protein interactions. The adaptor proteins, such as Fas-associated death domain (FADD) or TNFR-associated death domain protein (TRADD), also contain a DD so that they can interact with DRs to propagate the apoptotic signal (Fig. I.6). Importantly, death ligands can also interact with the decoy receptors, which do not possess cytoplasmic DD and thus cannot activate the apoptotic pathway (Mahmood and Shukla 2010).

On ligand binding, the DRs recruit the adaptor proteins, which in turn recruit and aggregate several molecules of pro-caspase 8, forming the Death-Inducing Signaling Complex (DISC). In this activating platform, the molecules of pro-caspase 8 are in close proximity, allowing its autoprocessing and activation. Active caspase 8 then proteolytically processes and activates the executor caspases 3 and 7, promoting further caspase-mediated events that culminate in apoptosis (Taylor et al. 2008, Czabotar et al. 2014). In type I cells, the activation of caspase 8 may be sufficient to execute cell death. Type II cells require further mitochondria-based signal amplification by enabling the crosstalk

with the intrinsic apoptotic machinery. This amplification loop involves the caspase 8-mediated cleavage of a pro-apoptotic protein of the B-cell lymphoma-2 (BCL-2) family, called BH3-interacting domain death agonist (BID). Its truncated form (tBID) contributes to the release of mitochondrial factors that will activate effector caspases (Tait and Green 2010).

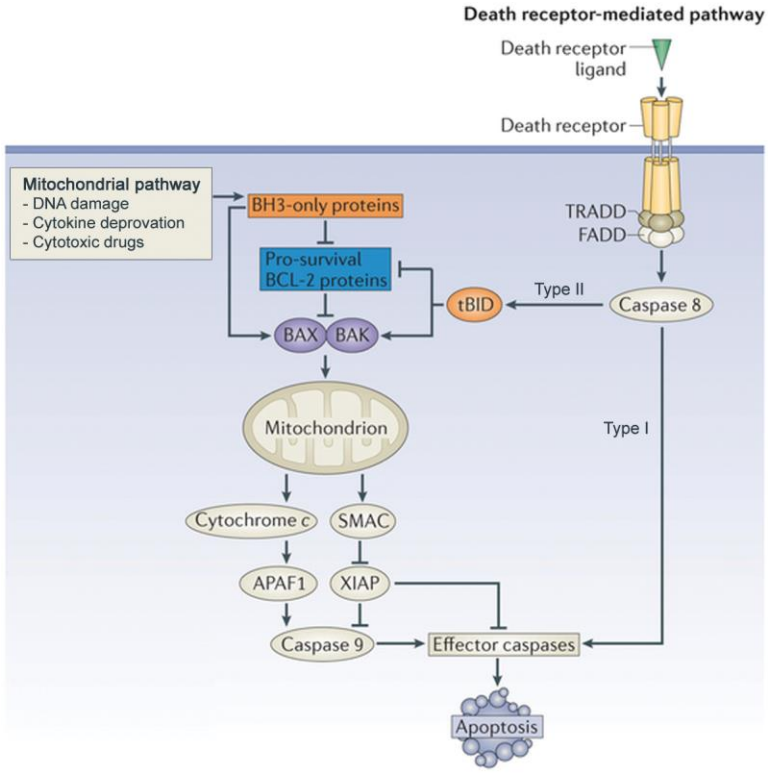

Figure I.6. Extrinsic and intrinsic apoptotic pathways. The extrinsic pathway is initiated with death receptors activation and the subsequent recruitment of the adaptor proteins FADD and/or TRADD, leading to caspase 8 activation. In type I cells, caspase 8 directly triggers apoptosis by activating effector caspases. In type II cells, further signal amplification through mitochondria is required. The intrinsic or mitochondrial pathway is activated upon different stresses, which result in the permeabilization of the mitochondrial outer membrane, the release of cytochrome *c* to the cytosol and the activation of the effector caspases. Adapted from Czabotar et al. 2014.

1.3.2. INTRINSIC APOPTOTIC PATHWAY

The main pathway for caspase activation in vertebrates is the intrinsic pathway, in which mitochondria play a central role (Green and Kroemer 2004). It is initiated in response to various external or internal stress stimuli, such as DNA damage, ER stress, reactive oxygen species (ROS) production, exposure to cytotoxic drugs or radiation, among others. These insults eventually trigger an intracellular cascade of events that result in the mitochondrial outer membrane permeabilization (MOMP), which is required for most apoptotic stimuli to induce caspase activation (Youle and Strasser 2008, Tait and Green 2010, Czabotar et al. 2014). MOMP allows the subsequent release of

several apoptogenic factors from the mitochondrial intermembrane space into the cytosol, including cytochrome *c*, SMAC/DIABLO, OMI/HtrA2, apoptosis-inducing factor and endonuclease G (Table I.1) (Tait and Green 2010).

IMS FACTORS	ROLE IN APOPTOSIS
Cytochrome *c*	Apoptosome activation
SMAC/DIABLO	XIAP antagonist
OMI/HtrA2	XIAP antagonist
Apoptosis-inducing factor	Chromatin condensation and DNA fragmentation. Contributes to CICD
Endonuclease G	DNA fragmentation. Contributes to CICD

Table I.1. Intermembrane space (IMS) proteins released upon mitochondrial outer membrane permeabilization and their role in apoptosis. Some of these factors contribute to caspase-independent cell death (CICD) (Adapted from Tait and Green 2010).

Besides being a key component of electron transport during oxidative phosphorylation, cytochrome *c* is necessary for the activation of caspases following MOMP. In the cytosol, cytochrome *c* binds the apoptotic protease-activating factor-1 (APAF-1) and activates it in an ATP-dependent manner, inducing APAF-1 conformational changes and oligomerization into a heptameric, wheel-like structure, the apoptosome. This complex recruits pro-caspase 9 and facilitates its dimerization and further activation, which in turn activates the effector caspases (Youle and Strasser 2008, Tait and Green 2010). Given the crucial role of the apoptosome in mediating cell death, a number of proteins and small molecules have been reported to regulate its function, including XIAP, Hsp70 or AKT (Tait and Green 2010, Bratton and Salvesen 2010). To counteract this inhibition, SMAC/DIABLO and OMI/HtrA2 are released from the mitochondria to inhibit XIAP. This allow the activation of the effector caspases, which finally proteolyze regulatory and structural cellular substrates to induce the apoptotic phenotype (Youle and Strasser 2008, Tait and Green 2010).

After MOMP, cell death can also be engaged even in the absence of caspase activity, a process termed caspase-independent cell death (CICD). Its morphologic, biochemical and kinetical features are different to the apoptotic ones and may vary between cell types. MOMP allows the release of intermembrane space factors which might actively trigger cell death independently of caspases. In addition, the mitochondrial function is gradually impaired, including a loss of the respiratory chain function and a drop in the membrane potential and the ATP synthesis. Ultimately, this leads to bioenergetics crisis and cell death (Pradelli et al. 2010b, Tait et al. 2014).

1.4. BCL-2 FAMILY MEMBERS

Mitochondrial integrity and the intrinsic apoptotic pathway are controlled by the evolutionarily conserved BCL-2 family of proteins, which can be classified into three groups based on structural and functional homologies (Fig. I.7) (Czabotar et al. 2014, Moldoveanu et al. 2014).

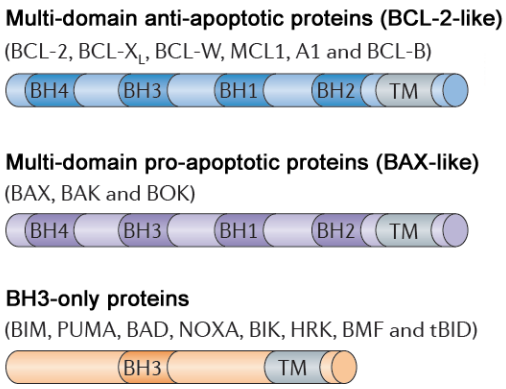

Figure I.7. Schematic representation of the structure of BCL-2 family proteins. BH, BCL-2 homology domain; TM, transmembrane domain. Adapted from Czabotar et al. 2014.

Anti-apoptotic proteins (BCL-2-like)

This subfamily includes BCL-2 related gene A1 (A1/BFL-1), BCL-2, BCL-2-related gene-long isoform (BCL-X_L), BCL-W, myeloid cell leukemia-1 (MCL-1) and BCL-B. All members share four BCL-2 homology (BH) domains (BH1-4). Most of them also contain a transmembrane (TM) domain for anchoring to organelles, mainly to mitochondria, but are also found in the ER and the cytosol. The domains BH1, BH2 and BH3 are folded to form a hydrophobic surface groove that allows interaction with other pro-apoptotic members. The BCL-2-like proteins are critical for cell survival as they preserve the integrity of the outer mitochondrial membrane (OMM) through inhibiting other pro-apoptotic members of the family. When overexpressed in transgenic mice, all the anti-apoptotic proteins of the BCL-2 family confer resistance to a wide range of apoptotic stimuli (Czabotar et al. 2014, Moldoveanu et al. 2014). Some of these proteins are required for the survival of certain cell types; for instance, BCL-2 and MCL-1 are necessary to extend the life of mature B and T lymphocytes (Strasser 2005).

Pro-apoptotic multi-domain proteins (BAX-like)

This subfamily includes BCL-2-associated X protein (BAX) and BCL-2-antagonist/killer-1 (BAK). Originally, they were reported to contain BH1, 2 and 3, but recently the BH4 domain has also been

identified (Kvansakul et al. 2008, Czabotar et al. 2014, Moldoveanu et al. 2014). In healthy cells, BAX and BAK exist as monomers. Upon a pro-apoptotic stimulus, these proteins get activated and oligomerize at the OMM to enable MOMP and the subsequent release of apoptogenic factors. In stark contrast to the previous group, overexpression of BAX-like proteins induces apoptosis. Mice lacking *Bax* and *Bak* have serious abnormalities caused by defects in developmentally programmed cell death. BCL-2-related ovarian killer (BOK) shares similar structure to BAX and BAK and is known to have a pro-apoptotic function. Nevertheless, mice lacking BOK are largely normal, so the exact role of this BAX-like protein in apoptosis remains to be fully elucidated (Czabotar et al. 2014, Moldoveanu et al. 2014).

Pro-apoptotic proteins with only the BH3 domain (BH3-only)

This subfamily comprises BCL-2 antagonist of cell death (BAD), BCL-2-like-11 (BIM), BCL-2 interacting killer (BIK), BID, harakiri (HRK, aslo known as DP5), BCL-2-modifying factor (BMF), NOXA and p53-upregulated modulator of apoptosis (PUMA). As indicated by their name, the BH3-only proteins share a single region with other BCL-2 family members, the BH3 domain, which is essential for their pro-apoptotic activity. Through the BH3 domain, these pro-apoptotic proteins interact with other BCL-2 family members creating a complex regulatory network to control cell survival and death in response to different stresses.

Several other proteins have been reported to contain a BH3-only domain within their structures and possess pro-apoptotic activity and/or the ability to interact with anti-apoptotic BCL-2 family proteins. These include BNIP3/NIX, BNIP3L or MOAP-1, the autophagy effector Beclin 1, or the E3 ligase MULE/ARF-BP1, among others (Lomonosova and Chinnadurai 2008).

Alternative splicing of BCL-2 family members may completely change their function. Some examples of anti-apoptotic proteins whose splicing variants are pro-apoptotic include BCL-X_S or MCL-1_S (Boise et al. 1993, Bae et al. 2000). On the contrary, alternative splicing of the BH3-only BID_{EL} or BID_L generates BID_S, which lacks the BH3 domain and thus plays an anti-apoptotic role (Renshaw et al. 2004). Many studies have achieved the knockout or overexpression mouse model of the BCL-2 family members, allowing the study of their physiological role, redundancy and interactions *in vivo* and their contribution to tumor progression and resistance to therapy (Czabotar et al. 2014). In addition, various non-apoptotic roles have been suggested for the BCL-2 family members. MCL-1 has different roles depending on its localization. In the OMM, it exerts an anti-apoptotic function, while a truncated form of MCL-1 in the mitochondrial matrix facilitates normal mitochondrial function. On the other hand, BCL-2 translocates to the ER and sequesters Beclin-1, thereby inhibiting autophagy.

When a BH3-only protein binds to BCL-2, it releases Beclin-1 and allows the induction of autophagy (Czabotar et al. 2014, Renault and Chipuk 2014).

1.4.1. INTERACTIONS BETWEEN BCL-2 FAMILY MEMBERS

The apoptotic threshold is set by the interactions between the BCL-2 family members. The BH3 amphypatic helix of the BH3-only proteins binds to the hydrophobic groove of the pro-survival proteins. Due to subtle differences in these interacting surfaces, BH3-only proteins bind pro-survival BCL-2 proteins with different affinities. Specifically, BIM, PUMA and tBID can bind to all pro-survival proteins; while other BH3-only are selective for subsets of their pro-survival relatives (Fig. I.8) (Czabotar et al. 2014, Moldoveanu et al. 2014).

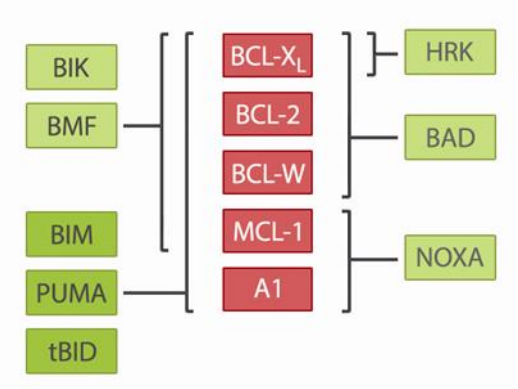

Figure I.8. The functional interaction network between pro- and anti-apoptotic BCL-2 family members. Adapted from Moldoveanu et al. 2014.

Three models addressing the interactions between BCL-2 family members have been proposed (Fig. I.9). In the direct activation model, certain BH3-only proteins termed activators (namely BIM, tBID and PUMA) bind to and directly activate the effectors BAX and BAK. Pro-survival BCL-2-like proteins bind to and inhibit the activator proteins. The other BH3-only proteins (BIK, BMF, HRK, BAD and NOXA) are called sensitizers. They lack the activator function, and the pro-apoptotic effects are exerted by neutralizing pro-survival BCL-2-like proteins, thereby releasing the bound BH3-only activators to allow BAX/BAK activation (Fig. I.9A). In contrast, the indirect model considers that pro-survival BCL-2-like proteins inhibit the effectors BAX and BAK. The BH3-only proteins bind to and neutralize the pro-survival proteins, allowing the release and subsequent activation of BAX and BAK (Fig. I.9B). Nowadays, the current consensus accepts that both models can occur

depending on the context. This unified model considers that pro-survival BCL-2-like proteins can neutralize both BH3-only and effector proteins (Fig. I.9C).

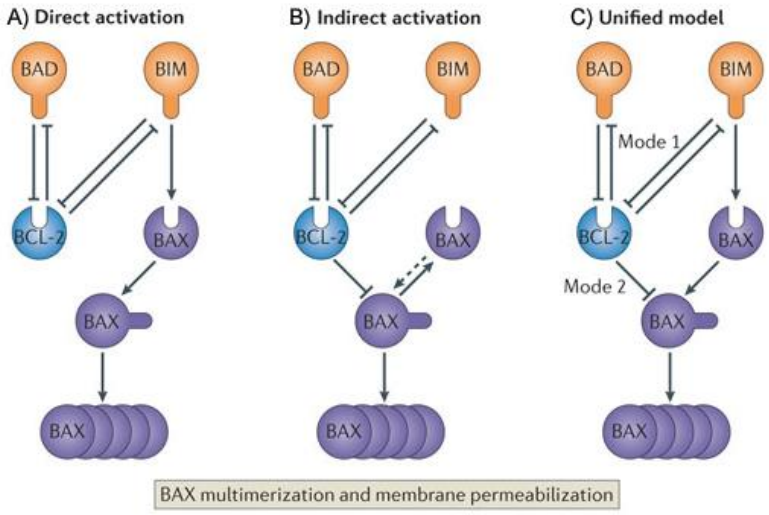

Figure I.9. Models of interaction among BCL-2 family members that control the apoptotic outcome. (A) The direct activation model. BH3-only sensitizers, such as BAD, bind to pro-survival proteins, like BCL-2, to release BH3-only activators (e.g. BIM) and allow the activation of the effectors (BAX and BAK). **(B)** The indirect activation model. BH3-only proteins, such as BAD and BIM, neutralize pro-survival BCL-2 proteins and allow the activation of the effectors. **(C)** The unified model combines the direct and the indirect models. BH3-only proteins interact with pro-survival BCL-2 proteins to release the BH3-only activators (mode 1) or activated BAX/BAK (mode 2). Taken from Czabotar et al. 2014.

1.4.2. ACTIVATION OF BH3-ONLY PROTEINS BY VARIOUS STIMULI

As the BCL-2 family members mediate the induction of the mitochondrial apoptotic pathway, their expression and function are tightly regulated by transcriptional and post-transcriptional mechanisms, including modulations of gene expression, protein stability and conformational changes (Adams and Cory 2007, Kelly and Strasser 2011).

The multiplicity of BH3-only proteins allows a precise control over the induction of apoptosis. In this sense, although they can have partially redundant physiological functions, each BH3-only member responds to specific insults. Among these insults, there are both physiological stimuli, such as deprivation of cytokines, signaling receptors or loss of adhesion to the matrix cells (a type of cell death called anoikis); as well as signals induced by activated oncogenes, DNA damage, chemotherapeutic agents, UV or γ radiation (Fig. I.10).

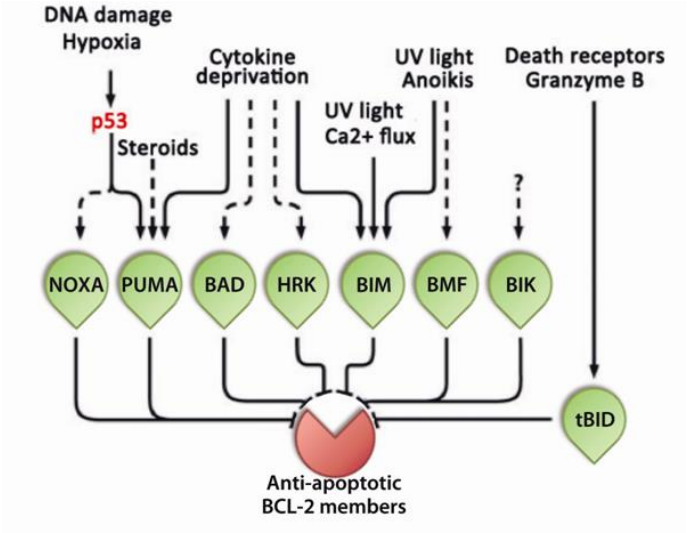

Figure I.10. Activation of BH3-only proteins by various stimuli. Adapted from Kelly and Strasser 2011.

1.4.3. PORE FORMATION DURING APOPTOSIS

In healthy cells, BAK is already inserted in the OMM, whereas BAX is mainly cytosolic. BAX constantly migrates from the cytosol to the OMM, but it accumulates at the OMM during apoptosis. BH3-only activators trigger the exposure of the BH3 domain of both BAX and BAK, fostering the dimerization. Through an unknown mechanism, dimers join to form oligomers of unknown size that permeabilize the membrane (Czabotar et al. 2014, Westphal et al. 2014). The nature of the pore that BAX and BAK form to promote MOMP is still under debate. Initially, it was thought that the two pro-apoptotic proteins could enhance the permeability of existing proteinaceous or lipidic pores, such as VDAC or ceramide channels. In contrast, BAX and BAK could be also forming a pore without requiring other proteins. More recent findings suggest that BAX, BAK and mitochondrial lipids cooperate to engage MOMP (Fig. I.11) (Renault and Chipuk 2014).

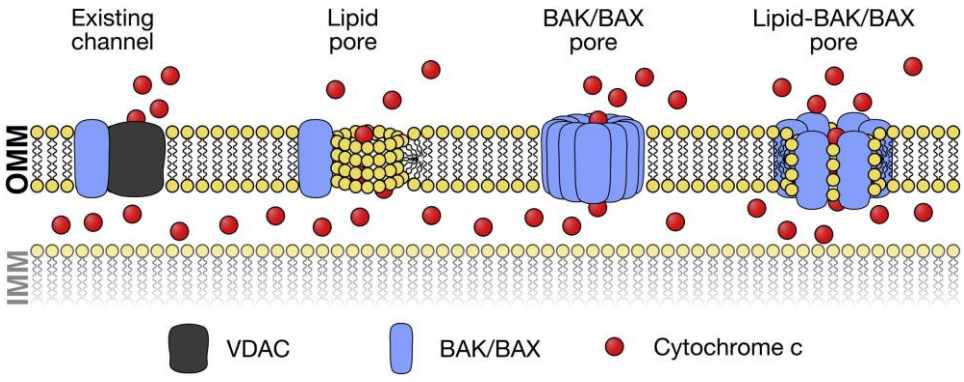

Figure I.11. Models of BAX and BAK pore formation during apoptosis. Taken from Renault and Chipuk 2014.

1.5. APOPTOSIS IN CANCER

Tissue homeostasis is the maintenance of normal tissue morphology and function, which relies on the accurate regulation of cell proliferation, stem cell activity, differentiation, quiescence and cell death. The balance among these processes is the result of the integration of a variety of intracellular and extracellular signals. In some cases, such balance is altered with abnormal accumulation of cells, which can lead to cancer (Hanahan and Weinberg 2011).

Throughout the sequential evolution towards becoming malignant, cells acquire several common capabilities to circumvent the principle barriers that prevent uncontrolled cell expansion. These attributes are the so-called hallmarks of cancer, which include sustained proliferative signaling, evasion of growth suppressors, resistance to cell death, replicative immortality and activation of angiogenesis, invasion and metastasis. Underlying these hallmarks are genome instability, which causes the genetic diversity that accelerates their acquisition; and inflammation, which promotes multiple hallmark functions. Advances in understanding cancer biology identified two emerging hallmarks of potential generality, namely reprogramming of energy metabolism and evading immune destruction. In addition, the acquisition of hallmark traits is fostered by the tumor microenvironment, a repertoire of recruited, apparently normal cells surrounding the tumor (Fig. I.12) (Hanahan and Weinberg 2011).

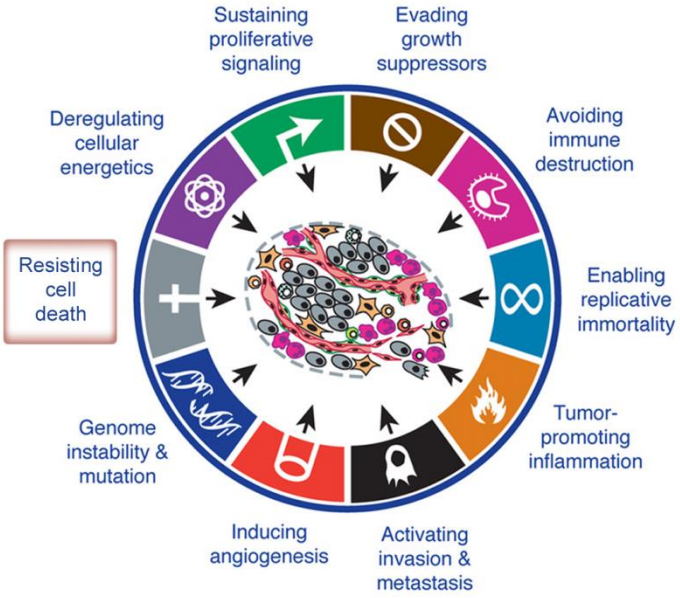

Figure I.12. The hallmarks of cancer. Eight hallmark capabilities and two enabling characteristics. Adapted from Hanahan and Weinberg 2011.

Apoptosis plays an important role in tumor growth, tumor progression and resistance to therapy. Hence, genes that suppress or induce physiological cell death are often deregulated in cancer (Hanahan and Weinberg 2011). Defects in the mechanisms of apoptosis induction allow tumor cells to survive beyond their physiological life, to avoid the need of extracellular factors for survival and to resist hypoxia and cell stress caused within the tumor. In addition, resistance to apoptosis gives room for the accumulation of genetic alterations that can contribute to deregulation of cell cycle, alteration of the tissue differentiation pattern, stimulation of angiogenesis, or increase in cell mobility and invasiveness (Reed 2003, Labi and Erlacher 2015).

Mechanisms of apoptosis induction are complex and involve numerous signaling pathways. Consequently, cancer cells may acquire resistance to cell death through various strategies. On the one hand, cancer cells may evade apoptosis through transcriptional, translational and post-translational modifications of the BCL-2 family proteins. In some cases, cancer cells may increase the expression of anti-apoptotic genes and/or decrease the pro-apoptotic genes. Alternatively, resistance to apoptosis may be acquired through stabilizing or destabilizing anti- or pro-apoptotic proteins, respectively. In addition, post-translational modifications of apoptotic proteins may change their function, resulting in defective apoptosis (Fernald and Kurokawa 2013, Czabotar et al. 2014).

Another mechanism to overcome apoptosis is the inactivation of p53 pathway, which was found mutated in half of human cancers, demonstrating its importance in cancer development (Vousden and Lane 2007). However, many pharmacological interventions used in cancer therapy relied, at least partially, on p53 pathway activation to induce apoptosis, which finally results in chemoresistance. Other alterations involved in resisting apoptosis include loss of DNA damage or hypoxia sensors, or alterations in survival pathways, including mitogen-activated protein kinases (MAPK), phosphatidylinositol-3-kinase (PI3K)/AKT, protein kinase C (PKC) or nuclear factor of kappa light polypeptide gene enhancer in B-cells (NF-$\varkappa$B) routes (Adams and Cory 2007).

1.5.1. THE ROLE OF APOPTOSIS IN CANCER THERAPY

Nowadays, the combination of surgery, radiation and chemotherapy is used to restore the normal signaling pathways to induce cell cycle arrest and/or apoptosis. Many current chemotherapeutic agents are inductors of apoptosis. Indeed, activation of the mitochondrial apoptotic pathway seems to be required for the therapeutic efficacy of most conventional chemotherapeutic agents (Czabotar et al. 2014). Depending on the nature of such apoptotic stimuli and the cellular context, distinct signaling pathways employ specific BH3-only proteins to induce apoptosis. A wide range of anti-cancer agents, including DNA damaging compounds, proteasome inhibitors or glucocorticoids, may

trigger mRNA or protein expression changes of several BCL-2 family members and, in particular of BH3-only proteins, to induce apoptosis (Fig. I.13) (Labi et al. 2006, Walensky 2006, Czabotar et al. 2014)

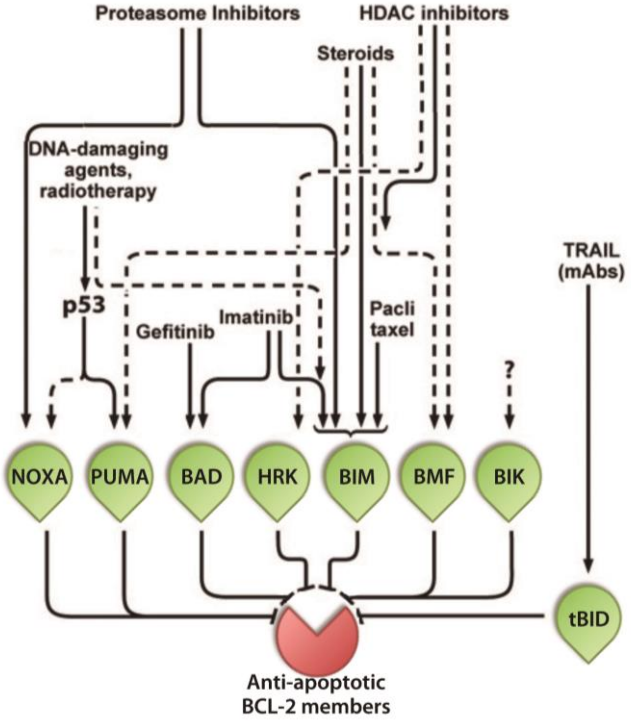

Figure I.13. Anti-cancer agents and their known ability to engage BH3-only proteins. Solid arrows indicate a strong activation, dashed arrows indicate weak activation. Adapted from Labi et al. 2006, Walensky 2006.

Unfortunately, although these drugs and therapeutic methods should have the potential to eliminate cancer cells, few strategies for cancer treatment are truly effective (Hanahan and Weinberg 2011, Czabotar et al. 2014). Therefore, it has become crucial to develop new therapeutic strategies based on the design and study of specific anti-cancer molecules able to overrule the apoptotic machinery that render cells resistant to apoptosis.

2. CHRONIC LYMPHOCYTIC LEUKEMIA

2.1. CLL BIOLOGY AND DIAGNOSIS

Chronic lymphocytic leukemia (CLL) represents the most common adult leukemia in the western world, mainly affecting elderly individuals. It is a malignant lymphoproliferative disorder of monoclonal B lymphocytes that accumulate in the blood, bone marrow, lymph nodes and other lymphoid tissues (Zenz et al. 2010). As a result of this abnormal expansion, CLL cells can account for up to 99% of circulating peripheral blood mononuclear cells (Chen and McMillan 2008). CLL cells are morphologically mature but functionally immature, showing a deficient production of antibodies, which favors the appearance of infectious and autoimmune diseases (Chiorazzi et al. 2005, Zenz et al. 2010).

CLL can be functionally considered as a dual disease. On the one hand, it involves a quiescent circulating population present in peripheral blood. These CLL cells are arrested in G0/G1 phase of the cell cycle and they can survive for a few months. Therefore, lack of proper apoptotic signaling pathways was considered the main cause for B cell accumulation. However, it is now widely recognized that quiescent CLL cells present in the periphery have undergone several rounds of proliferation compared to their normal counterparts, as shown by shortened telomeres (Chiorazzi 2007, Hayden et al. 2012). Indeed, survival of CLL cells depends on interactions with the microenvironment, consisting of T cells, macrophages, and stromal cells, which induce the activation of survival and proliferative signaling pathways. These interactions can occur in proliferating centers within the solid tissues, including bone marrow and the lymph nodes (Zenz et al. 2010, Hayden et al. 2012).

CLL can be diagnosed if the lymphocyte counts in the blood are higher than $5x10^9$/L, with a characteristic immunological profile defined by the expression of CD5, CD19, CD20 and CD23 along with low expression of CD10, IgM, IgD and cyclin D1. CLL is characterized by an extremely heterogeneous clinical course, ranging from indolent forms with very slow evolution to aggressive forms with short course. Therefore, the use of prognosis factors is especially important to adopt the most appropriate decision in the patient management and also to predict the disease evolution and the response to treatment. The current criteria are based on clinical stage (Binet and Rai classification), serum markers (for example, thymidine kinase, β2-microglobulin and soluble CD23), cell marker expression (CD38 and zeta-associated protein 70) and various genetic parameters (Zenz et al. 2010, Hallek 2015). In fact, two subsets of CLL cases have been identified according to the status of somatic hypermutations in the immunoglobulin heavy chain variable region (IGHV) genes, clearly presenting different prognostication and treatment. Specifically, CLL cells with unmutated IGHVs can activate key signaling pathways upon B-cell receptor (BCR) activation and are genetically more

unstable, which may explain the poorer overall survival of the patients. On the contrary, IGHV-mutated CLL cells weakly activate BCR signaling and are relatively anergic, which can explain the better overall survival of this subset of CLL patients (Zenz et al. 2010).

2.2. GENETIC ABERRATIONS AND GENE MUTATIONS IN CLL

Deletion (del) of 13q14 is the structural aberration most frequently found in CLL, occurring in ~55% of all cases. The presence of only this abnormality often implies a benign course of the disease. Two microRNAs, miR-15a and 16-1, were identified in the critical region of del(13q14). In addition, trisomy 12 is one of the most frequent aberration (10–20% of patients with CLL), though the genes involved in the pathogenesis of CLL are unknown (Zenz et al. 2010, Hallek 2015) and its prognostic importance remains controversial (Seiffert et al. 2012).

Although they are rarely found in early-stage disease, patients with advanced or chemotherapy-resistant disease frequently show deletions in 11q, which harbors the gene *ATM*; and in 17p13, which harbors the gene *TP53* (Zenz et al. 2010, Hallek 2015). Interestingly, the recently reported whole genome sequencing project in CLL has revealed various recurrent somatic gene mutations, which include the genes *TP53*, *ATM*, among others (Puente et al. 2011, Quesada et al. 2012). It is noteworthy that p53 and ATM are key proteins in DNA damage signaling and DNA repair (Jackson and Bartek 2009). The fact that different genetic alterations, i.e. deletions and mutations, in these two genes appear more frequently in patients with secondary resistance to DNA-damaging chemotherapy (Puente et al. 2011, Quesada et al. 2012) highlights the critical role of these two proteins in mediating apoptosis in response to DNA damage in CLL cells.

2.3. TREATMENT OF CLL

Most patients are asymptomatic at diagnosis of CLL, and treatment starts upon progression to the symptomatic disease. Historically, CLL was treated with chemotherapy including an alkylating agent and a purine analogue. The addition of a monoclonal antibody against CD20 to the classical chemotherapy improved the survival of CLL patients. This triple combination, known as chemoimmunotherapy, has become the currently recommended front-line treatment for CLL patients. Specifically, the purine analogue fludarabine, the alkylating agent cyclophosphamide and the anti-CD20 monoclonal antibody ritixumab (FCR) appear to be the most preferred treatment of choice in young, fit patients with good renal function. Other regimens are more applicable in elder and/or frailer patients who are unlikely to tolerate it (Nabhan and Rosen 2014, Hallek 2015).

Recently, the Food and Drug Administration has approved the use of ibrutinib, idelalisib and obinutuzumab, three new agents for the treatment of CLL. Ibrutinib and idelalisib inhibit Bruton tyrosine kinase (BTK) and PI3Kδ, respectively. These kinases are involved in the BCR signaling, which is crucial for the survival of CLL cells. In addition, a new monoclonal anti-CD20, obinutuzumab, has proved efficacy in patients that cannot properly tolerate more aggressive chemoimmunotherapies (Sanford et al. 2015). Another promising new therapeutic agent is ABT-199, a BH3-mimetic that inhibits BCL-2 protein (Souers et al. 2013). Treatment with ABT-199 results in a high rate of durable remission in patients with relapsed or refractory CLL, as well as in patients with impaired p53 pathway (Hallek 2015).

TYPES OF TREATMENT FOR CHRONIC LYMPHOCYTIC LEUKEMIA	
Alkylating agents	Chlorambucil Cyclophosphamide Bendamustine
Purine analogues	Fludarabine Pentostatin Cladribine
Monoclonal antibodies (anti-CD20)	Rituximab Alemtuzumab Obinutuzumab
B-cell receptor pathway inhibitors	Ibrutinib (targets BTK) Idelalisib (targets PI3Kδ)

Table I.2. Drugs used in CLL therapy. Adapted from Nabhan and Rosen 2014.

Although the overall survival of CLL patients has increased with the first-line therapy, the side-effects and the chemoresistance limit their efficacy, and eventually all patients relapse (Zenz et al. 2010). Therefore, it is necessary to identify new agents with selective toxicity for malignant B cells and to develop therapeutic strategies that overcome cellular resistance mechanisms to cytotoxic agents, which are often caused by inactive p53 pathway, in order to obtain sustained remission rates in patients with adverse prognostic factors.

3. NEW STRATEGIES FOR CANCER TREATMENT

3.1. THE PURINE NUCLEOSIDE AICAR

3.1.1. AICAR AS AN AMP-ACTIVATED PROTEIN KINASE ACTIVATOR

AICAR (5-aminoimidazole-4-carboxamide riboside, acadesine or Acadra®, represented in figure I.14) is a cell-permeable purine nucleoside for which three pharmacological applications were identified about 20 years ago: i) stimulation of the cardiac production of adenosine under ischemic conditions; ii) inhibition of hepatic gluconeogenesis, with therapeutic potential in diabetes; and iii) activation of the AMP-activated protein kinase (AMPK), initially applied to inhibit the hepatic synthesis of triglycerides and cholesterol (Van Den Neste et al. 2010).

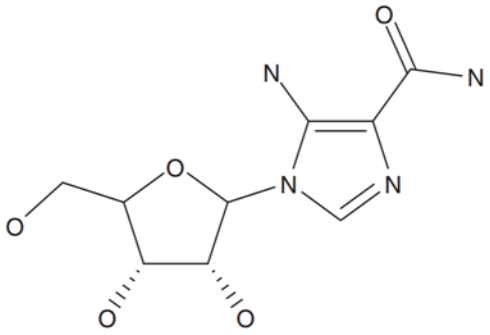

Figure I.14. Structure of AICAR, 5-aminoimidazole-4-carboxamide riboside, acadesine or Acadra®. Taken from Van Den Neste et al. 2010.

AMPK is a well-conserved eukaryotic serine/threonine protein kinase that acts as sensor of energy status. It is expressed in essentially all eukaryotic cells as heterotrimeric complexes, containing the catalytic α subunit and the regulatory β and γ subunits. AMPK plays a key role during metabolic stress, when AMP:ATP and ADP:ATP ratios increase. AMPK is activated allosterically by AMP or through increased phosphorylation in Thr172 of the catalytic α subunit by upstream kinases, namely LKB1 and Ca^{2+}/calmodulin-activated protein kinase kinases β (CAMKKβ) (Hardie et al. 2012). In addition, recent work suggests non-canonical activation of AMPK induced by oxidative stress or genotoxic treatments. The main function of AMPK is to restore cellular energy homeostasis by switching on catabolic pathways and switching off ATP-consuming processes. Furthermore, AMPK is also crucial in the regulation of whole body energy balance, especially by mediating effects of hormones on the hypothalamus to promote feeding and circadian rhythms of metabolism and feeding behavior (Hardie et al. 2012).

3.1.2. AICAR AS A THERAPEUTIC AGENT FOR SEVERAL HEMATOLOGICAL MALIGNANCIES

Our group described that AICAR induces apoptosis in various cell types, including CLL, mantle cell lymphoma (MCL), and splenic marginal zone B-cell lymphoma (SMZL) cells, without affecting primary T lymphocytes (Campàs et al. 2003, 2005).

AICAR enters into the cells through nitrobenzylthioinosine (NBTI)-sensitive transporters, which mainly includes equilibrative nucleosides transporter 1 (ENT1). Then, AICAR is further phosphorylated to ZMP (also known as AICA-ribotide) by adenosine kinase. Both steps are required for AICAR-induced apoptosis in CLL cells (Campàs et al. 2003, Santidrián et al. 2010). ZMP has been described to activate AMPK by allosteric stimulation due to its structural analogy with AMP and by promoting its phosphorylation by upstream kinases (Corton et al. 1995, Suter et al. 2006). Accordingly, AICAR triggers the phosphorylation of AMPK at Thr172 in CLL, MCL and SMZL cells, correlating with induction of apoptosis (Campàs et al. 2003, Campàs 2004). Strikingly, AICAR was proved to induce cell death independently of AMPK. First, AICAR enters follicular lymphoma (FL) cells and induces phosphorylation of AMPK, but most FL samples tested are resistant to AICAR-induced apoptosis (Campàs et al. 2005). In Jurkat cells, AICAR induces apoptosis without inducing the phosphorylation of AMPK neither requiring ZMP accumulation (López et al. 2003). In CLL cells, direct activation of AMPK does not induce apoptosis, and mouse B lymphocytes lacking *Ampkα* are sensitive to the pro-apoptotic effects of AICAR (Santidrián et al. 2010). In chronic myelogenous leukemia (CML) cells, AICAR triggered autophagic cell death in a PKC-dependent but AMPK-independent manner (Robert et al. 2009).

Following AICAR treatment, apoptosis is induced through the intrinsic pathway, involving cytochrome *c* release and the activation of caspases 3 and 9. Importantly, the caspase inhibitor benzyloxycarbonyl-Val-Ala-Asp-fluoromethylketone (Z-VAD.fmk) blocks AICAR-induced apoptosis (Campàs et al. 2003, Santidrián et al. 2010). Inhibitors of protein kinase A (PKA) or MAPKs, including inhibitors of p38, extracellular signal-regulated kinase (ERK) and c-Jun N-terminal kinase (JNK), are unable to block AICAR-induced apoptosis in CLL cells (Campàs et al. 2003).

Fludarabine and other nucleoside analogues are highly effective in the treatment of CLL but they induce apoptosis of T cells (Bellosillo et al. 1999) leading to immunosuppression (Keating 1993). Hence, the higher sensitivity of B cells opens a therapeutic window for AICAR as a treatment for CLL. T cells from CLL patients are only slightly affected by AICAR at high doses. Intracellular levels of ZMP are higher in B cells than in T cells from CLL patients upon treatment with 0.5 mM AICAR (Campàs et al. 2003), which can explain the different sensitivity of the cells.

Defects in p53 are rare in newly diagnosed CLL patients, though its frequency increases among patients with advanced and chemotherapy-resistant disease (Shindiapina et al. 2014). Drugs that induce apoptosis in a p53-dependent manner induce the phosphorylation and subsequent accumulation of p53. Importantly, AICAR does not result in accumulation nor phosphorylation of p53 (Campàs et al. 2003) and induces apoptosis irrespective of *TP53* or *ATM* mutational status in CLL cells (Santidrián et al. 2010). Accordingly, AICAR efficiently triggered apoptosis in mouse lymphocytes lacking *p53* (González-Gironès 2012). This is a significant difference compared to other nucleoside analogues, such as fludarabine, that require p53 activation for apoptosis induction (Byrd et al. 2004).

AICAR mechanism of apoptosis induction has been further characterized in CLL cells. Treatment with AICAR induces a ZMP-dependent increase in the mRNA levels of the BH3-only members *BIM*, *BNIP3*, *BNIP3L*, *HRK*, *MOAP1*, *NOXA* and *PUMA*, but not all genes are modified concomitantly in the same CLL sample (Santidrián et al. 2010, González-Gironès 2012). Interestingly, BIM and NOXA were reported to play a crucial role in AICAR-induced apoptosis. Mouse B lymphocytes and MEFs lacking *Bim* and *Noxa* were resistant to the pro-apoptotic effects of AICAR (Santidrián et al. 2010, González-Gironès 2012).

A multicenter phase I/II study of AICAR was performed in CLL patients, with a favourable efficacy and safety profile. Patients showed reduced number of CLL cells and lymphadenopathy (Van Den Neste et al. 2013). Although the results were variable because of the small population, AICAR emerged as a promising agent for the treatment of relapsed or refractory CLL patients. Interestingly, the pro-apoptotic effects of AICAR increased in combination with the most common chemotherapeutic agents for CLL treatment. Specifically, AICAR showed synergistic effects with the glucocorticoid dexamethasone, and additive effects with fludarabine, chlorambucil and mafosfamide in CLL cells (González-Gironès 2012). In MCL cells, AICAR showed synergistic effects in combination with rituximab both *in vitro* and *in vivo*, although it did not occur in CLL cells (Montraveta et al. 2014).

The detailed description of the mechanism of induction of apoptosis gives room for the identification of targets that can establish novel strategies for cancer treatment. Therefore, one of the main goals of this thesis has been the characterization of AICAR-induced apoptosis.

3.2. THE NEW PROHIBITIN-BINDING COMPOUND FLUORIZOLINE

Resistance to cell death is one of the hallmarks of cancer development and it compromises the efficacy of conventional anti-cancer agents (Hanahan and Weinberg 2011). Hence, there is need for the development of novel apoptosis-inducing compounds as potential therapies for cancer. With this aim, our group established a collaboration with Dr. Lavilla and Dr. Albericio (Barcelona Science Park - UB) to synthetize a library of new, potent, safe and selective apoptosis-inducing compounds. Specifically, two families of new chemical entities were prepared, based on fluorinated thiazole or fluorinated indole scaffolds. Their anti-cancer activity was assessed in various cancer cell lines as well as in primary CLL cells. Interestingly, the structure-activity relationship analysis permitted the rational optimization of those chemical structures with better biological activities to further improve their potency as pro-apoptotic compounds. Among all the compounds tested, the diaryl trifluorothiazoline PG10 or compound **1a**, hereafter referred to as fluorizoline (Fig. I.15), was selected as the best apoptosis inductor (González-Gironès 2012, Pérez-Perarnau 2013, Pérez-Perarnau et al. 2014).

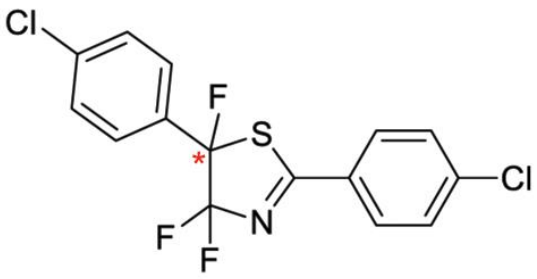

Figure I.15. Chemical structure of compound 1a or fluorizoline, showing the trifluorinated thiazoline scaffold and the chiral carbon (*).

Most biological molecules are optically active and present several enantiomers. Often only one of the enantiomers is responsible for the desired biological effects, while the other enantiomer is less active, inactive, or sometimes even responsible for adverse effects. Consequently, drugs composed of only one enantiomer (enantiopure) can be developed to enhance the biological efficacy (Smith 2009). Fluorinated thiazoles are prepared as racemic mixtures containing two enantiomers. The separation of the two enantiomers was achieved for compound **1b** or PG0, proving that only one enantiomer is responsible for the pro-apoptotic activity (Pérez-Perarnau et al. 2014). Unfortunately, the racemic mixture separation of fluorizoline has not been performed.

Fluorizoline induces apoptosis in a wide range of cancer cell lines, including prostate, breast, uterus, brain, pancreas, lung, and liver. Importantly, these cell lines have different p53 status, thus proving

that fluorizoline exerts its anti-tumor action in a p53-independent manner (Pérez-Perarnau et al. 2014). This differentiates fluorizoline from other drugs currently used in cancer therapy, whose mechanism of action is mediated by p53, a tumor suppressor gene frequently mutated or deleted in many cancer types (Vousden and Lane 2007, Polager and Ginsberg 2009). In addition, treatment with fluorizoline resulted in mitochondrial fragmentation, cristae remodeling and cytochrome *c* release. Of note, apoptosis-related gene expression profile revealed that NOXA was consistently upregulated in various cancer cell lines. Its importance in fluorizoline mechanism of action was further proved by downregulating *NOXA* in HeLa cells, which conferred resistance to fluorizoline treatment (Pérez-Perarnau 2013). Finally, our group collaborated with Dr. Handa (Tokyo Institute of Technology, Japan) to perform a high-performance affinity purification with magnetic nanobeads. This assay allowed the identification of the proteins that were directly binding to fluorizoline: prohibitin 1 and 2 (PHBs) (Pérez-Perarnau et al. 2014).

3.2.1. THE PROHIBITIN FAMILY

PHB1 and PHB2 (also known as B-cell-receptor-associated protein 37 - BAP-37, or repressor of estrogen receptor activity - REA) are evolutionary conserved and ubiquitously expressed proteins that belong to the stomatin-prohibitin-flotilin-HflC/K (SPFH) superfamily, which share a domain of ~160 amino acid residues known as SPFH or PHB domain. SPFH proteins tend to oligomerize and form large multimeric complexes localized in lipid rafts microdomains of different cellular membranes (Browman et al. 2007). Indeed, PHBs form a macromolecular structure of ~1.2 MDa at the inner mitochondrial membrane (IMM). PHB1 and 2 interact with each other to form a ring-like structure of 20-25nm, which is thought to contain about 12 to 16 PHB1 and PHB2 heterodimers. It has been proposed that the PHB mitochondrial complex anchores to the membrane through the N-terminal domain, while the C-terminal coiled-coil domain facilitates oligomerization into the large complexes (Fig. I.16) (Merkwirth and Langer 2009).

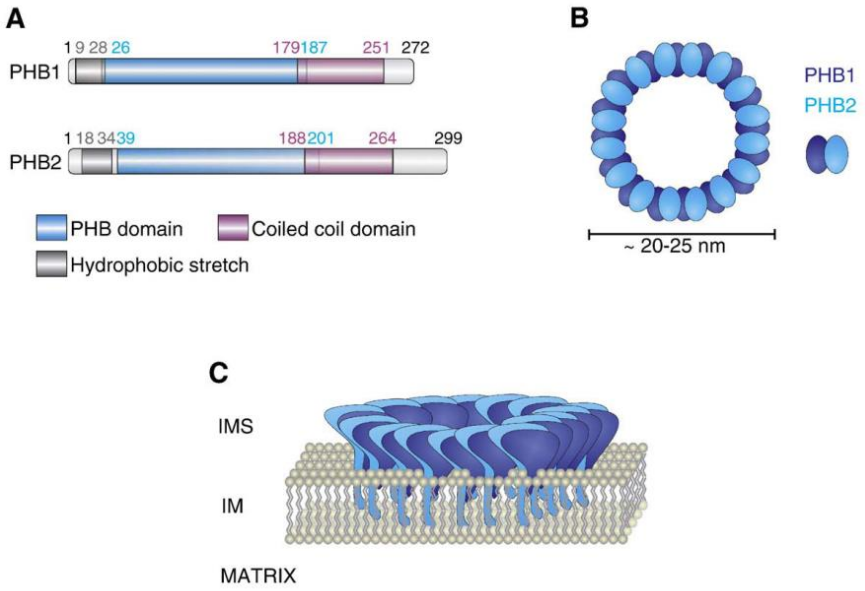

Figure I.16. Schematic representation of PHB domain structures and dimer assembling into ring-like structures. (A) Domain structures of mammalian PHBs. Numbers refer to the respective amino acid residues in murine PHBs. **(B)** Dimers of PHB1 and PHB2 as building blocks of PHB complexes. Approximately 12-16 heterodimers are thought to assemble into ring-like PHB complexes with alternating subunit composition. The average stoichiometry of the complex is speculative. **(C)** Suggested model of membrane-bound prohibitin complex. The PHB complex is anchored to the mitochondrial inner membrane (IM) via N-terminal hydrophobic stretches. PHB and coiled-coil domains are exposed to the intermembrane space (IMS). Modified from Merkwirth and Langer 2009.

PHBs ring-like structure and the sequence similarity to lipid-raft associated proteins of the SPFH family suggest a protein and lipid scaffold function for PHBs in the inner mitochondrial membrane (Osman et al. 2009b). In this sense, PHBs may contribute to the spatial organization of the IMM as protein scaffolds, by recruiting proteins to specific sites (Fig. I.17A), or by creating protein-free lipid areas (Fig. I.17B). As lipid scaffolds, PHBs may create lipid-enriched microdomains (Fig. I.17C). This compartmentalization of the membrane composition may serve as a mechanism for separating cellular functions within the cellular membranes (Browman et al. 2007, Osman et al. 2009b).

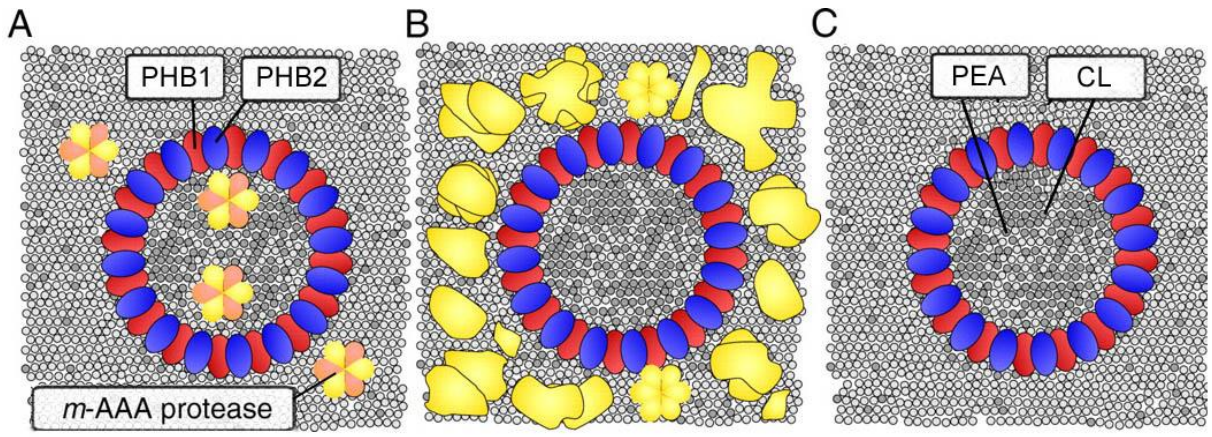

Figure I.17. Speculative models for PHBs as lipid and protein scaffolds. (A) PHBs complexes as protein scaffolds. **(B)** Fence-like function of PHBs complexes. **(C)** PHBs complexes as lipid scaffolds. Phoshpatidylethanolamine (PEA), cardiolipin (CL). Modified from Osman et al. 2009b.

PHBs are interdependent at the protein level, thus depletion of one PHB leads to the loss of the other PHB without affecting its expression (Merkwirth and Langer 2009, Artal-Sanz and Tavernarakis 2009, Osman et al. 2009b). Severe phenotypes are linked to the loss of PHBs in multicellular organisms. PHBs are essential for the development of higher eukaryotes, as their loss leads to embryonic lethality in *Caenorhabditis elegans* and mice (Artal-Sanz et al. 2003, Park et al. 2005, He et al. 2008). At the cellular level, reduction in PHBs levels results in impaired proliferation (Kasashima et al. 2006, Schleicher et al. 2008, Merkwirth et al. 2008, Sievers et al. 2010, Jiang et al. 2015), and increased sensitivity towards apoptotic stimuli (Merkwirth et al. 2008, Gregory-Bass et al. 2008, Patel et al. 2010, Zhou et al. 2013a, Chowdhury et al. 2013). In this line, overexpression of PHBs confers resistance to pro-apoptotic stimuli (Fusaro et al. 2002, Zhou et al. 2013a, 2013b, Thuaud et al. 2013, Chowdhury et al. 2013, Han et al. 2014, Wang et al. 2014).

Mitochondria are dynamic organelles that continuously change their shape, from spherical to elongated, as a consequence of fusion and fission (Kasahara and Scorrano 2014). The lack of PHBs has severe consequences for the reticular mitochondrial network and results in the accumulation of fragmented mitochondria with an altered ultrastructure of the cristae (Kasashima et al. 2006, Merkwirth et al. 2008).

These morphological alterations observed in the absence of PHBs were attributed to the increased processing of optic atrophy 1 (OPA1), a dynamin-related GTPase in the IMM that that mediates mitochondrial fusion and maintains the cristae structure (Olichon et al. 2003, Arnoult et al. 2005, Merkwirth et al. 2008). There are up to eight variants of OPA1 generated by alternative splicing, being variants 1 and 7 the most dominantly expressed ones. Proteolytic cleavage results in 5 different

forms: a and b (long, L-OPA1), and c, d and e (short, S-OPA1) (Ishihara et al. 2006). OPA1 functions as a hetero-oligomeric complex of the large and the small forms (Ishihara et al. 2006, Frezza et al. 2006) and ensures the correct closing of the cristae junctions, creating the intracristae space where most of the cytochrome *c* resides (Scorrano et al. 2002, Frezza et al. 2006). During apoptosis, OPA1 complexes are disassembled (Frezza et al. 2006, Yamaguchi et al. 2008, Landes et al. 2010, Jiang et al. 2014), allowing the reorganization of the mitochondrial cristae and facilitating cytochrome *c* release from the intracristae space to the intermembrane space (Fig. I.18) (Scorrano et al. 2002, Yamaguchi et al. 2008). Hence, the marked processing of OPA1 links the increased sensitivity to pro-apoptotic stimuli that was also observed in the absence of PHBs (Merkwirth et al. 2008).

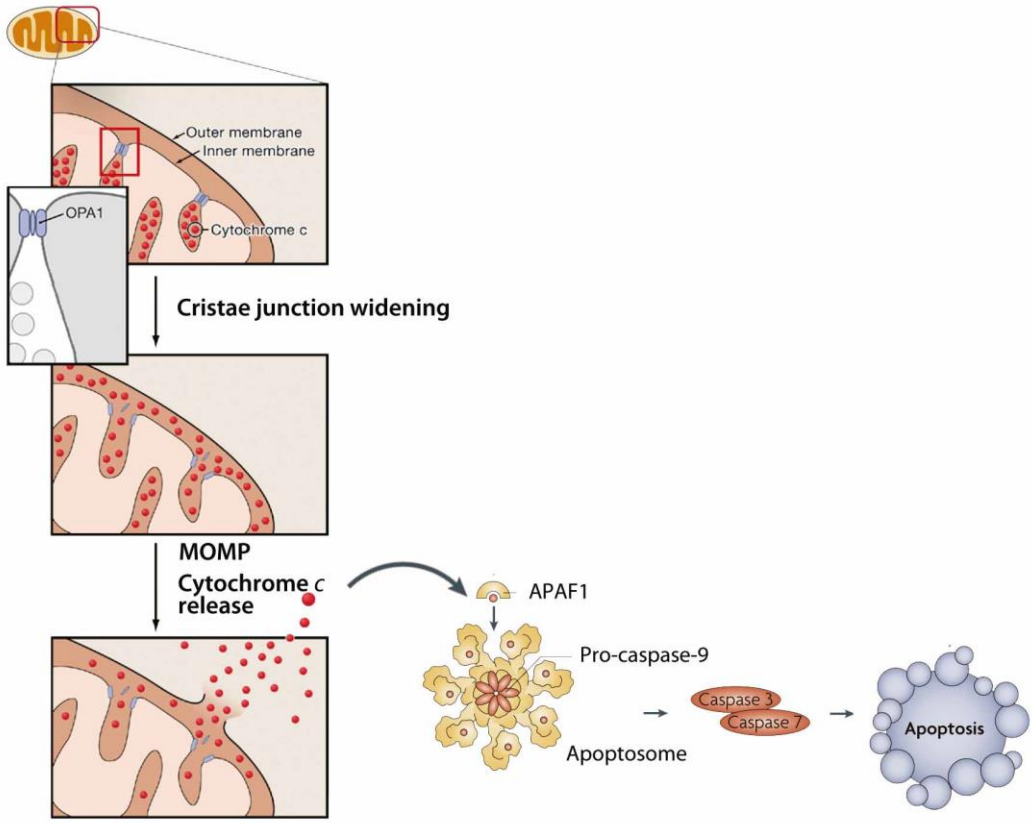

Figure I.18. OPA1 maintains cristae junctions and prevents cytochrome *c* release. OPA1 plays a critical role in maintaining the mitochondrial cristae structure. During apoptosis, OPA1 complexes are disassembled, cristae junctions widen and cytochrome *c* diffuses to the intermembrane space. MOMP allows cytochrome *c* release to the cytosol to trigger downstream events that will result in apoptosis. Adapted from Gottlieb, 2006 and further modified in Pérez-Perarnau 2013.

All these findings point towards a key role for PHBs in the maintenance of the functional integrity of mitochondria, which ultimately allows proper cell and tissue homeostasis (Artal-Sanz and Tavernarakis 2009, Osman et al. 2009b, Merkwirth et al. 2012, Supale et al. 2013, Ising et al. 2015).

3.2.2. THE ROLE OF PROHIBITINS IN PHOSPHOLIPID HOMEOSTASIS

In the inner mitochondrial membrane, PHBs were proposed to act as lipid scaffolds, which would be crucial for the homeostasis of mitochondrial glycerophospholipids (GPLs) (Osman et al. 2009b, Richter-Dennerlein et al. 2014). GPLs are the most abundant lipids, present in almost all mammalian membranes (Hermansson et al. 2011). GPLs consist of a hydrophilic head connected to a glycerol with two fatty acids (hydrophobic tails). There are different GPL classes, including phosphatidylcholine (PC), phosphatidylethanolamine (PEA), phosphatidylinositol (PIN), phosphatidylserine (PS), phosphatidylglycerol (PG) and cardiolipin (CL), which differ in the structure of their head group. Each class in turn contains diverse molecular species, which have the same head group but fatty acid acyl chains with different length and number of double bonds, and their synthesis is highly interconnected (Hermansson et al. 2011) (Fig. I.19).

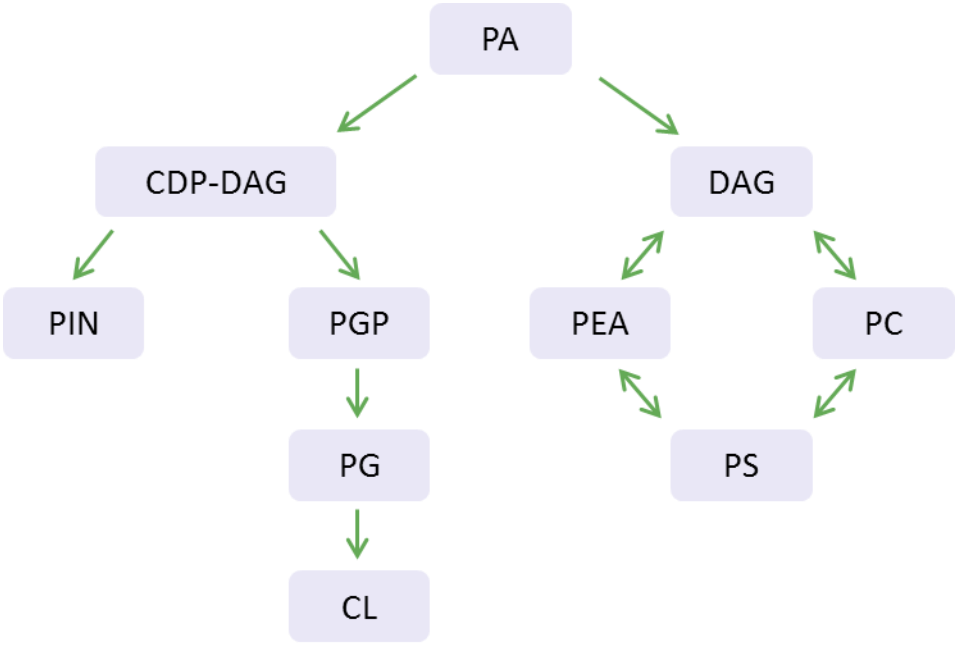

Figure I.19. Pathways of glycerophospholipid biosynthesis in mammalian cells. Phosphatidic acid (PA), diacylglycerol (DAG), phosphatidylethanolamine (PEA), phosphatidylcholine (PC), phosphatidylserine (PS), cytidine diphosphate (CDP)-DAG, phosphatidylinositol (PIN), phosphatidylglycerol phosphate (PGP), phosphatidylglycerol (PG), and cardiolipin (CL). Adapted from Hermansson et al. 2011.

Due to the wide range of different alkyl chain combinations, each GPL class consists of many structurally different molecular species. The meaning of such diversity remains to be fully elucidated, but it may relate to the multiple functions of GPLs, such as signal transduction, vesicle trafficking and membrane fluidity (Hermansson et al. 2011, Hishikawa et al. 2014).

The presence of PHBs is especially crucial for CL and PEA homeostasis (Osman et al. 2009a, Richter-Dennerlein et al. 2014). It was recently reported that mitochondria from PHBs-downregulated HEK293 cells have impaired CL and PEA content (Richter-Dennerlein et al. 2014). Of note, CL has been linked to the execution of apoptosis. CL was suggested to act as a platform crucial for caspase 8 activation, as well as a docking site for tBID and BAX at the mitochondria. In addition, a portion of cytochrome *c* is bound to CL in the IMM. Consistently, decreased in CL levels or increased oxidation of the unsaturated CL acyl chains led to a reduction of the amount of membrane-bound cytochrome *c*, which facilitates its release to the cytosol (Schug and Gottlieb 2009, Raemy and Martinou 2014).

3.2.3. PROHIBITINS AND CANCER

The role of PHBs in cancer has been extensively debated, as evidences of both pro- and anti-tumorigenic roles of PHBs have been described (Theiss and Sitaraman 2011, Thuaud et al. 2013). Low levels of PHBs were associated with enhanced tumor growth in prostate and gastric cancer, glioma and hepatocellular carcinoma (Liu et al. 2009, Ko et al. 2010, Fletcher et al. 2012, Dart et al. 2012, Qian et al. 2013). In some cancer cells, PHB1 localizes in the nucleus and regulates the activity of various transcription factors. Specifically, PHB1 interacts with p53 to increase its activity in breast and prostate cell lines (Fusaro et al. 2003, Chander et al. 2010). It was also reported that PHB1 represses the activity of E2F transcription factors by recruiting the Retinoblastoma protein and chromatin-remodeling molecules, leading to cell cycle arrest (Wang et al. 1999a, 1999b, 2002, Fusaro et al. 2002). In addition, PHBs reduce tumor growth by inhibiting the activity of androgen and estrogen receptors (Gamble et al. 2007, He et al. 2008, Kim et al. 2009, Dart et al. 2012).

On the contrary, there is a growing body of evidences supporting a pro-tumorigenic role of PHBs in cancer growth and development. Of note, PHB1 localizes in lipid rafts in the plasma membrane and allows the activation of c-Raf by Ras to finally activate the MEK-ERK signaling pathway (Rajalingam et al. 2005), which requires the phosphorylation of PHB1 by AKT (Chiu et al. 2013). The ERK pathway plays a key role in promoting the survival, proliferation and metastasis of a high percentage of human tumors (Balmanno and Cook 2009, Samatar and Poulikakos 2014). Furthermore, high levels of PHB1 were increased in various tumor cells, likely due to the presence of a c-Myc regulatory element in the PHB promoter (Mishra et al. 2005, Theiss and Sitaraman 2011). PHBs mediate cell proliferation and anchorage-independent growth in several cancer cell lines (Sievers et al. 2010), strongly suggesting a potential role of PHBs in cancer progression. In chemoresistant ovarian cancer cells, PHB1 expression correlated with drug-resistance, and downregulation of PHBs increased the

sensitivity towards apoptotic stimuli in ovarian cancer cell lines (Gregory-Bass et al. 2008, Patel et al. 2010). PHBs were reported to play a pro-survival role, not only against apoptosis but also towards other insults, such as oxidative stress or inflammatory responses (Theiss and Sitaraman 2011, Thuaud et al. 2013). This cytoprotective function provides support for a pro-tumorigenic role of PHBs.

3.2.4. PROHIBITINS AS POTENTIAL THERAPEUTIC TARGETS FOR CANCER TREATMENT

There are several drugs with anti-cancer effects that involve PHBs (reviwed in Thuaud et al. 2013). First, it was described that capsaicin, an active component of chili peppers, binds to PHB2 to induce cytochrome *c* release from mitochondria (Kuramori et al. 2009). Second, the marine depsipeptide aurilide, obtained from the sea hare *Dolabella auricularia*, was shown to selectively bind to PHB1 in mitochondria, leading to rapid mitochondrial fragmentation and the induction of apoptosis (Sato et al. 2011). Third, Rocaglamide-A (Roc-A), a member of the flavaglines class of compounds, binds to both PHB1 and PHB2 at the cell membrane to inhibit Raf activation and Raf-MEK-ERK-mediated cell cycle progression and cell proliferation in tumor cell lines, without inducing mitochondrial fragmentation (Polier et al. 2012). Interestingly, Roc-A and other related flavaglines have pro-apoptotic activities both *in vitro* and *in vivo* in various cancer cells, yet it remains unknown whether PHBs are involved in their mechanism of apoptosis induction (Ribeiro et al. 2012, Thuaud et al. 2013). Next, it was recently shown that the natural compound xanthohumol blocks the estradiol-induced growth of breast cancer cells by disrupting BIG3-PHB2 interaction, thus allowing PHB2 to repress estrogen receptor transcriptional activity (Yoshimaru et al. 2014). The complexity of the synthesis or availability of these compounds may hinder their use in therapeutics. In contrast, fluorizoline synthesis is practical, versatile, short and reproducible, being amenable to gram-scale batches (Pérez-Perarnau et al. 2014).

All in all, the implication of PHBs in cell proliferation and cancer, together with the evidence that its function can be modulated, strongly suggest that targeting PHBs would be a useful therapeutic approach for treatment of various diseases, including cancer. Consequently, the PHBs-binding compound fluorizoline emerged as a very interesting pro-apoptotic agent and we were encouraged to further study its mechanism of action.

OBJECTIVES

The main objective of the doctoral thesis has been the analysis of new pro-apoptotic compounds that trigger the apoptotic signaling pathway independently of p53 in cancer cells. We aimed to further dissect the mechanism of apoptosis induction in order to provide novel targets that would facilitate the development of therapeutic strategies for cancer treatment and drug discovery.

The main objective has been divided into the following specific points:

1. Study of the pro-apoptotic effects of AICAR.
    a. Characterization of AICAR-induced apoptosis in mouse embryonic fibroblasts.
    b. Analysis of putative mechanisms of apoptosis induction by AICAR in chronic lymphocytic leukemia cells.

2. Characterization of fluorizoline-induced apoptosis.
    a. Study of the requirement of prohibitins for the pro-apoptotic effects of fluorizoline.
    b. Analysis of the apoptotic pathway triggered by fluorizoline treatment.

RESULTS

1. Study of the pro-apoptotic effects of AICAR

1.1. AICAR INDUCES APOPTOSIS IN A ZMP-DEPENDENT BUT AMPK-INDEPENDENT MANNER IN MOUSE EMBRYONIC FIBROBLASTS

One of the main objectives of this thesis has been the characterization of the mechanism of apoptosis induction by AICAR, a nucleoside analogue that induces apoptosis in chronic lymphocytic leukemia (CLL) cells. These primary cells are difficult to transfect, and thus it was necessary to find an alternative model to further study AICAR mechanism of action. Dr. González Gironès started to work with mouse embryonic fibroblasts (MEFs), being a useful model due to the possibility of obtaining knockout cell lines. First, it was necessary to validate MEFs as a suitable model for the study of AICAR-induced apoptosis. In other words, AICAR mechanism of action should be similar in both models. In CLL cells, AICAR is taken up into the cells through nitrobenzylthioinosine (NBTI)-sensitive transporters, and is further phosphorylated to ZMP by adenosine kinase. Both steps are required for AICAR-induced apoptosis and modulation of the apoptosis-related gene expression profile in CLL cells (Campàs et al. 2003, Santidrián et al. 2010).

In MEFs, AICAR entrance to the cell was necessary to induce apoptosis (González-Gironès 2012). Together with Dr. González Gironès, we studied whether AICAR phosphorylation to ZMP was required for AICAR pro-apoptotic effects in MEFs, as observed in CLL cells. To this end, WT MEFs were pre-incubated with the adenosine kinase inhibitor 5-iodotubercidin and then treated with 1 mM AICAR for 48 hours. AICAR-induced apoptosis was completely blocked by 5-iodotubercidin, indicating that ZMP formation is necessary for AICAR cytotoxic effects in MEFs (Fig. 1.1A). We then analyzed AICAR-mediated changes in the mRNA expression profile of apoptosis-related genes in MEFs by retrotranscriptase multiplex ligation-dependent probe amplification (RT-MLPA). Incubation of WT MEFs with 1 mM AICAR for 24 h increased *Noxa* and *Apaf* mRNA levels, and decreased *Bcl-2* and S*urvivin* mRNA levels, correlating with the apoptotic outcome. We also observed significant downregulation of *Moap1*, *Bok* and *Htra2* mRNA levels, as well as an increase in *Hiap1* mRNA levels (Fig. 1.1B). Interestingly, all these changes were ZMP-dependent as they were suppressed with 5-iodotubercidin pretreatment.

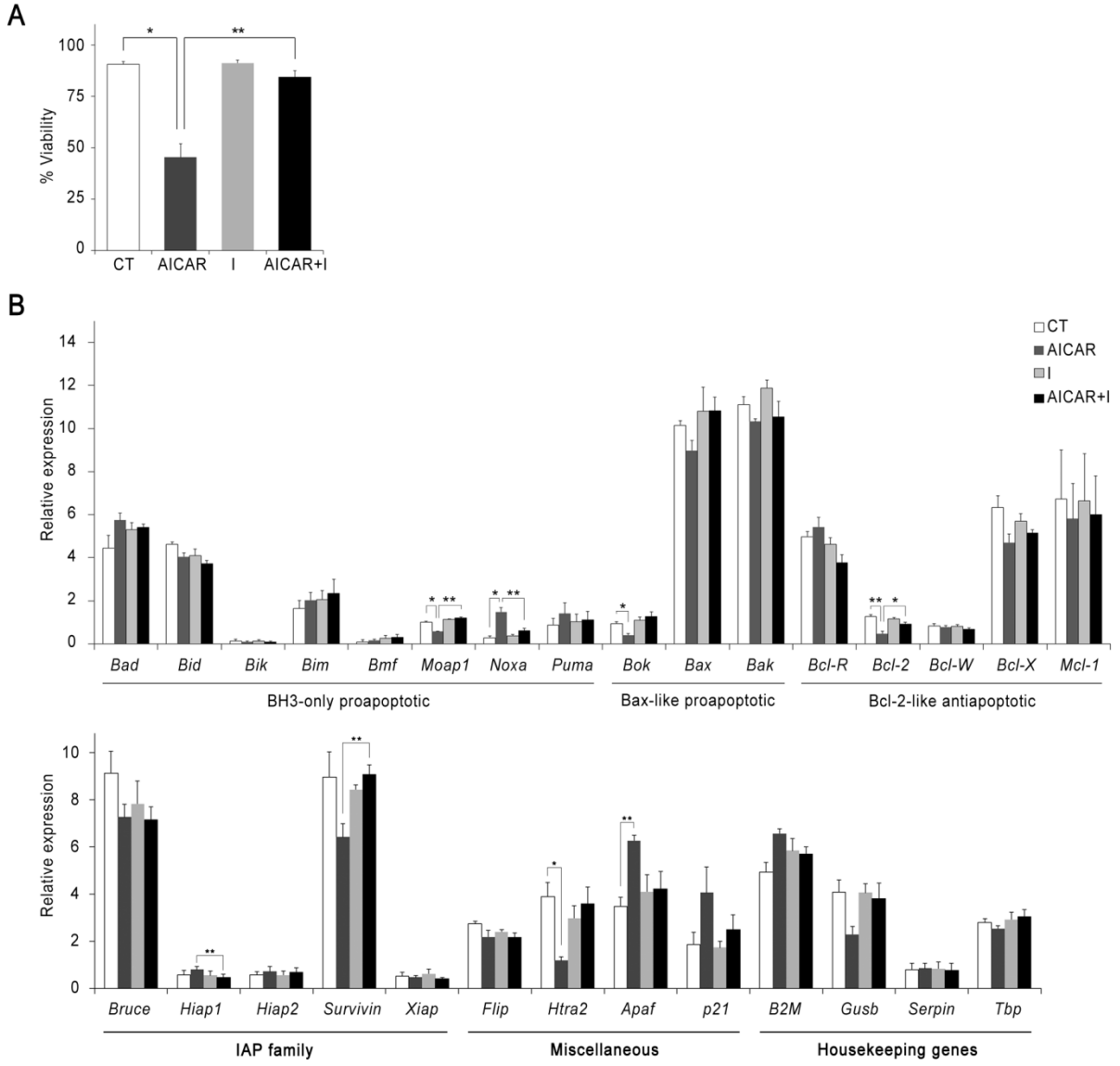

Figure 1.1. AICAR-induced apoptosis and modulations of apoptosis-related genes require phosphorylation to ZMP. WT MEFs were untreated (CT) or pretreated with 0.2 μM 5-iodotubercidin (I) for 30 min and then incubated with 1 mM AICAR for 24 h and 48h. **(A)** Viability was measured after 48h of treatment with 1mM AICAR by flow cytometry and it is expressed as the percentage of non-apoptotic cells (annexin V-/PI-negative). **(B)** mRNA levels of apoptosis-related genes were analyzed by RT-MLPA upon 24 h of treatment with 1 mM AICAR. Data are shown as mean ± SEM (n=3, including data obtained by Dr. González Gironès). *$p < 0.05$, **$p < 0.01$.

AICAR has been widely used as an AMPK activator, as ZMP mimics AMP activating effects on AMPK (Corton et al. 1995, Suter et al. 2006). Nevertheless, there are many reports showing AMPK-independent effects of AICAR (Martelli et al. 2012). In this line, direct activation of AMPK in CLL cells did not induce apoptosis, and mouse lymphocytes lacking *Ampkα* underwent apoptosis following AICAR treatment (Santidrián et al. 2010). Accordingly, Dr. González Gironès had previously shown that AICAR could effectively induce apoptosis in MEFs lacking the two catalytic

subunits of AMPK, α1 and α2 *(Ampk*α DKO MEFs). In fact, *Ampk*α DKO MEFs were more sensitive than WT MEFs, suggesting a pro-survival role of AMPK in MEFs (González-Gironès 2012). Thus, we sought to analyze whether AICAR-induced modulations in apoptosis-related gene expression profile in MEFs were mediated by AMPKα. *Ampk*α DKO MEFs and their corresponding WT MEFs were treated with 2 mM AICAR for 24 h and cell viability was assessed as a control of AICAR treatment. In agreement with previous results, WT MEFs did not undergo apoptosis upon treatment with AICAR at 24 h. In contrast, lack of AMPKα sensitized cells to AICAR treatment, proving that AICAR does not require AMPKα for apoptosis induction (Fig. 1.2A). Next, we analyzed the relative expression of apoptosis-related genes by RT-MLPA. AICAR induced the upregulation of *Noxa*, *Hiap1* and *Apaf* as well as the downregulation of *Bcl-2* mRNA levels in both WT and *Ampk*α DKO MEFs (Fig. 1.2B). These results demonstrate that AICAR induces mRNA modulations of these apoptosis-related genes in an AMPK-independent manner.

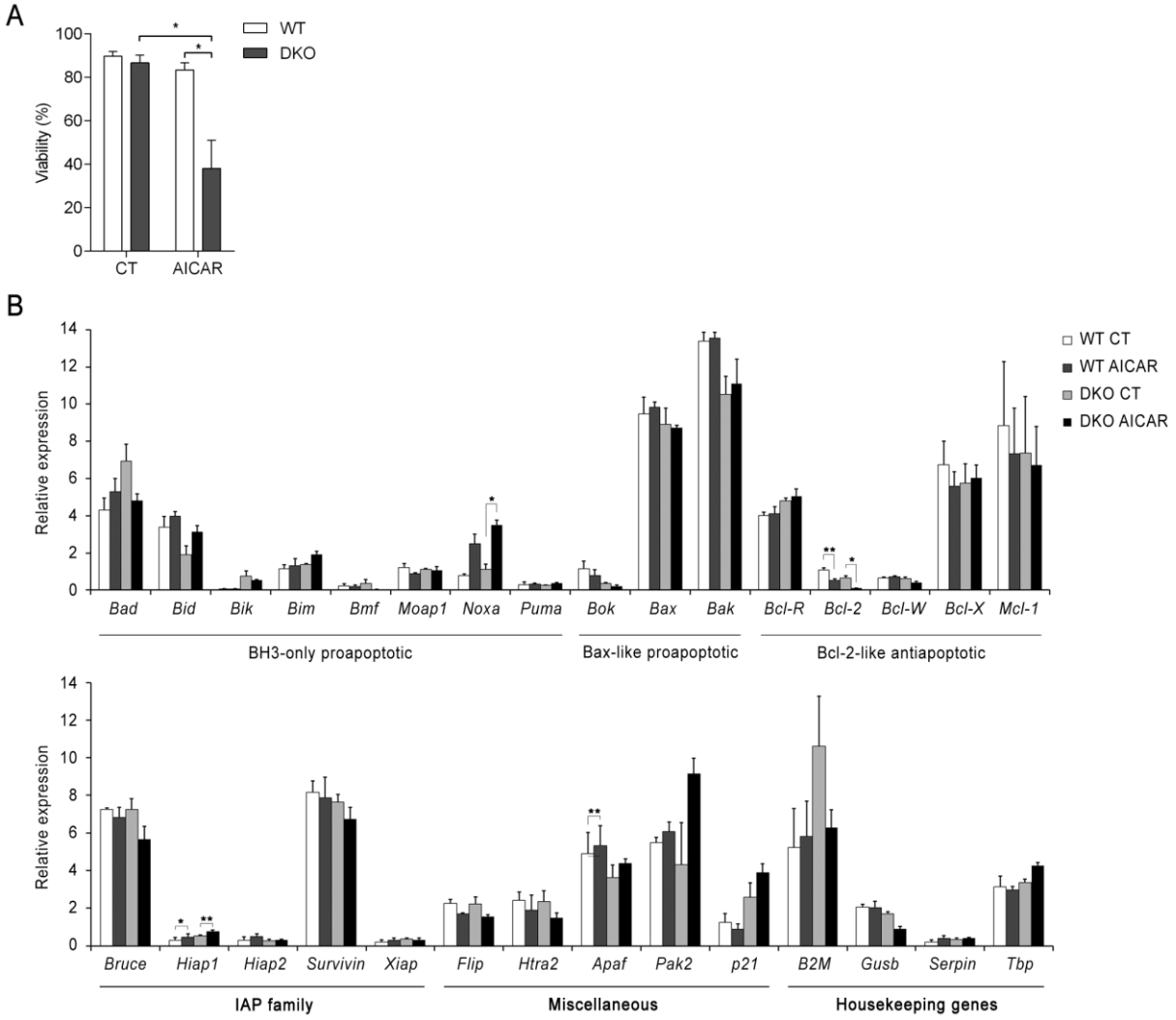

Figure 1.2. AICAR induces apoptosis and changes in the apoptosis-related gene expression profile in an AMPK-independent manner. WT and *Ampkα1*$^{-/-}$/*Ampkα2*$^{-/-}$ (DKO) MEFs were untreated (CT) or treated with 2 mM AICAR for 24 h. **(A)** Viability was measured by flow cytometry and it is expressed as the percentage of non-

apoptotic cells (annexin V-/PI-negative). **(B)** Cells were lysed and then mRNA levels of apoptosis-related genes were analyzed by RT-MLPA as described in "Patients, materials and methods". Data are shown as mean ± SEM (in A, n=5; in B, n=3 including data obtained by Dr. González Gironès). *p < 0.05, **p < 0.01.

To further prove that AICAR was inducing apoptosis independently of AMPK, we assessed whether direct activation AMPK could trigger apoptosis in MEFs. AICAR triggered efficient apoptosis, while the direct AMPK activator A-769662 failed to induce apoptosis in WT MEFs (Fig. 1.3A). In contrast, both AICAR and A-769662 induced phosphorylation of AMPKα and its substrate acetyl-CoA carboxylase (ACC), which indicates activation of AMPK (Fig. 1.3B). These results show that AICAR-mediated apoptosis does not require AMPK activation.

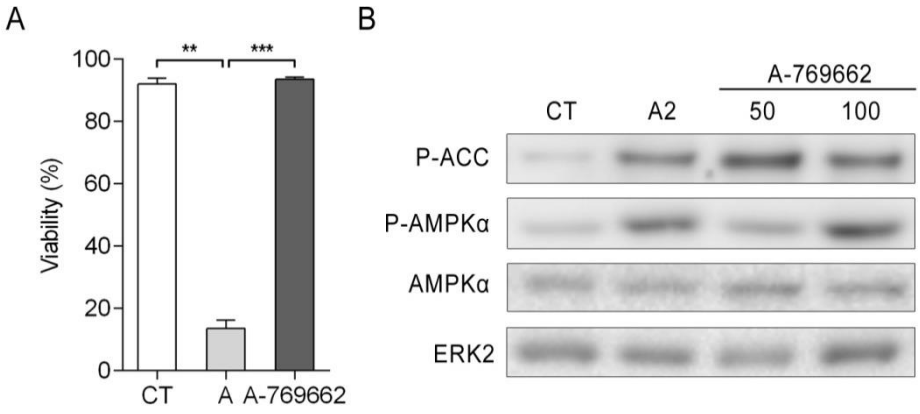

Figure 1.3. Direct activation of AMPK does not induce apoptosis in WT MEFs. (A) WT MEFs were untreated (CT) or treated with either 2 mM AICAR (A) or 50 μM of the direct AMPK activator A-769662 for 48 h. Viability was measured by flow cytometry and it is expressed as the mean ± SEM (n=3) of the percentage of non-apoptotic cells (annexin V-/PI-negative). ** p < 0.01, ***p < 0.001. **(B)** WT MEFs were untreated (CT) or treated with either 2 mM AICAR (A2) or 50 or 100 μM A-769662 for 24 hours. Protein levels of phospho-acetyl-CoA carboxylase at Serine 79 (P-ACC), phospho-AMPKα at Threonine 172 (P-AMPKα), and total AMPKα were analyzed by western blot. ERK2 was used to standardize protein levels.

1.2. STUDY OF THE BCL-2 FAMILY MEMBERS INVOLVED IN AICAR-INDUCED APOPTOSIS IN MEFs

Our group reported that BIM, NOXA and PUMA are involved in AICAR-induced apoptosis in CLL cells (Santidrián et al. 2010). However, RT-MLPA analysis of AICAR treatment in MEFs showed no significant changes on *Bim* and *Puma* expression levels (Fig. 1.1B). We further characterized the modulation of these genes upon different times of AICAR treatment by real time quantitative PCR (RT-qPCR). As a control, we included *Noxa* and *Bcl-2*, which are significantly modulated upon AICAR treatment. MEFs were incubated for 3, 6, 9, 12 and 24 h with AICAR and mRNA levels were analyzed. *Bim* mRNA levels were significantly increased from 6 h until 24 h of AICAR treatment, while *Puma* mRNA levels were only induced after 24 h of AICAR treatment. As expected, AICAR treatment significantly induced increases in *Noxa* and downregulation of *Bcl-2* mRNA levels (Fig. 1.4).

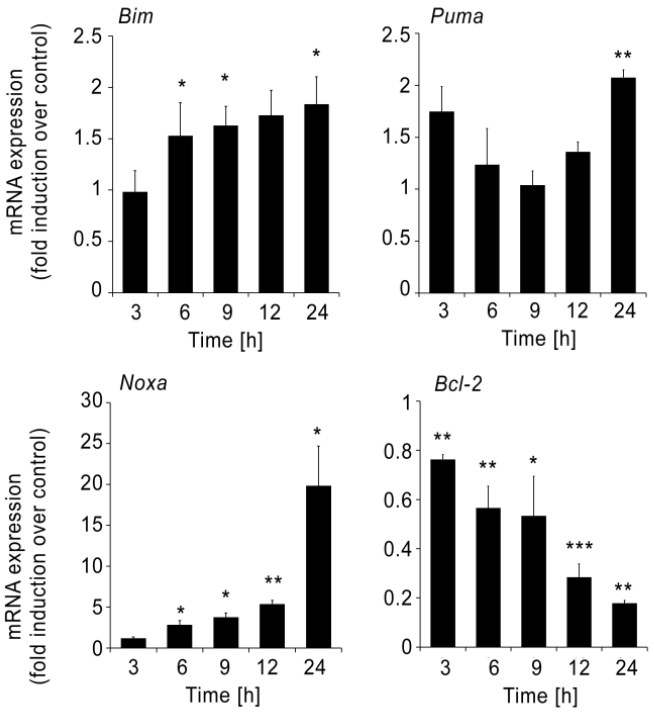

Figure 1.4. AICAR modulates *Bim*, *Puma*, *Noxa* and *Bcl-2* mRNA levels in WT MEFs. WT MEFs were untreated or treated with 2 mM AICAR for 3, 6, 9, 12 and 24 h. *Bim*, *Puma*, *Noxa* and *Bcl-2* mRNA levels were measured by RT-qPCR. The mRNA levels of all genes were normalized to those of *Gapdh* and referenced to the untreated cells of the corresponding time. Data are shown as mean ± SEM (n=3). *p < 0.05, **p < 0.01, ***p < 0.001 AICAR-treated *versus* untreated MEFs.

Next, we analyzed whether the modulation of these genes at the transcriptional level could lead to changes on the corresponding protein levels. NOXA and PUMA protein levels could not be analyzed due to lack of proper antibodies detecting the mouse protein in MEFs. Importantly, we detected significant increases of BIM_{EL} and BIM_{L} protein levels upon 24 h of AICAR treatment (Fig. 1.5A-B).

AICAR did not significantly modulate BCL-2 protein levels despite the reduction on *Bcl-2* mRNA levels, a finding consistent with the long half-life of this protein (Merino et al. 1994).

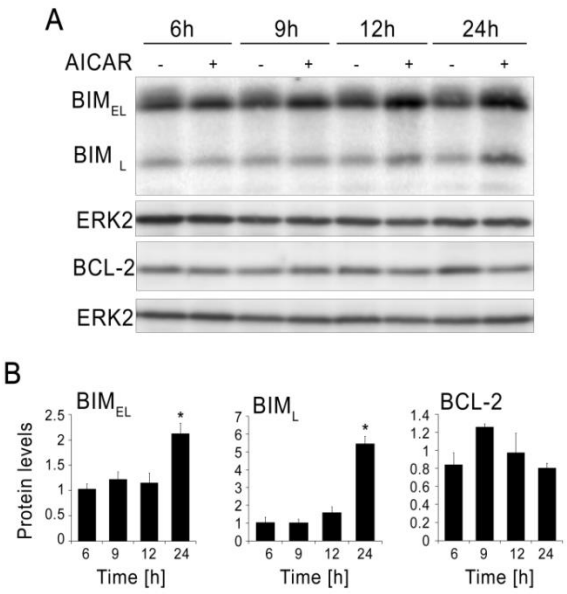

Figure 1.5. AICAR induces BIM protein levels in WT MEFs. WT MEFs were untreated or treated with 2 mM AICAR for 6, 9, 12 and 24 h. **(A)** BIM and BCL-2 protein levels were analyzed by western blot. ERK2 was used to standardize protein levels. This is a representative image of three independent experiments that were performed. **(B)** Protein levels were quantified by densitometry using ImageJ software, normalized to ERK2 protein levels and referenced to untreated cells of the corresponding time. Data are shown as mean ± SEM (n=3). *p < 0.05 AICAR-treated *versus* untreated MEFs.

In order to study the contribution of PUMA in AICAR-induced cell death, we assessed the effect of AICAR treatment in MEFs lacking this BH3-only protein. The loss of *Puma* not only failed to protect MEFs from AICAR-induced apoptosis, but slightly sensitized them (Fig. 1.6).

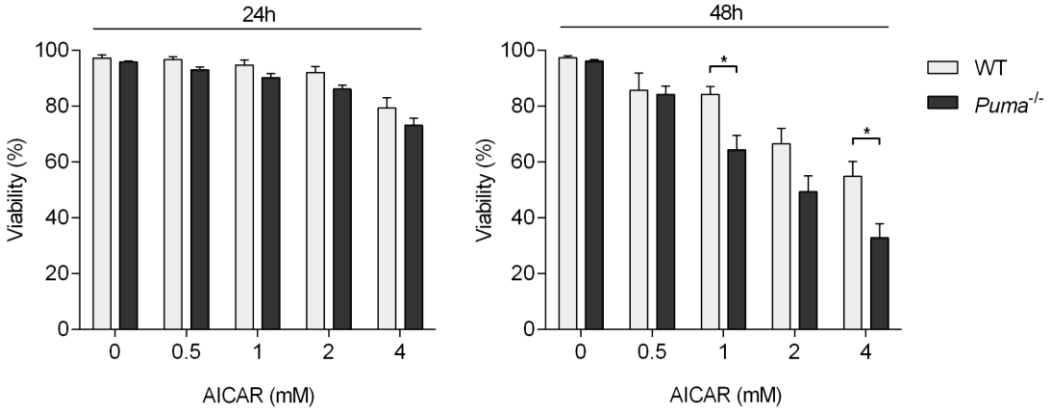

Figure 1.6. Loss of *Puma* does not confer resistance to AICAR-induced apoptosis. WT and *Puma*$^{-/-}$ MEFs were untreated or treated with 0.5, 1, 2 and 4 mM AICAR for 24 and 48 h. Viability was measured by flow cytometry and it is expressed as the mean ± SEM (n=4) of the percentage of non-apoptotic cells (annexin V-/PI-negative). *p < 0.05.

Interestingly, results from our group showed that *Bim*$^{-/-}$/*Noxa*$^{-/-}$ MEFs were highly resistant to AICAR treatment compared to the corresponding WT MEFs (González-Gironès 2012). All together, these data demonstrate that both BIM and NOXA, but not PUMA, are key players in AICAR-induced apoptosis in MEFs.

1.3. ROLE OF p53 IN AICAR-INDUCED APOPTOSIS IN MEFs

p53 was proposed to mediate the anti-proliferative effects of AICAR (Jones et al. 2005, Tang et al. 2011). In order to analyze its role in MEFs, we decided to use *p53*$^{-/-}$ MEFs and compare their response to WT MEFs. In these experiments, we treated MEFs with a wider range of doses of AICAR than we usually did. Strikingly, we observed that 0.15 and 0.25 mM AICAR were inducing high rates of apoptosis in WT MEFs, while 0.5 mM AICAR triggered apoptosis to a lesser extent. From 0.5 mM AICAR and on, apoptosis was induced in a dose-dependent manner. Of note, the induction of apoptosis upon treatment with low doses of AICAR seemed to be p53 dependent, as *p53*$^{-/-}$ MEFs were undergoing apoptosis just with doses higher than 0.5 mM AICAR. In contrast, higher doses of AICAR were able to induce apoptosis in a p53-independent manner, because WT and *p53*$^{-/-}$ MEFs underwent apoptosis alike (Fig. 1.7).

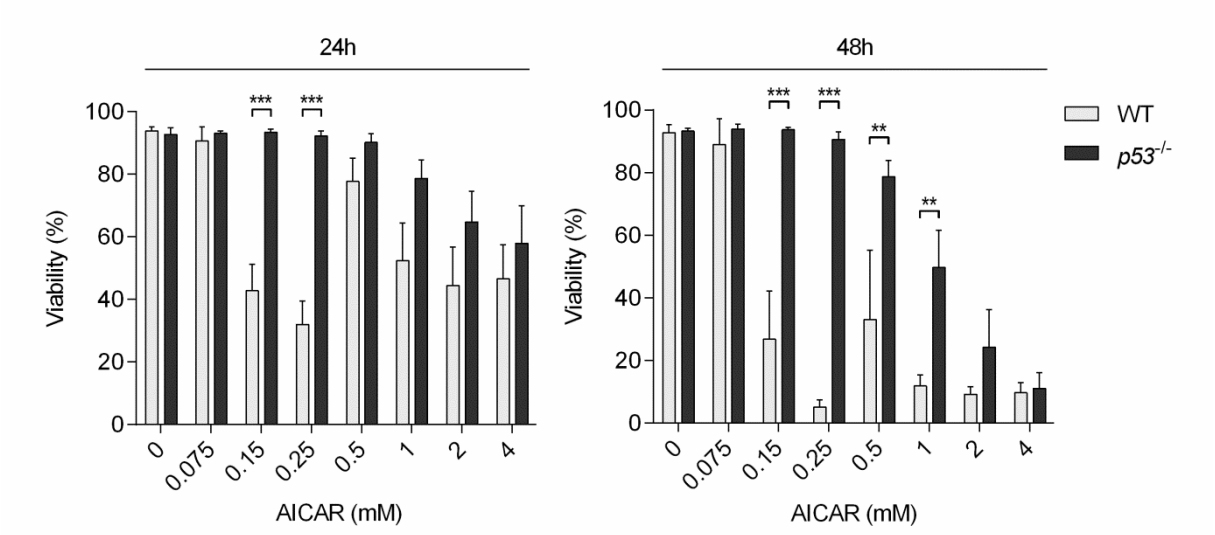

Figure 1.7. Role of p53 in AICAR-induced apoptosis. WT and *p53*$^{-/-}$ MEFs were untreated or treated with increasing doses of AICAR for 24 and 48 h. Viability was measured by flow cytometry and it is expressed as the mean ± SEM (n=4) of the percentage of non-apoptotic cells (annexin V-/PI-negative). **p < 0.01, ***p < 0.001.

In view of such peculiar results, we sought to analyze how other WT MEFs would respond to low doses of AICAR in order to discard clone specific behaviors. We used four different WT MEFs that we had in the laboratory:

A) WT MEFs from Dr. Korsmeyer's laboratory, provided by Dr. Jacint Boix (Universitat de Lleida).
B) WT MEFs from Dr. Korsmeyer's laboratory, provided by Dr. Cristina Muñoz (IDIBELL).
C) WT MEFs from Dr. Villunger (Medical University Innsbruck).
D) WT MEFs from Dr. Benoit Viollet's laboratory, provided by Dr. Aramburu (Universitat Pompeu Fabra).

Interestingly, the latter cell line (D) had been immortalized with the C-terminal domain of p53, which inactivates the pathway. Thus, we expected that WT D MEFs would respond as *p53*$^{-/-}$ MEFs. The different MEFs were untreated or treated with increasing doses of AICAR and viability was assessed by flow cytometry. Although A, B and C WT MEFs presented different sensitivity to AICAR treatment, the three cell lines displayed the same profile of apoptosis induction: low doses of AICAR had higher pro-apoptotic capacity than 0.5 mM AICAR, and higher doses were again capable of inducing apoptosis. As expected, WT D MEFs and *p53*$^{-/-}$ MEFs underwent apoptosis only after treatment with high doses of AICAR (Fig. 1.8). All together, these results show that low doses of AICAR trigger apoptosis in a p53-dependent manner, though higher doses are able to trigger apoptosis independently of p53.

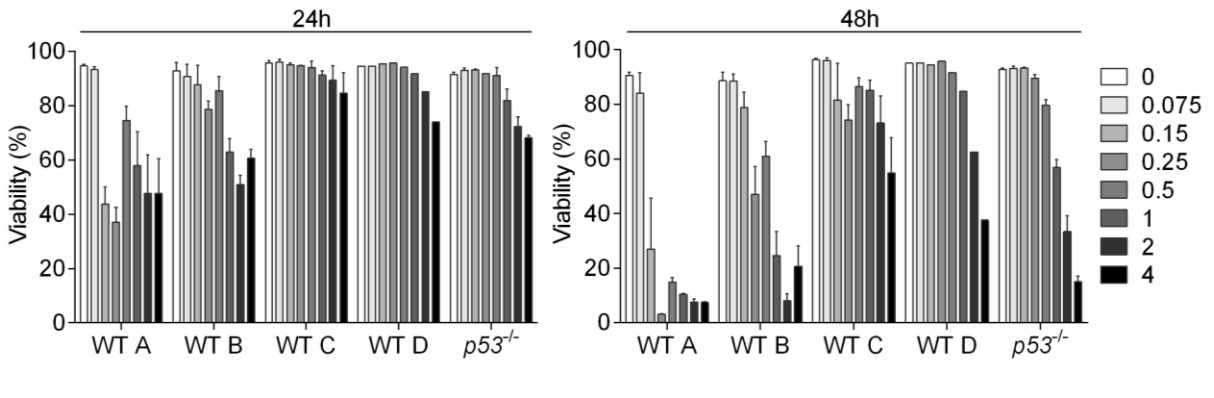

Figure 1.8. Low doses of AICAR induce p53-dependent apoptosis in MEFs. Different WT MEFs (A: WT MEFs from Dr. Korsmeyer's laboratory, provided by Dr. Jacint Boix; B: WT MEFs from Dr. Korsmeyer's laboratory, provided by Dr. Cristina Muñoz; C: WT MEFs from Dr. Villunger; D: WT MEFs from Dr. Viollet's laboratory, provided by Dr. Aramburu), and *p53*$^{-/-}$ MEFs were untreated or treated with increasing doses of AICAR (mM) for 24 and 48 h. Viability was measured by flow cytometry and it is expressed as the percentage of non-apoptotic cells (annexin V-/PI-negative). Data are shown as mean ± SEM (n=2 for WT A, B, C and *p53*$^{-/-}$ MEFs; n=1 for WT D MEFs).

1.4. PYRIMIDINE STARVATION AS A PUTATIVE MECHANISM OF ACTION OF AICAR

In 2013, a manuscript was published proposing a new model for AICAR mechanism of action in multiple myeloma (MM) cells (Bardeleben et al. 2013). AICAR triggered ZMP-dependent but AMPK-independent apoptosis in different MM cell lines. A metabolomics screen revealed that AICAR led to increased purine metabolism and decreased pyrimidine metabolism. Specifically, two intermediates in *de novo* pyrimidine synthesis showed altered levels: orotate was increased while UMP was decreased, suggesting an inhibition of the UMP synthase (UMPS) enzyme (see steps 5 and 6 in Fig. 1.9). AICAR-induced apoptosis was blocked by addition of uridine and cytidine, and thymidine partially did it. The authors proposed that AICAR reduces phosphoribosyl-pyrophosphate (PRPP) levels, one of the substrates of UMPS, resulting in a pyrimidine starvation that finally induces apoptosis in MM cells.

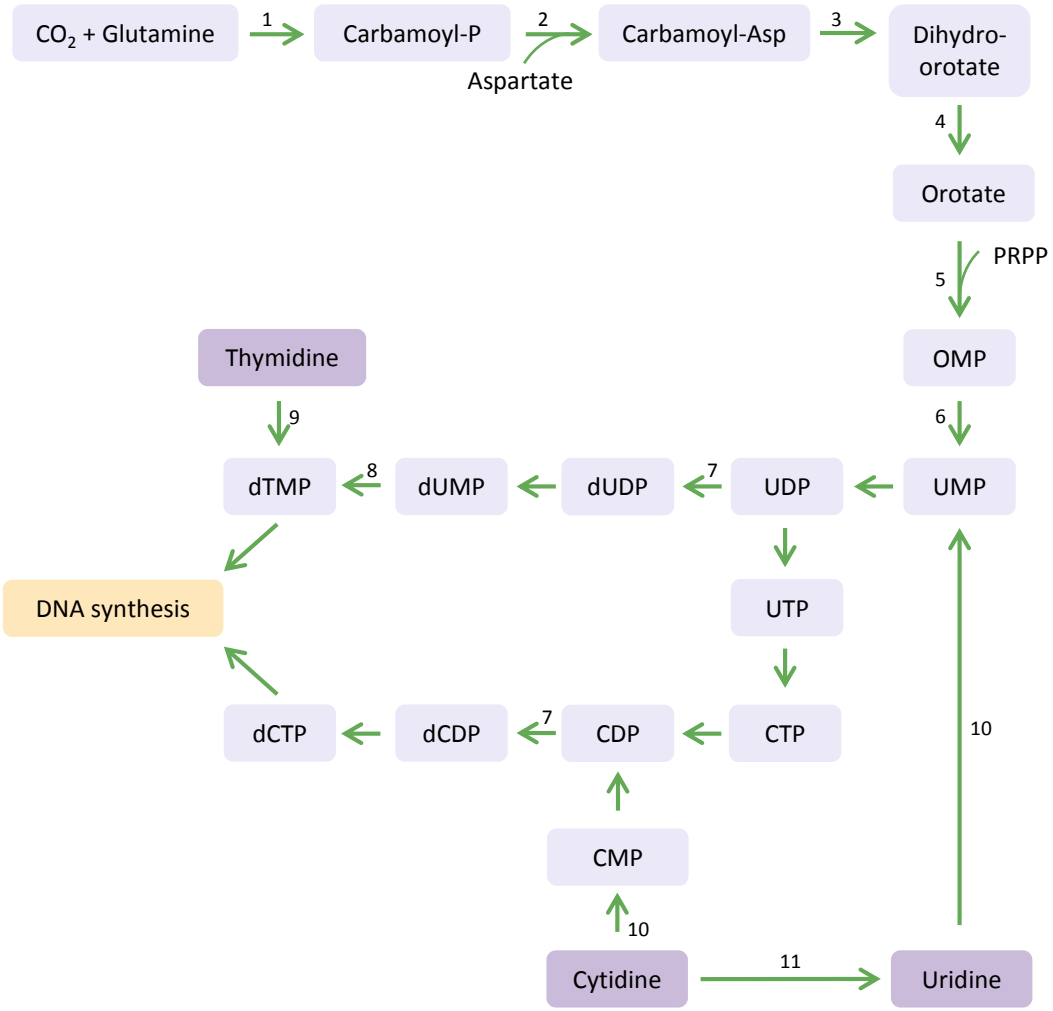

Figure 1.9. Pathways of pyrimidine metabolism. *De novo* pyrimidine synthesis: 1, carbamoylphosphate synthetase II; 2, ATCase; 3, dihydroorotase (1, 2 and 3 comprise CAD); 4, dihydroorotate dehydrogenase; 5, orotate phosphoribosyl-transferase; 6, OMP decarboxylase (5 and 6 comprise UMP synthase); 7, ribonucleotide diphosphate reductase; 8, thymidilate synthase. Pyrimidine salvage: 9, thymidine kinase 1; 10, uridine/cytidine kinase. Pyrimidine

catabolism: 11, cytidine deaminase. Carbamoyl-P, carbamoyl-phosphate; Carbamoyl-Asp, carbamoyl-aspartate; PRPP, phosphoribosyl-pyrophosphate; OMP, orotidine monophosphate; UMP, uridine monophosphate; TMP, thymidine monophosphate; CMP, cytidine monophosphate. Based on Balasubramaniam et al. 2014.

In view of such interesting results, we decided to assess whether addition of pyrimidines could rescue AICAR-induced apoptosis in CLL cells. To this end, CLL cells were co-treated with AICAR and uridine or cytidine for 48 hours and viability was assessed by flow cytometry. Low doses of uridine and cytidine (in the range used in the MM manuscript) could not abolish AICAR pro-apoptotic effects. Interestingly, if uridine concentration was increased 100 times, AICAR-induced apoptosis was effectively inhibited (Fig. 1.10).

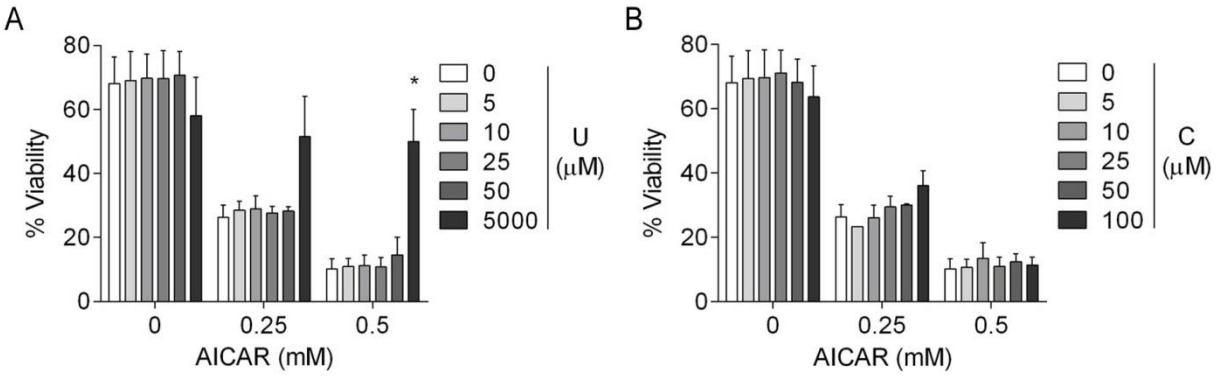

Figure 1.10. Low doses of uridine or cytidine do not block AICAR-induced apoptosis. CLL cells were untreated or treated with 0.25 mM or 0.5 mM AICAR, in the presence or absence of increasing doses of uridine (U) **(A)** and cytidine (C) **(B)** for 48 hours. Viability was measured by flow cytometry and it is expressed as the percentage of non-apoptotic cells. Data are shown as mean ± SEM (0.25 mM AICAR, n=2; 0.5 mM AICAR, n=3). *$p < 0.05$ AICAR-treated *versus* AICAR and uridine-treated cells.

These results suggested that the used doses were too low and thus not enough to block AICAR-induced apoptosis. Therefore, we assessed the viability of CLL cells treated with AICAR in the absence or presence of high doses of uridine and cytidine. In addition, we included a wide range of doses of thymidine, because it was shown that this pyrimidine can partially inhibit AICAR-induced apoptosis in MM cells (Bardeleben et al. 2013). Interestingly, uridine and thymidine inhibited AICAR-induced apoptosis in a dose-dependent manner in CLL cells (Fig. 1.11A, C, D). In contrast, high doses of cytidine were inducing apoptosis by themselves, even enhancing AICAR-induced apoptosis in some conditions (Fig. 1.11B).

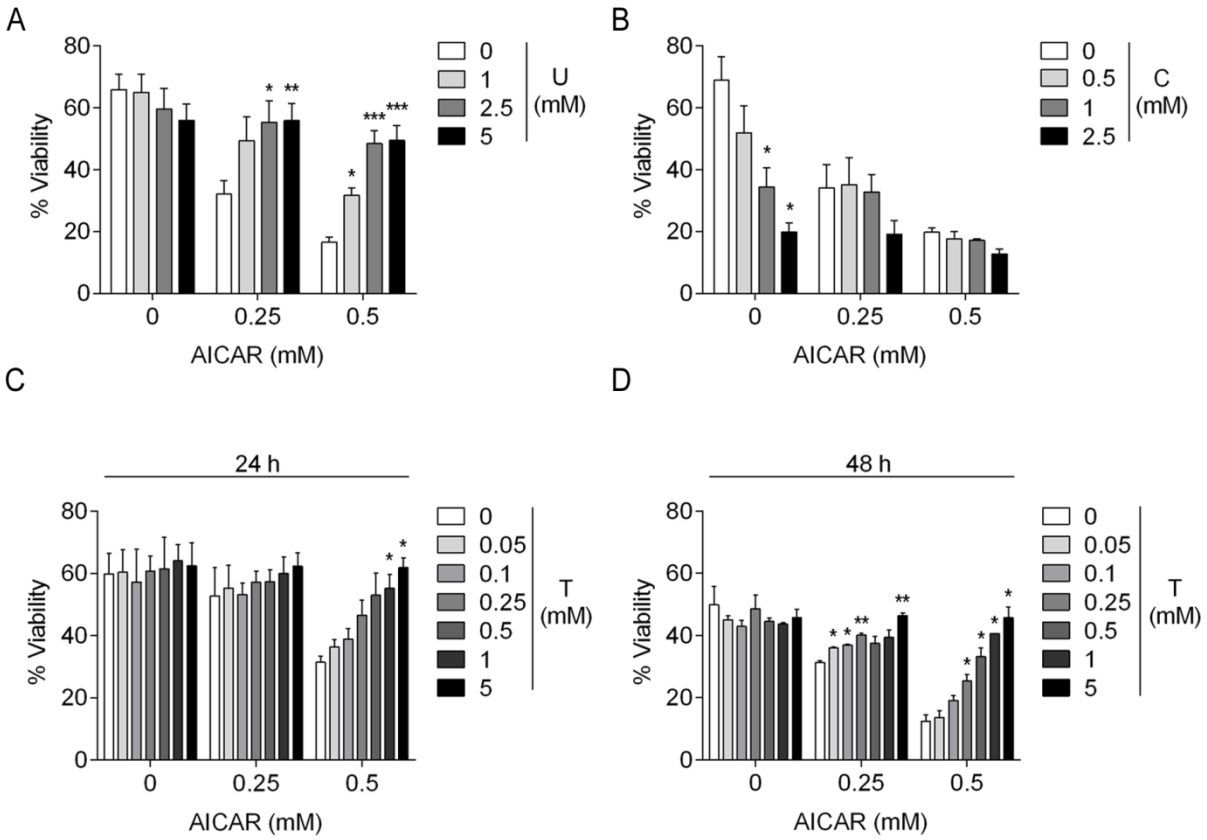

Figure 1.11. High doses of uridine or thymidine, but not cytidine, block AICAR-induced apoptosis. CLL cells were untreated or treated with 0.25 mM or 0.5 mM AICAR, in the presence or absence of increasing doses of uridine (U) **(A)** or cytidine (C) **(B)** for 48 hours; or thymidine (T) for 24 **(C)** and 48 hours **(D)**. Viability was measured by flow cytometry and it is expressed as the percentage of non-apoptotic cells (annexin V-/PI-negative). Data are shown as mean ± SEM (for uridine, 0.25 mM AICAR, n≥5; 0.5 mM AICAR, n≥3. For cytidine, 0.25 mM AICAR, n=4; 0.5 mM AICAR, n=2. For thymidine, n=2). *p < 0.05, **p < 0.01, ***p < 0.001 AICAR-treated *versus* AICAR and pyrimidine-treated cells.

These data show many differences in the inhibition of AICAR-induced apoptosis mediated by addition of pyrimidines in CLL cells compared to MM cells. Apart from the used doses, cytidine was able to block AICAR-induced apoptosis in MM cells (Bardeleben et al. 2013) but not in CLL cells. In addition, thymidine could only partially abolish AICAR-induced apoptosis in MM cells (Bardeleben et al. 2013) but efficiently blocked it in CLL cells. It is conceivable that AICAR mechanism of action is different in these two cell types. Nonetheless, as we were using experimental methods that differed from the ones used in the aforementioned report, we decided to use the MM cell line RPMI 8226, one of the cell lines that were studied by Bardeleben and collegues, as a control for our experiments. They measured active caspase 3 by flow cytometry and observed around 40% of caspase 3 positive cells after 48 hours of treatment with 0.25 mM AICAR in RPMI 8226 cells (Bardeleben et al. 2013). Strikingly, in our hands RPMI 8226 cells were much more resistant to AICAR as measured by

phoshpatidylserine (PS) exposure (Fig. 1.12). Treatment with 0.25 mM AICAR reduced the mean viability from 93% to 80%.

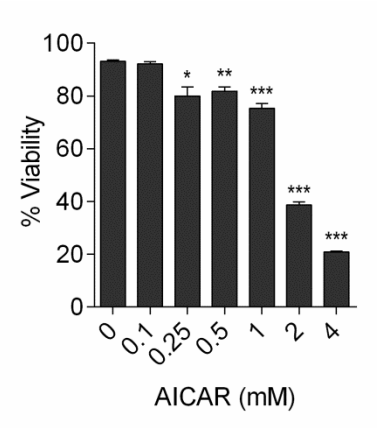

Figure 1.12. Dose-response of AICAR in RPMI 8226 cells. RPMI 8226 cells were treated with different doses of AICAR for 48 hours. Viability was measured by flow cytometry and it is expressed as the mean ± SEM (n=3) of the percentage of non-apoptotic cells (annexin V-/PI-negative). *p < 0.05, **p < 0.01, ***p < 0.001 treated *versus* untreated cells.

We next analyzed the rescue of AICAR-induced apoptosis by pyrimidine addition in RPMI 8226 cells. Incubation with different doses of uridine could block the small reduction in viability induced by treatment with 0.25 mM AICAR (Fig. 1.13A), in agreement with the results previously reported (Bardeleben et al. 2013). Nevertheless, uridine could not revert the effects of higher doses of AICAR, in which higher rates of apoptosis were observed. In fact, uridine increased the pro-apoptotic effects of treatment with 2 mM AICAR, which were absent in the treatment with uridine alone. Of note, the doses of uridine that were used in these experiments were much higher than the ones reported in the paper (0.5 to 5 *versus* 0.05 and 0.1 mM). Thus, the incapacity to inhibit apoptosis cannot be attributed to a limited amount of uridine.

In the MM cells report, low doses of cytidine could prevent AICAR-induced apoptosis, yet higher doses increased AICAR-induced apoptosis despite not being cytotoxic on their own. In our hands, none of the used doses of cytidine were capable of inhibiting AICAR-induced apoptosis. In fact, addition of cytidine enhanced the pro-apoptotic effects observed after treatment with 2 mM AICAR despite not being cytotoxic on their own (Fig. 1.13B).

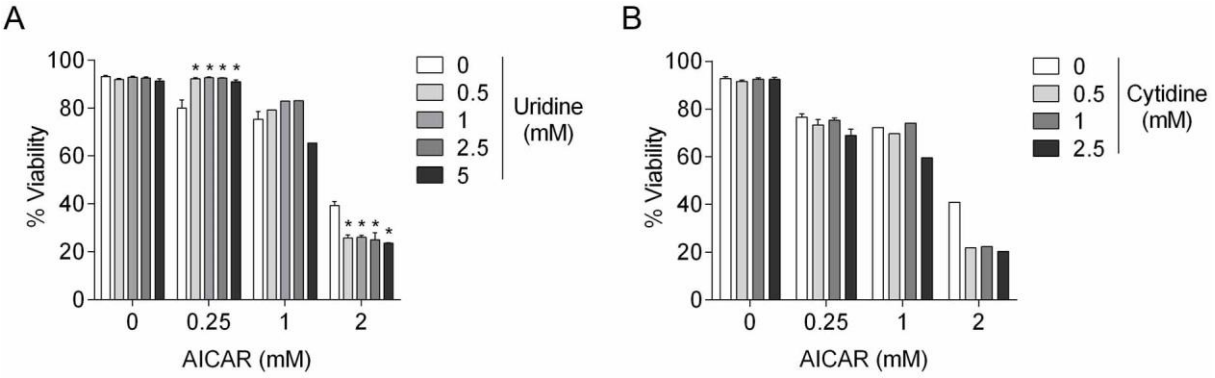

Figure 1.13. Viability assay after treatment with AICAR and uridine or cytidine in RPMI 8226 cells. RPMI 8226 cells were treated with different concentrations of AICAR in the presence or absence of uridine **(A)** or cytidine **(B)** for 48 hours. Viability was measured by flow cytometry and it is expressed as the percentage of non-apoptotic cells (annexin V-/PI-negative). Data are shown as mean ± SEM (for uridine, 0 and 0.25 mM AICAR, n=3; 1 mM AICAR, n=1; 2 mM AICAR, n=2. For cytidine, 0 and 0.25 mM AICAR, n=2; 1 and 2 mM AICAR, n=1), *$p < 0.05$ AICAR-treated *versus* AICAR and uridine-treated cells.

Despite the lack of consistency between the results in RPMI 8226 obtained by Bardeleben and us, the fact that high doses of uridine and thymidine could block AICAR-induced apoptosis in CLL cells encouraged us to further study the involvement of pyrimidines.

Nucleosides uptake into the cell is mediated by the nucleosides transporter (NT) proteins. There are two main NTs families: concentrative NT (CNT) and equilibrative NT (ENT). The former comprises hCNT1, hCNT2 and hCNT3 proteins, that exert their function in a Na^+ coupled manner. The latter includes hENT1 and hENT2 proteins, which mediate the transport depending on the relative substrate concentrations across the membrane. hENT1 and hENT2 can be distinguished according to their sensitivity to inhibition by NBTI, being hENT1 much more sensitive than hENT2 (Pastor-Anglada et al. 2004, Fernández-Calotti et al. 2011, Young et al. 2013, Pastor-Anglada and Pérez-Torras 2015). AICAR is a nucleoside analogue that is taken up into cells by NBTI-sensitive transporters (Campàs et al. 2003). Considering that AICAR and other nucleosides share the transporters that mediate their entrance to the cell, it is conceivable that the addition of nucleosides may impair AICAR influx. Indeed, previous results from our group showed that adenosine protected CLL cells from AICAR-induced apoptosis by blocking AICAR entrance to the cell (Campàs et al. 2003). To test whether uridine and thymidine were acting likewise, we assessed phosphorylation of ACC, an indicator of AICAR entrance, in CLL cells treated with a combination of AICAR and uridine or thymidine. As a control, viability was measured by flow cytometry in each experiment. AICAR efficiently induced apoptosis in CLL cells, which was abrogated by treatment with uridine or thymidine (Fig. 1.14).

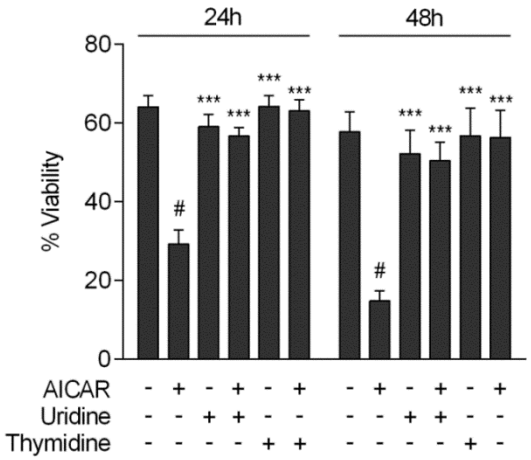

Figure 1.14. Uridine and thymidine block AICAR-induced apoptosis. CLL cells from 9 patients were untreated or treated with 0.5 mM AICAR in the absence or presence of 5 mM uridine or thymidine for 24 and 48 hours. Viability was measured by flow cytometry and it is expressed as the mean ± SEM (n=9) of the percentage of non-apoptotic cells (annexin V-/PI-negative). # $p < 0.05$ untreated *versus* AICAR-treated cells. ***$p < 0.001$ pyrimidine-treated *versus* AICAR-treated cells.

Samples from 3 different CLL patients were analyzed after 2, 4, 6, 9, 16, 20 and 24 hours of treatment with AICAR in combination with uridine or thymidine. A complete time course could not be performed with all the samples due to reduced available number of cells in the CLL samples. Figure 1.15 summarizes the different experiments that were performed and the results obtained.

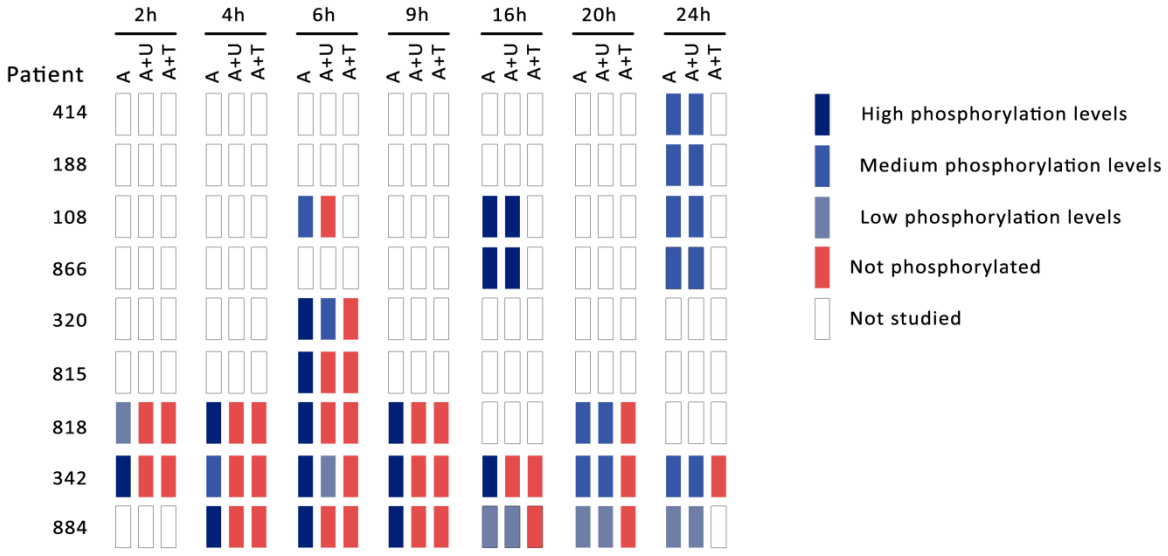

Figure 1.15. Summary of the western blot analyses of ACC phosphorylation performed in different samples of CLL patients. CLL cells were untreated or treated with 0.5 mM AICAR (A) in the absence or presence of 5 mM uridine (U) or thymidine (T). ACC phosphorylation was assessed by western blot at different time points.

Figure 1.16 shows one of the time course experiments with one sample of a CLL patient.

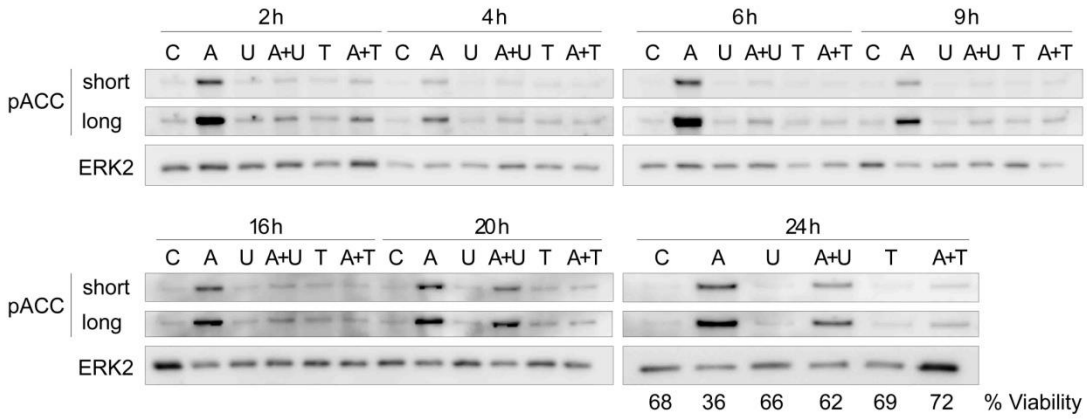

Figure 1.16. Western blot analysis of ACC phosphorylation in a sample of a CLL patient. CLL cells were untreated (C) or treated with 0.5 mM AICAR (A), in the absence or presence of 5 mM uridine (U) or 5 mM thymidine (T) for different times. Viability was measured after 24 h of treatment by flow cytometry and it is expressed as the percentage of non-apoptotic cells. This is one representative patient of three that were analyzed (see figure 1.15 with the list of patients analyzed).

The initial time point and the intensity of ACC phosphorylation varied among the analyzed CLL patients. Nevertheless, we observed a general tendency: AICAR induced early and strong ACC phosphorylation, which was weaker at longer time points. Addition of thymidine completely blocked AICAR-induced ACC phosphorylation in all the time points analyzed, suggesting that thymidine inhibits AICAR entrance to the cell. On the other hand, addition of uridine seemed to delay ACC phosphorylation: it was inhibited at earlier time points, but it reached the levels induced by AICAR alone at longer time points. It is worth mentioning that, in most of the samples analyzed, combination of AICAR and uridine did not reach the high intensity of ACC phosphorylation observed in early time points of AICAR treatment, only the reduced ones observed at longer time points. It is difficult to know whether uridine-mediated delay in ACC phosphorylation can account for the inhibition of AICAR-induced apoptosis. It would have been interesting to perform an HPLC analysis to measure the levels of ZMP (as an indicator of AICAR entrance to the cell), as well as orotate and PRPP levels (as indicators of UMPS activity). These analyses would have given much more information about the modulation in pyrimidine metabolism after AICAR treatment.

We decided to give up the study of the involvement of pyrimidine starvation in AICAR-induced apoptosis in CLL cells as the data obtained were pointing at an inhibition of AICAR entrance to the cell.

1.5. AICAR-INDUCED PRODUCTION OF REACTIVE OXYGEN SPECIES REQUIRES CASPASE ACTIVATION

AICAR is an adenosine analogue that is metabolized within purine catabolism. Increased purine catabolism can lead to hyperuricemia and reactive oxygen species (ROS) generation as a consequence of high activity of xanthine oxidase. This enzyme is involved in the final steps of purine catabolism, it catalyzes hypoxanthine to xanthine and further to uric acid, generating ROS (Fig. 1.17) (Pacher et al. 2006). Previous results from our group showed that CLL cells treated with AICAR had increased production of ROS, i.e., superoxide anion ($O_2^{\cdot-}$) as detected by dihydroethidium (DHE) staining. AICAR-induced ROS production and apoptosis were partially blocked by treatment with allopurinol and febuxostat, two inhibitors of xanthine oxidase (González-Gironès 2012). These results suggested that AICAR could be inducing apoptosis through ROS production owing to hyperactivation of xanthine oxidase.

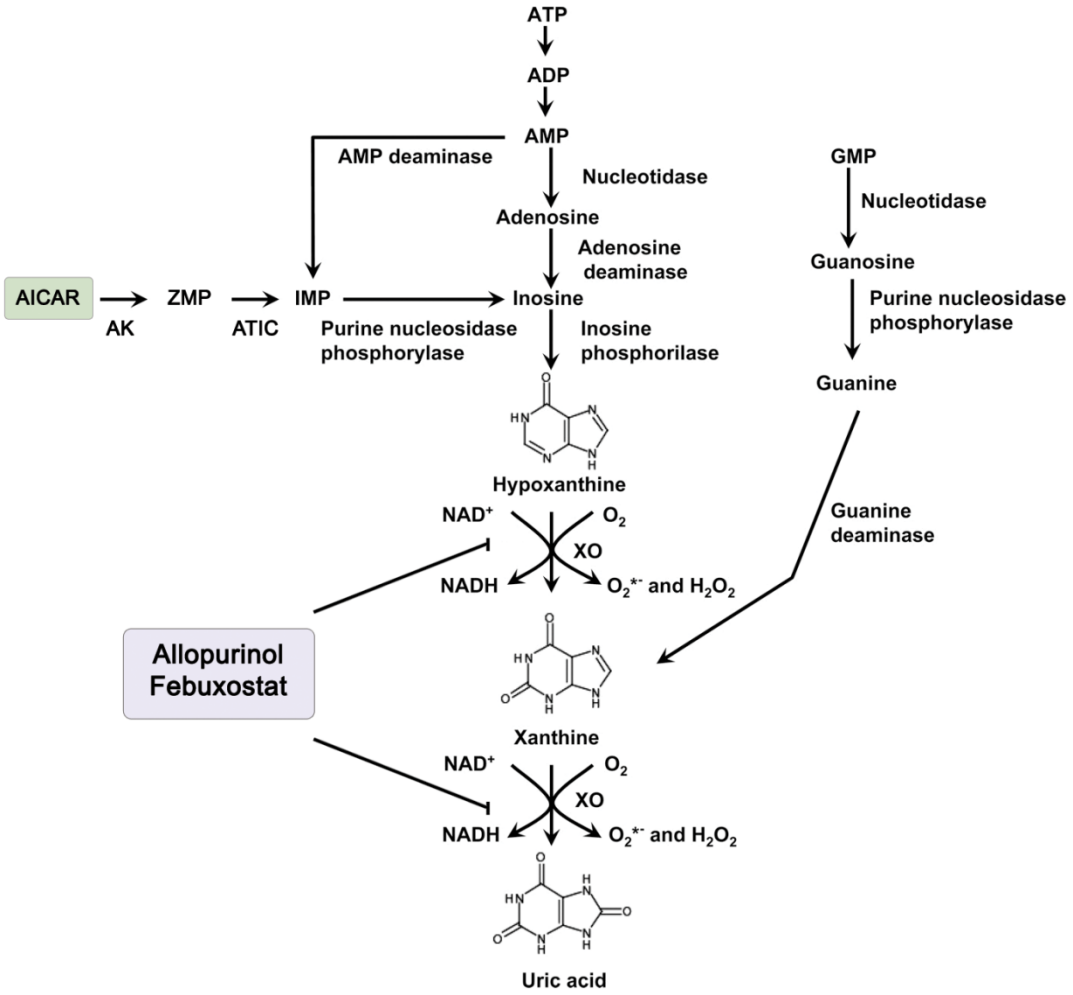

Figure 1.17. Purine catabolism pathways and xanthine oxidase inhibitors. AK, adenosine kinase; ATIC, AICAR transformylase IMP cyclohydrolase; XO, xanthine oxidase. Modified from Pacher et al. 2006.

Nevertheless, it was reported that caspase activation results in ROS formation (Ricci et al. 2004). Hence, we sought to assess whether AICAR-mediated production of superoxide anion was a cause or a consequence of apoptosis induction. To this end, two samples from CLL patients were pre-treated with the pan-caspase inhibitor Q-VD-OPh and then treated with AICAR for 6, 9, and 24 hours. We observed a reduction in the viability of the cells and an increase in the production of superoxide upon 24 hours of AICAR treatment, which were blocked by pre-treatment with Q-VD-OPh (Fig. 1.18). Therefore, AICAR-induced ROS production is an event occurring downstream of caspases activation and thus cannot be its mechanism of apoptosis induction.

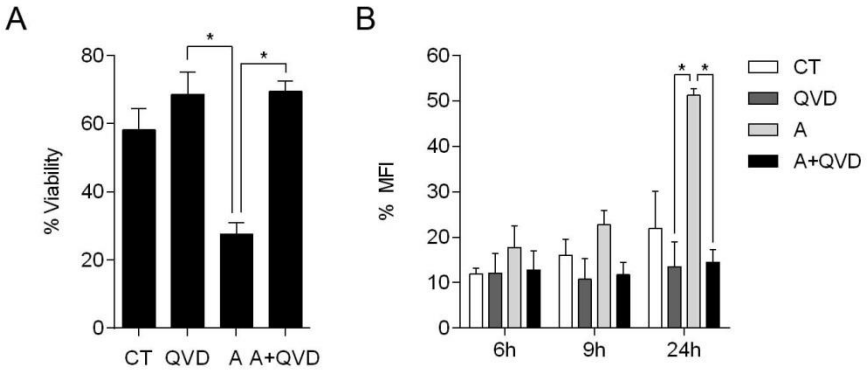

Figure 1.18. AICAR-induced apoptosis and ROS production require caspases activation. Samples from two CLL patients were pre-incubated in the absence (CT) or presence of 20 μM Q-VD-OPh for 30 minutes and then untreated or treated with 0.5 mM AICAR (A) for 6, 9 and 24 hours. **(A)** Viability was measured by flow cytometry upon 24 hours of AICAR treatment and it is expressed as the mean ± SEM (n=2) of the percentage of non-apoptotic cells (annexin V/PI-negative). *$p < 0.05$. **(B)** Superoxide production was detected at 6, 9 and 24 h by flow cytometry with DHE staining and it is shown as geometric mean of the fluorescence intensity (MFI) ± SEM (n=2).

2. Characterization of fluorizoline-induced apoptosis

2.1. OPA1 PROCESSING UPON FLUORIZOLINE TREATMENT

Previous results from our group showed that fluorizoline binds directly to prohibitin (PHB) 1 and 2 (Pérez-Perarnau et al. 2014). It was necessary to prove that PHBs were indeed mediating fluorizoline-induced apoptosis. With this aim, our group first used an indirect strategy, based on the study of optic atrophy 1 (OPA1). This protein is a dynamin-related GTPase in the inner mitochondrial membrane (IMM) that mediates mitochondrial fusion and maintains the cristae structure (Olichon et al. 2003, Arnoult et al. 2005, Merkwirth et al. 2008). HeLa cells express mainly two transcripts of OPA1, variants 1 and 7, which are cleaved resulting in the accumulation of five OPA1 forms: two long (a and b, L-OPA) and three short forms (c, d and e; S-OPA) (Ishihara et al. 2006). Depletion of PHBs leads to increased processing of OPA1, as well as mitochondrial fragmentation and cristae disorganization (Merkwirth et al. 2008). This phenotype was also observed upon fluorizoline treatment (Pérez-Perarnau 2013), which suggested that fluorizoline pro-apoptotic effects were indeed mediated by PHBs. OPA1 plays a key role in the maintenance of the mitochondrial cristae junctions, creating the intra-cristae space where the majority of cytochrome *c* resides. During apoptosis, OPA1 complexes are disassembled (Frezza et al. 2006, Yamaguchi et al. 2008, Landes et al. 2010, Jiang et al. 2014). This allows the reorganization of the mitochondrial cristae and facilitates cytochrome *c* release from the intracristae space to the intermembrane space (Scorrano et al. 2002, Yamaguchi et al. 2008).

Taking into account such an important role of OPA1 in apoptosis induction, it is conceivable that not only fluorizoline but also other apoptotic stimuli induce OPA1 processing and cristae disorganization. This would discard OPA1 processing as a demonstration that PHBs mediate fluorizoline-induced apoptosis, because it would be a general apoptotic feature as well.

To shed some light on this issue, we sought to analyze OPA1 protein levels upon treatment with different pro-apoptotic insults in HeLa cells. To this end, cells were treated with fluorizoline; staurosporine (STS), a cell death inducer control; capsaicin, which binds to PHBs and induces cytochrome *c* release (Kuramori et al. 2009); and Rocaglamide-A (Roc-A), which binds to PHBs and arrests cell cycle without apoptosis induction (Polier et al. 2012). Cell viability was assessed by flow cytometry, and OPA1 protein levels were analyzed by western blot. Interestingly, OPA1 processing correlated with apoptosis induction, regardless of the involvement of PHBs in the mechanism of action of the different drugs. Specifically, there was a clear reduction of L-OPA1 and an increase in S-OPA1, mainly c and e forms (Fig. 2.1).

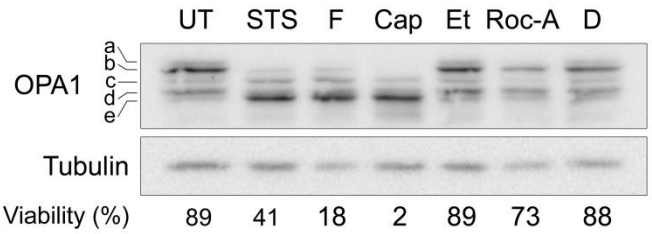

Figure 2.1. OPA1 processing correlates with apoptosis induction. HeLa cells were untreated (UT) or treated with 0.25 μM staurosporine (STS), 10 μM fluorizoline (F), 500 μM capsaicin (Cap), capsaicin vehicle control (ethanol, Et), 500 nM Rocaglamide-A (Roc-A) or Roc-A vehicle control (DMSO, D) for 24 hours. Viability was measured by flow cytometry and it is expressed as the percentage of non-apoptotic cells (annexin V-negative). Protein levels were analyzed by western blot. This is a representative experiment of two that were performed independently.

As different pro-apoptotic insults were inducing OPA1 processing, we next studied whether it was an event occurring after caspase activation. With this aim, HeLa cells were pre-treated with the pan-caspase inhibitor Q-VD-OPh and then treated with different pro-apoptotic stimuli: fluorizoline, actinomycin D (ActD), STS, Roc-A or capsaicin. Blocking caspase activation efficiently prevented fluorizoline- and ActD-induced apoptosis, while just partially blocked STS-induced cell death. HeLa cells treated with Roc-A showed only a minor decrease in viability, in agreement with previous results (Polier et al. 2012). Strikingly, the cytotoxic effects of capsaicin were not reverted by Q-VD-OPh pre-treatment, suggesting that capsaicin treatment leads to caspase-independent cell death (Fig. 2.2A). Western blot analysis showed that fluorizoline, ActD, STS and capsaicin treatment induced OPA1 processing, as seen by a reduction of L-OPA1 and accumulation of S-OPA1. Pre-treatment with Q-VD-OPh did not block loss of L-OPA1, though it blocked accumulation of S-OPA1 (Fig. 2.2B). Thus, there were two treatments, ActD and fluorizoline, in which Q-VD-OPh was able to block phosphatidilserine exposure but could not prevent loss of L-OPA1.

All these data suggest that disappearance of L-OPA1 is a common apoptotic event, upstream of caspase activation, which cannot be used as a proof that fluorizoline-induced apoptosis is mediated by PHBs.

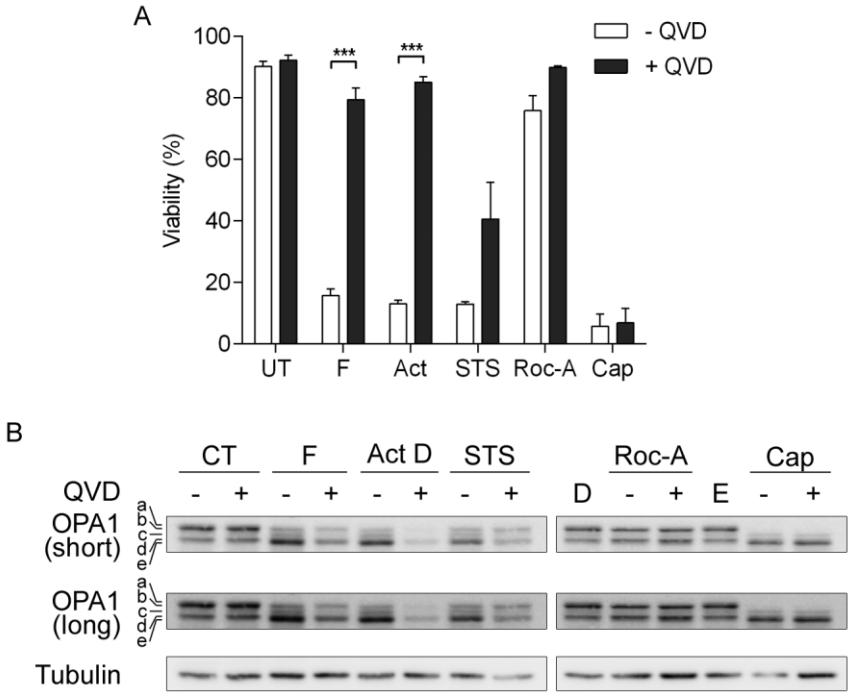

Figure 2.2. Treatment with different pro-apoptotic agents triggers loss of L-OPA1 independently of caspase activation. HeLa cells were pre-incubated with or without 20 μM Q-VD-OPh for 30 minutes and then untreated (UT) or treated with 10 μM fluorizoline (F), 5 μg/mL ActD, 0.25 μM STS, Roc-A vehicle control (DMSO, D), 500 nM Roc-A, capsaicin vehicle control (ethanol, Et), or 300 μM capsaicin (Cap) for 24 hours. **(A)** Viability was measured by flow cytometry and it is expressed as the percentage of non-apoptotic cells (annexin V-negative). Data are shown as mean ± SEM (n=2). ***$p < 0.001$. **(B)** Protein levels were analyzed by western blot (n=1, except for fluorizoline, n=3). Here we show short and long exposures of OPA1 blot.

2.2. IN SEARCH OF A MODEL FOR PROHIBITINS DEPLETION

In order to prove that the pro-apoptotic effects of fluorizoline require PHBs, we sought to analyze the response to fluorizoline treatment in the absence of PHBs. The first approach was the downregulation of PHBs by siRNA transfection in HeLa cells. Nevertheless, loss of PHBs led to morphological changes and cell detachment (Pérez-Perarnau 2013). This is in consistence with other reports which described similar phenotypes after PHB downregulation (Rajalingam et al. 2005, Kasashima et al. 2006, Sievers et al. 2010, Sato et al. 2011).

With the aim of overcoming this technical drawback, our group established a collaboration with Dr. Thomas Langer (Institute for Genetics, CECAD, Cologne, Germany). They had previously developed a cell line of mouse embryonic fibroblasts (MEFs) conditional knockout (KO) for *Phb2* (*Phb2*$^{fl/fl}$ MEFs) (Merkwirth et al. 2008). In contrast with the morphologic changes observed after siRNA-mediated PHBs silencing in HeLa cells, MEFs with deleted *Phb2* show impaired proliferation but maintain the cellular viability. This conditional KO model is based on Cre-lox system: exon 3 of *Phb2* gene is flanked by two loxP sites, which will be recognized and digested by Cre recombinase,

deleting part of *Phb2* gene. This abolishes *Phb2* expression, as mRNA levels of *Phb2* cannot be detected. At a protein level, PHB1 and PHB2 are interdependent, thus reduction of the levels of one protein entails the reduction of the other (Merkwirth et al. 2008). Hence, when using the conditional KO MEFs, deletion of *Phb2* leads to a deletion of both PHB1 and 2, the two proteins that directly bind to fluorizoline. As a control, we used wild-type (WT) MEFs, in which Cre recombinase transduction does not modify PHBs protein levels (Merkwirth et al. 2008).

A classical disadvantage of Cre-lox system is the low efficiency of Cre recombinase expression processes, e.g., virus transfection or plasmid overexpression. In order to improve this step, Langer and colleagues use a recombinant Cre recombinase called His-TAT-NLS-Cre (HTNC) (described at Peitz et al. 2002). The TAT peptide allows the cellular absorption of the enzyme, while the nuclear localization signal (NLS) allows its translocation to the nucleus. Thanks to histidines, the enzyme can be purified with nickel beads from a bacterial expression system. Thus, this system allows the direct administration of Cre recombinase to MEFs, dramatically increasing the efficiency of the gene deletion. All in all, MEFs conditional KO for *Phb2* rose as a really useful tool for the analysis of pro-apoptotic effects of fluorizoline in cells lacking their main molecular targets: PHB1 and 2.

We first sought to optimize the amount of Cre recombinase required for *Phb2* gene deletion. To this end, $Phb2^{fl/fl}$ MEFs were transduced with different concentrations of Cre recombinase for 20 hours and further grown for 72 hours. We then harvested the cells and assessed the efficiency of the deletion by PCR. As shown in figure 2.3, 6 μM Cre recombinase was the minimum concentration required for a total *Phb2* gene deletion, and thus was established for further experiments. The optimization of the concentration had to be done every time that a newly synthetized Cre recombinase was used for the first time.

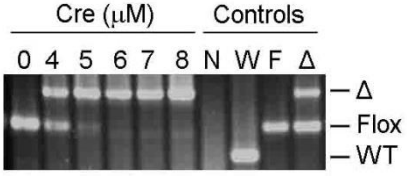

Figure 2.3. PCR analysis of *Phb2* gene deletion after Cre recombinase transduction. $Phb2^{fl/fl}$ MEFs were transduced with increasing doses of Cre recombinase for 20 hours. Afterwards, cells were washed with phosphate buffered saline (PBS) and grown with complete medium for 72 hours. Cells were harvested, DNA was isolated and PCR analysis was performed. Negative (N), WT (W), $Phb2^{fl/fl}$ (F) and $Phb2^{fl/-}$ (Δ) control amplification fragments are shown.

2.3. PROHIBITINS ARE REQUIRED FOR FLUORIZOLINE-INDUCED APOPTOSIS

2.3.1. VALIDATION OF THE MODEL

First of all, we sought to analyze WT and *Phb2*$^{fl/fl}$ MEFs basal response to fluorizoline treatment in the absence of Cre recombinase. It was important to find similar responses in the two cell lines so as further comparisons could be attributed to presence or absence of PHBs, not due to intrinsic sensitivity of the cell lines. Treatment with fluorizoline triggered apoptosis in WT and *Phb2*$^{fl/fl}$ MEFs in a similar manner in the absence of Cre recombinase. Actinomycin D (ActD), a cell death inducer control, was also capable of inducing similar rates of apoptosis in WT and *Phb2*$^{fl/fl}$ MEFs (Fig. 2.4A).

Accordingly, western blot analysis revealed that fluorizoline and ActD treatment led to cleavage of caspase 3 and poly ADP-ribose polymerase (PARP), which indicate apoptosis induction, in WT and *Phb2*$^{fl/fl}$ MEFs likewise (Fig. 2.4B). Interestingly, PHBs levels were increased upon ActD or fluorizoline treatment in both cell lines, as previously observed in apoptotic conditions in rat cells (Chowdhury et al. 2007, 2011).

OPA1 processing occurs during the apoptotic process (Alaimo et al. 2014, Jiang et al. 2014). This allows the remodeling of the mitochondrial cristae and facilitates cytochrome *c* release from the intracristae space to the intermembrane space (Scorrano et al. 2002, Yamaguchi et al. 2008). Consistently, both ActD and fluorizoline triggered OPA1 processing in the apoptotic conditions, where PARP and caspase 3 were also cleaved, in WT and *Phb2*$^{fl/fl}$ MEFs (Fig. 2.4B). Therefore, these results show that WT and *Phb2*$^{fl/fl}$ MEFs respond similarly to fluorizoline and thus are suitable for further studies.

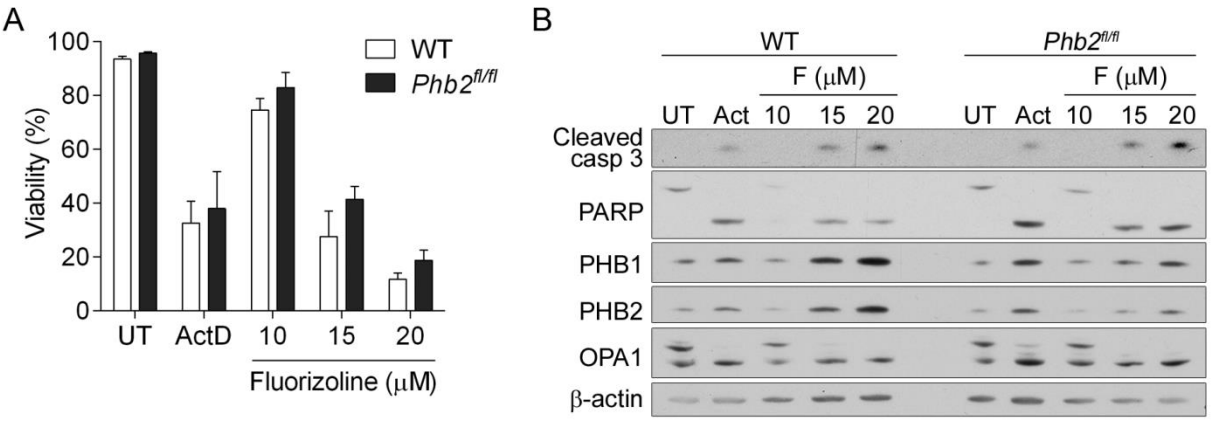

Figure 2.4. WT and *Phb2*$^{fl/fl}$ MEFs show similar apoptotic response to fluorizoline treatment. WT and *Phb2*$^{fl/fl}$ MEFs were untreated (UT) or treated with either 0.15 μg/mL ActD or increasing doses of fluorizoline (F) for 24 hours. **(A)** Viability was measured by flow cytometry and it is expressed as the mean ± SEM (n≥3) of the percentage of non-apoptotic cells (annexin V-negative). **(B)** Protein levels were analyzed by western blot. This is a representative image of at least three independent experiments.

PARP and caspase 3 activation were indicating that apoptosis was occurring upon treatment with fluorizoline. Apoptosis is orchestrated by caspases, a family of cysteine/aspartate proteases that proteolyze hundreds of proteins in a controlled manner (Taylor et al. 2008). We next assessed whether caspases activation were required for fluorizoline-induced apoptosis in MEFs, as previously reported for HeLa cells (Pérez-Perarnau 2013). To this end, we performed a viability assay with the pan-caspase inhibitor Q-VD-OPh. Incubation with fluorizoline decreased viability in WT and *Phb2*$^{fl/fl}$ MEFs, which was abrogated by the pre-treatment with Q-VD-OPh (Fig. 2.5). Hence, induction of apoptosis by fluorizoline is dependent on caspase activation.

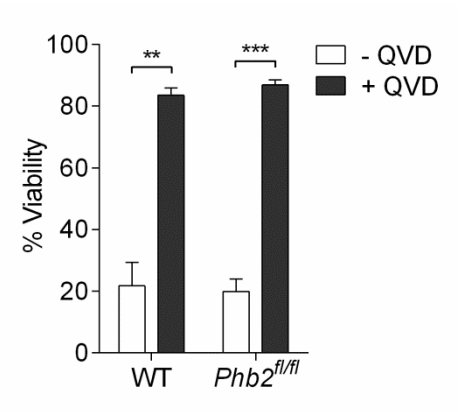

Figure 2.5. Caspase activation is required for fluorizoline-induced apoptosis in WT and *Phb2*$^{fl/fl}$ MEFs. WT and *Phb2*$^{fl/fl}$ MEFs were pre-incubated with or without 20 μM Q-VD-OPh for 30 minutes and then treated with 20 μM fluorizoline for 24 h. Viability was measured by flow cytometry and it is expressed as the mean ± SEM (n=3) of the percentage of non-apoptotic cells (annexin V-negative) relative to the control. **p < 0.01, ***p < 0.001.

2.3.2. CRE RECOMBINASE MEDIATED LOSS OF PROHIBITINS

Having validated WT and *Phb2*$^{fl/fl}$ MEFs as suitable models for the study of fluorizoline-induced apoptosis, we sought to analyze their response to fluorizoline in the absence of PHBs. To his end, WT and *Phb2*$^{fl/fl}$ MEFs were transduced with 6 μM Cre recombinase for 72 hours and then treated with increasing doses of fluorizoline for 24 hours. WT MEFs were sensitive to fluorizoline treatment, while loss of PHBs in Cre-transduced *Phb2*$^{fl/fl}$ MEFs (*Phb2*$^{-/-}$ MEFs) conferred strong resistance to fluorizoline-induced apoptosis. In contrast, both cell lines showed a similar response to ActD (Fig. 2.6A).

Consistently, fluorizoline treatment induced the cleavage of caspase 3 and poly ADP-ribose polymerase (PARP) in WT MEFs, whereas their processing was clearly reduced in *Phb2*$^{-/-}$ MEFs (Fig. 2.6B). Contrary to fluorizoline, ActD triggered similar cleavage of caspase 3 and PARP in WT and *Phb2*$^{-/-}$ MEFs, providing support for the specificity of PHBs as targets of fluorizoline.

In agreement with former results, processing of OPA1 was observed in ActD- and fluorizoline-treated WT MEFs, the same conditions in which PARP and caspase 3 were cleaved (Fig. 2.6B). Cre-mediated depletion of *Phb2* was accompanied by an increased processing of OPA1 in *Phb2*$^{-/-}$ MEFs (Fig. 2.6B), as previously described (Merkwirth et al. 2008). All together, these results show that absence of PHBs confers resistance to fluorizoline-induced apoptosis.

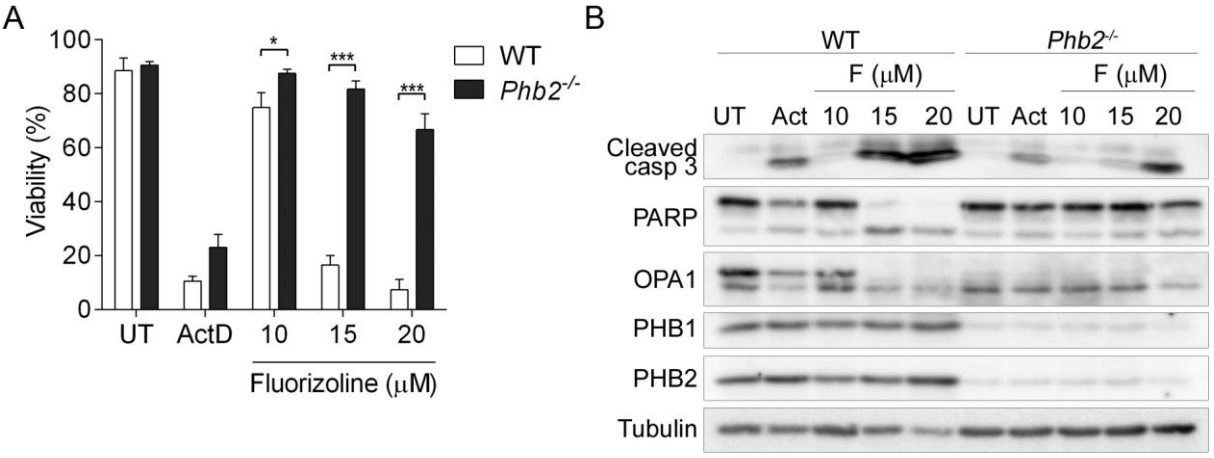

Figure 2.6. Cre-mediated loss of PHBs confers resistance to fluorizoline pro-apoptotic effects in *Phb2*$^{fl/fl}$ MEFs. Cre recombinase was transduced in WT and *Phb2*$^{fl/fl}$ MEFs (*Phb2*$^{-/-}$) for 72 hours. Then cells were untreated (UT) or treated with either 0.15 μg/mL ActD or increasing doses of fluorizoline (F) for 24 hours. **(A)** Viability was measured by flow cytometry and it is expressed as the percentage of non-apoptotic cells (annexin V-negative). Mean ± SEM (n≥3). *p < 0.05, ***p < 0.001. **(B)** Protein levels were analyzed by western blot. These are representative images of at least three independent experiments.

2.3.3. GENETIC RESCUE OF PROHIBITINS DEPLETION

We sought to further corroborate that loss of PHBs was indeed the cause of resistance to fluorizoline-induced apoptosis. To this end, we used *Phb2*$^{fl/fl}$::*Phb2* MEFs, which harbor *Phb2* gene downstream from a stop-cassette with flanking loxP sites. Cre recombinase transduction results in simultaneous deletion of genomic *Phb2* along with the deletion of the floxed transcriptional stop-cassete, which allows the expression of the transgene *Phb2* (Fig. 2.7). Thus, this cell line would be an optimal control for Cre recombinase-mediated loss of PHBs.

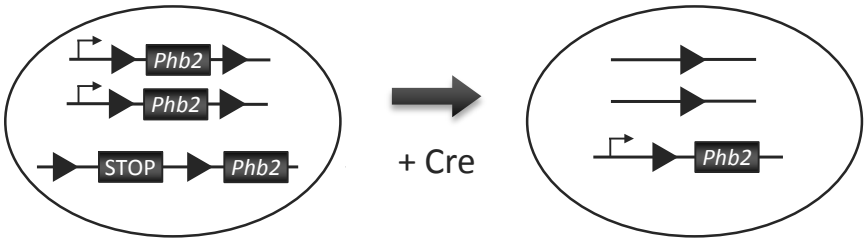

Figure 2.7. Schematic representation of Cre-induced expression of *Phb2* in *Phb2$^{fl/fl}$::Phb2* MEFs. Based on Merkwirth et al. 2008.

First, we analyzed *Phb2$^{fl/fl}$*::*Phb2* MEFs basal response to fluorizoline treatment in the absence of Cre recombinase. It was important to find similar responses to WT or *Phb2$^{fl/fl}$* MEFs so as further comparisons could be attributed to presence or absence of PHBs, not due to intrinsic sensitivity of the cell lines. However, *Phb2$^{fl/fl}$*::*Phb2* MEFs displayed less sensitivity to fluorizoline-induced apoptosis compared to WT or *Phb2$^{fl/fl}$* MEFs (Fig. 2.8). In addition, ActD did not affect viability of *Phb2$^{fl/fl}$*::*Phb2* MEFs, showing that this cell line is generally less sensitive to apoptotic stimuli. Hence, we discarded *Phb2$^{fl/fl}$*::*Phb2* MEFs as a good genetic rescue model.

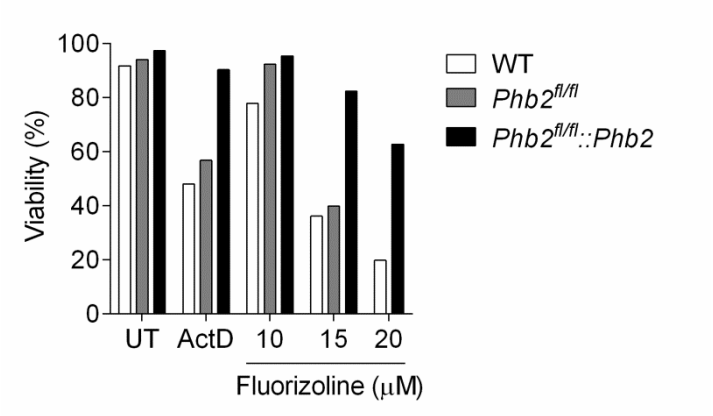

Figure 2.8. Dose-response curve of fluorizoline in WT, *Phb2$^{fl/fl}$* and *Phb2$^{fl/fl}$*::*Phb2* MEFs. WT, *Phb2$^{fl/fl}$* and *Phb2$^{fl/fl}$*::*Phb2* MEFs were untreated (UT) or treated with 0.10 μg/mL ActD, or increasing doses of fluorizoline for 24 hours. Viability was measured by flow cytometry and it is expressed as the percentage of non-apoptotic cells (annexin V-negative). This experiment was performed once.

Recently, a manuscript from Dr. Langer's group was published describing a similar cell line, namely *Phb2$^{fl/fl}$*::CNAP-*Phb2* MEFs. In this case, Cre recombinase transduction allowed endogenous *Phb2* gene deletion along with the re-expression of an exogenous *Phb2* which was tagged to the epitope CNAP (Richter-Dennerlein et al. 2014). Again, we performed a viability assay to assess their response to fluorizoline treatment. *Phb2$^{fl/fl}$*::CNAP-*Phb2* MEFs were sensitive to fluorizoline pro-apoptotic effects, though to a smaller extent compared to WT and *Phb2$^{fl/fl}$* MEFs (Fig. 2.9).

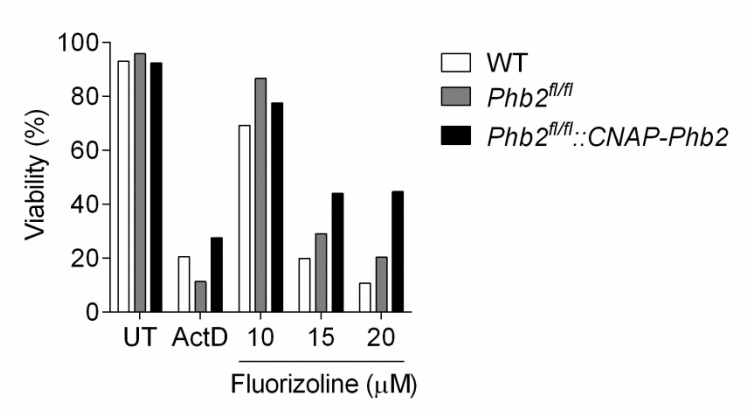

Figure 2.9. Dose-response curve of fluorizoline in WT, *Phb2*$^{fl/fl}$ and *Phb2*$^{fl/fl}$*::CNAP-Phb2* MEFs. WT, *Phb2*$^{fl/fl}$ and *Phb2*$^{fl/fl}$*::CNAP-Phb2* MEFs were untreated (UT) or treated with either 0.15 μg/mL ActD or increasing doses of fluorizoline for 24 hours. Viability was measured by flow cytometry and it is expressed as the percentage of non-apoptotic cells (annexin V-negative). This experiment was performed once.

As the differences on the sensitivity to fluorizoline were not dramatic, western blot analysis were performed to characterize the apoptotic response in more detail. Treatment with ActD and fluorizoline triggered the processing of caspase 3 and PARP in WT and *Phb2*$^{fl/fl}$ MEFs alike, yet it was clearly reduced in *Phb2*$^{fl/fl}$*::CNAP-Phb2* MEFs (Fig. 2.10). These results show that *Phb2*$^{fl/fl}$*::CNAP-Phb2* MEFs are more resistant to apoptotic stimuli and therefore, were also ruled out as genetic rescue model.

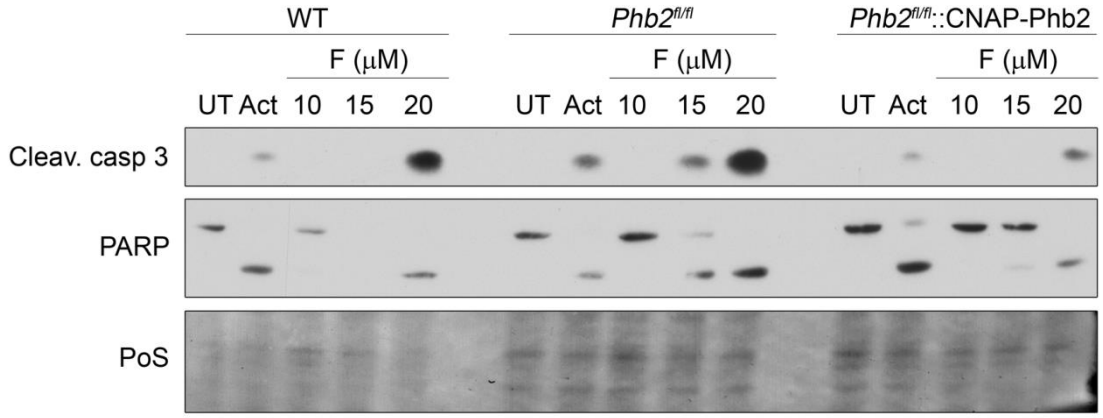

Figure 2.10. Western blot analysis of WT, *Phb2*$^{fl/fl}$ and *Phb2*$^{fl/fl}$*::CNAP-Phb2* MEFs. These cell lines were untreated (UT) or treated with either 0.15 μg/mL ActD or increasing doses of fluorizoline (F) for 24 hours. Protein levels were analyzed by western blot. These are representative images of two independent experiments. Ponceau staining (PoS) was used as a loading control.

2.3.4. siRNA-MEDIATED DOWNREGULATION OF PROHIBITINS

Having discarded both available genetic rescue cell lines as good models to study the mechanism of action of fluorizoline, we decided to corroborate the results obtained in Cre-mediated *Phb2*$^{-/-}$ by downregulating *Phb2* levels using siRNA. In this way, another approach would be used in order to further prove that PHBs are required for fluorizoline-induced apoptosis. WT and *Phb2*$^{fl/fl}$ MEFs were transfected with *Phb2* siRNA for 72 hours and then treated with fluorizoline for 24 hours. Consistent with the previous results, fluorizoline pro-apoptotic effects were blocked when PHBs were downregulated, as shown by viability analysis (Fig. 2.11).

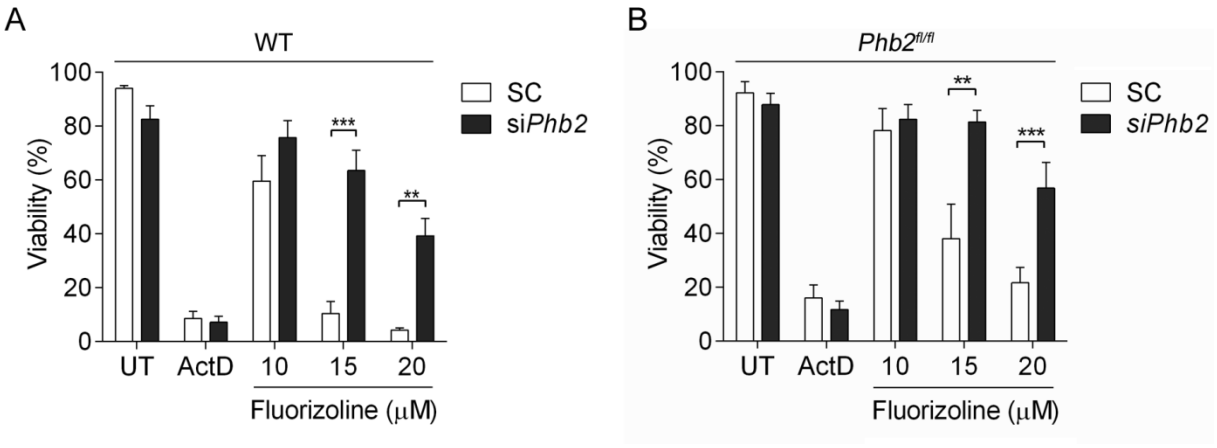

Figure 2.11. Viability assay in *Phb2*-downregulated WT and *Phb2*$^{fl/fl}$ MEFs. WT **(A)** and *Phb2*$^{fl/fl}$ **(B)** MEFs were transfected with scramble (SC) or *Phb2* siRNA (si*Phb2*) for 72 hours. Afterwards, cells were treated with either 2.5 μg/mL Actinomycin D (ActD) or increasing doses of fluorizoline for 24 hours. Viability was measured by flow cytometry and it is expressed as the percentage of non-apoptotic cells (annexin V-negative). Mean ± SEM (n≥3). **p < 0.01, ***p < 0.001.

Next, we performed western blot analyses to further characterize the apoptotic response to fluorizoline treatment. Caspase 3 and PARP cleavage were induced by ActD and fluorizoline in scramble-transfected cells, while their cleavage was reduced in *Phb2* siRNA-transfected cells in both WT and *Phb2*$^{fl/fl}$ MEFs (Fig. 2.12). In agreement with figure 2.6B, ActD and fluorizoline induced OPA1 processing in scramble-transfected cells, while downregulation of PHBs led to OPA1 processing irrespective of the treatment. All together, these data prove that absence of PHBs confers resistance to fluorizoline-induced apoptosis.

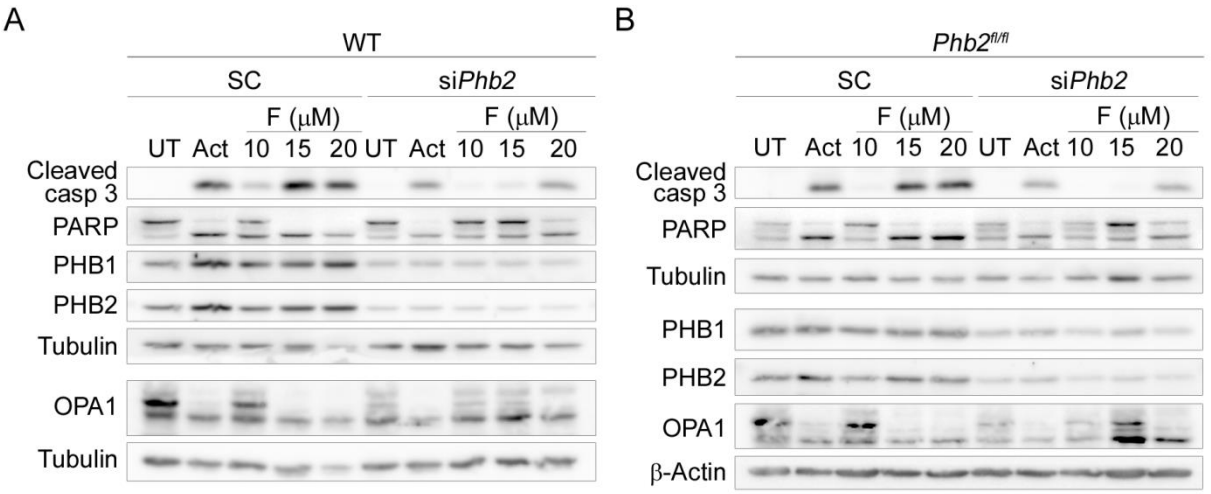

Figure 2.12. Western blot analysis in *Phb2*-downregulated WT and *Phb2*$^{fl/fl}$ MEFs. WT **(A)** and *Phb2*$^{fl/fl}$ **(B)** MEFs were transfected with scramble (SC) or *Phb2* siRNA (si*Phb2*) for 72 hours. Afterwards, cells were treated with either 2.5 μg/mL Actinomycin D (Act) or increasing doses of fluorizoline (F) for 24 hours. Protein levels were analyzed by western blot. These are representative images of at least three independent experiments.

2.4. SLP-2 IS NOT INVOLVED IN FLUORIZOLINE-INDUCED APOPTOSIS

PHBs belong to the stomatin-prohibitin-flotilin-HflC/K (SPFH) superfamily, whose members tend to oligomerize and form large multimeric complexes that localize in lipid rafts microdomains in various cellular membranes (Browman et al. 2007). Stomatin-like protein 2 (SLP-2) also belongs to this superfamily and has been described to interact with cardiolipin and PHBs in the IMM, forming membrane microdomains that facilitate mitochondrial biogenesis and function (Da Cruz et al. 2008, Christie et al. 2011).

Considering the structural similarity of the SPFH family members, it is conceivable that fluorizoline may also affect other SPFH proteins apart from PHBs. As SLP-2 KO (SKO) MEFs were available at Dr. Langer's laboratory, we decided to examine how these cells would respond to fluorizoline treatment. With this aim, *Phb2*$^{fl/fl}$ and SKO MEFs were incubated with different doses of fluorizoline for 24 hours and viability was measured by flow cytometry. Both cell lines displayed similar sensitivity to fluorizoline-induced apoptosis (Fig. 2.13), ruling out SLP-2 as a required target for fluorizoline mechanism of action.

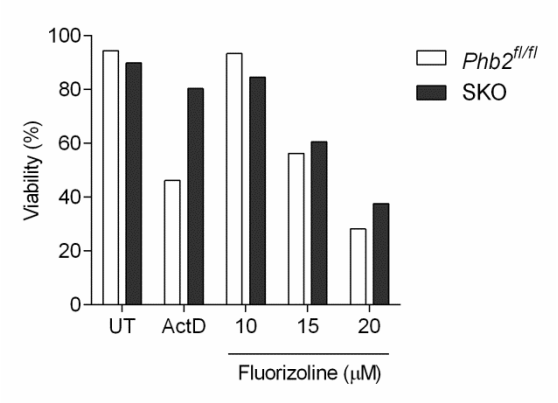

Figure 2.13. Fluorizoline triggers apoptosis in *Phb2*$^{fl/fl}$ and SKO MEFs alike. *Phb2*$^{fl/fl}$ and SKO MEFs were untreated (UT) or treated with 0.15 μg/mL Actinomycin D (ActD), or increasing doses of fluorizoline for 24 hours. Viability was measured by flow cytometry and it is expressed as the percentage of non-apoptotic cells (annexin V-negative). This experiment was performed once.

2.5. GENERATION OF A *Phb2*$^{-/-}$ STABLE CELL LINE

Although *Phb2*$^{-/-}$ MEFs were reported to have impaired proliferation (Merkwirth et al. 2008), after Cre recombinase transduction some cell proliferation was observed in *Phb2*$^{fl/fl}$ MEFs. This encouraged us to try to generate a stable cell line lacking *Phb2* which could avoid the requirement of *Phb2* depletion for each experiment. With this aim, *Phb2*$^{fl/fl}$ MEFs were transduced with Cre recombinase for 20 hours and further grown for 72 hours. Then, single cells were sorted separately in individual wells in a 96-well plate and allowed to grow for several days (Fig. 2.14).

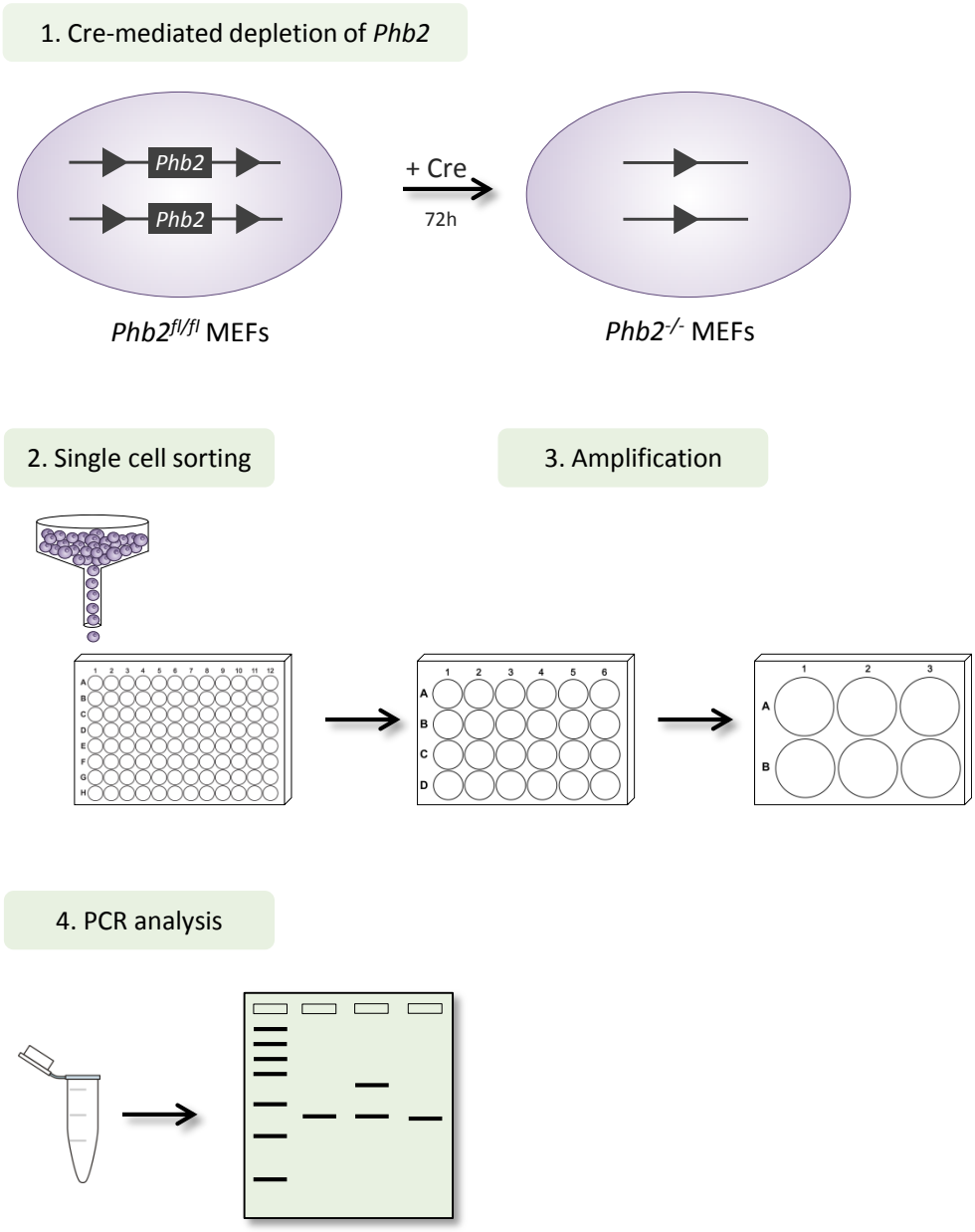

Figure 2.14. Schematic representation of the generation of a *Phb2*$^{-/-}$ stable cell line.

Among 192 clones that were seeded, 79 were selected and grown in bigger plates for further study. Considering that loss of *Phb2* could result in impaired proliferation, clones were chosen at different days in order to include clones with different proliferation rates. We isolated DNA from 58 clones and performed a PCR analysis to assess the status of the *Phb2* gene. None of the clones presented a complete deletion of the *Phb2* gene. Of note, 47 clones had one allele depleted while the other one was still floxed (*Phb2*$^{fl/-}$); while the other 11 had both alleles floxed (*Phb2*$^{fl/fl}$). Figure 2.15 shows representative PCR analysis of different clones.

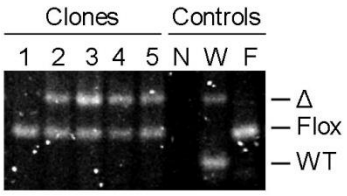

Figure 2.15. PCR analysis of *Phb2* gene in different clones. DNA of five different Cre-transduced *Phb2*$^{fl/fl}$ clones was isolated and PCR analysis was performed. Negative (N), *Phb2*$^{+/-}$ (W), and *Phb2*$^{fl/fl}$ (F) control amplification fragments are shown.

In spite of the lack of *Phb2*$^{-/-}$ clones, we sought to study how would heterozygous (*Phb2*$^{fl/-}$) respond to fluorizoline treatment. To this end, we selected three heterozygous and two control homozygous (*Phb2*$^{fl/fl}$) clones, incubated them with fluorizoline for 24 hours and analyzed the viability. This experiment was performed twice, and data from the clones with the same genetic status were pooled together in order to minimize the clone-specific differences unrelated to the *Phb2* gene status. Strikingly, *Phb2*$^{fl/-}$ and *Phb2*$^{fl/fl}$ clones displayed similar sensitivity to fluorizoline treatment (Fig. 2.16).

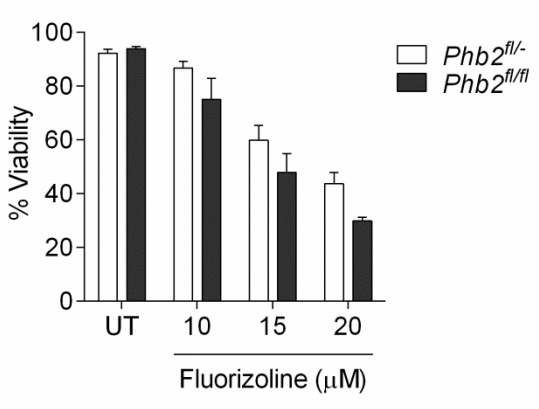

Figure 2.16. *Phb2*$^{fl/fl}$ and *Phb2*$^{fl/-}$ clones respond similarly to fluorizoline treatment. Three *Phb2*$^{fl/-}$ and two *Phb2*$^{fl/fl}$ clones were untreated (UT) or treated with increasing doses of fluorizoline for 24 hours. Viability was measured by flow cytometry and it is expressed as the mean ± SEM (n=2) of the percentage of non-apoptotic cells (annexin V-negative). Data from the clones with the same genetic status were pooled together (three heterozygous, two experiments, in one group; two homozygous, two experiments, another group) in order to minimize the clone-specific differences unrelated to the *Phb2* gene status.

We then analyzed the protein levels of PHBs and OPA1 in the five selected clones (Fig. 2.17). Interestingly, *Phb2*$^{fl/-}$ showed lower levels of PHBs when compared to *Phb2*$^{fl/fl}$. This reduction was accompanied by OPA1 processing (loss of L-OPA forms) as observed in those cells totally lacking

PHBs. Thus, *Phb2*$^{fl/-}$ clones have low levels of PHBs, which are not enough for blocking OPA1 processing, yet are enough for fluorizoline to induce apoptosis as effectively as in *Phb2*$^{fl/fl}$ clones.

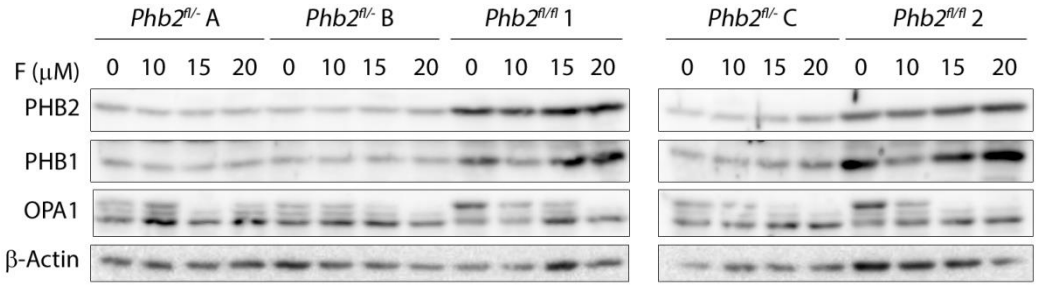

Figure 2.17. Western blot analysis of *Phb2*$^{fl/fl}$ and *Phb2*$^{fl/-}$ clones. Three *Phb2*$^{fl/-}$ clones (A, B, and C) and two *Phb2*$^{fl/fl}$ clones (1 and 2) were untreated or treated with 10, 15 or 20 μM fluorizoline (F) for 24 hours. Protein levels were analyzed by western blot. This is a representative image of two independent experiments.

To discard any putative problem with the *Phb2* depletion in the first attempt to generate a *Phb2*$^{-/-}$ stable cell line, we decided to further try it by transducing again with Cre recombinase in three *Phb2*$^{fl/-}$ clones. Unfortunately, among 26 selected clones, none was *Phb2*$^{-/-}$ (data not shown). Hence, the difficulty to obtain a *Phb2*$^{-/-}$ clone provides further support for a key role of PHBs in proliferation, and thus those cells lacking PHBs have a clear proliferation disadvantage.

2.6. EFFECTS OF FLUORIZOLINE ON PROHIBITINS COMPLEXES IN MITOCHONDRIA

In the inner mitochondrial membrane, PHB1 and 2 form membrane-bound complexes of 0.8-1 MDa (Merkwirth and Langer 2009). In addition, PHBs interact with other proteins leading to the formation of the prohibitin/mAAA protease (PMA) supercomplexes (Richter-Dennerlein et al. 2014). It is conceivable that treatment with fluorizoline might be affecting these complexes, so we decided to study their assembly by non-denaturing blue native gel electrophoresis (BN-PAGE). As shown in figure 2.18, treatment with fluorizoline did not affect the assembly of PHBs complex neither the PMA supercomplex in *Phb2*$^{fl/fl}$ MEFs. It is worth mentioning that owing to the huge molecular weight of these complexes, subtle changes in their composition may not be detected by BN-PAGE, e.g., loss or incorporation of small proteins. Hence, further experiments would be necessary to characterize more precisely fluorizoline-induced changes in PHBs complexes.

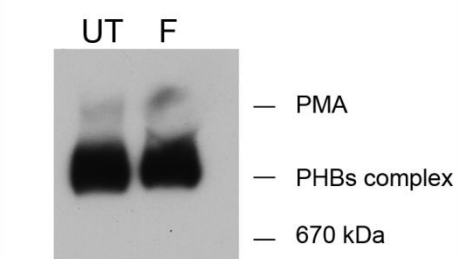

Figure 2.18. Blue Native-PAGE analysis of prohibitins in *Phb2*$^{fl/fl}$ MEFs. These cells were untreated (UT) or treated with 20 μM fluorizoline (F) for 24 hours. Mitochondria were isolated and analyzed by Blue Native-PAGE, followed by immunoblotting with a mixed solution of PHB1 and 2 antibodies. This experiment was performed once.

2.7. STUDY OF THE PHOSPHOLIPID COMPOSITION OF FLUORIZOLINE-TREATED MEFs

PHBs complexes and PMA have been suggested to act as lipid scaffolds in the IMM, which would be crucial for the homeostasis of mitochondrial phospholipids, especially for cardiolipin (CL) and phosphatidylethanolamine (PEA) (Osman et al. 2009b, Richter-Dennerlein et al. 2014).

Therefore, we sought to examine whether fluorizoline treatment was leading to changes in the phospholipid composition. To this end, we analyzed untreated or fluorizoline-treated *Phb2*$^{fl/fl}$ MEFs, as well as Cre-transduced *Phb2*$^{-/-}$ MEFs. Dr. Takashi Tatsuta (Dr. Langer's group, Institute for Genetics, CECAD, Cologne, Germany) performed the lipid analyses by mass spectometry, studying:

- The amount of different phospholipid classes: PEA, CL, phosphatidylcholine (PC), phosphatidylinositol (PIN), phosphatidylserine (PS), phosphatidic acid (PA), and phosphatidylglycerol (PG).
- The length and saturation profile of the acyl chains in each phospholipid species.

Fluorizoline treatment or Cre-mediated loss of PHBs did not induce major changes in the phospholipidome of *Phb2*$^{fl/fl}$ MEFs. The only statistically significant modification was an increase of PEA content induced by Cre recombinase transduction (Fig. 2.19).

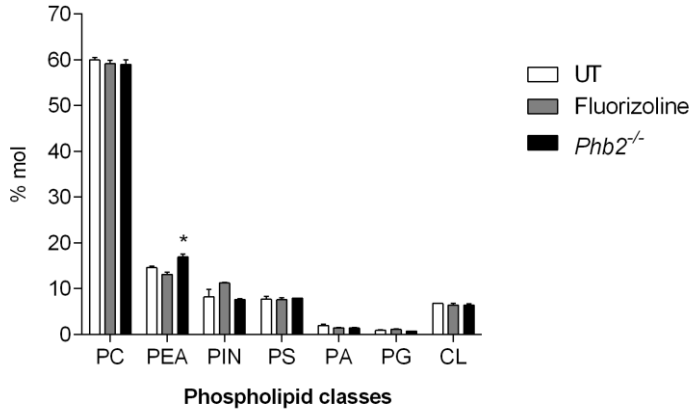

Figure 2.19. Phospholipidome of fluorizoline-treated or Cre-transduced *Phb2*$^{fl/fl}$ MEFs. *Phb2*$^{fl/fl}$ MEFs were untreated (UT), treated with 20 μM fluorizoline for 24 hours, or Cre-transduced for 72 hours (*Phb2*$^{-/-}$). Amounts of phosphatidylcholine (PC), phosphatidylethanolamine (PEA), phosphatidylinositol (PIN), phosphatidylserine (PS), phosphatidic acid (PA), phosphatidylglycerol (PG) and cardiolipin were analyzed by quantitative mass spectrometry and are represented as the mean ± SEM (n=3) of the percentage of pmols relative to the total sum. *p < 0.05.

This is in stark contrast with PHB-downregulated HEK293 mitochondrial phospholipid analysis, in which lack of PHBs correlated with a decrease in PEA and CL content as well as an increase in PIN content (Richter-Dennerlein et al. 2014).

Regarding the length and the saturation of the acyl chains, fluorizoline treatment induced an increase in PEA chain length (Fig. 2.20). The same tendency was observed in *Phb2*$^{-/-}$ MEFs, though no statistical significance was observed. The acyl chains tended to present more double bonds in fluorizoline-treated and Cre-transduced MEFs, but again without statistical significance.

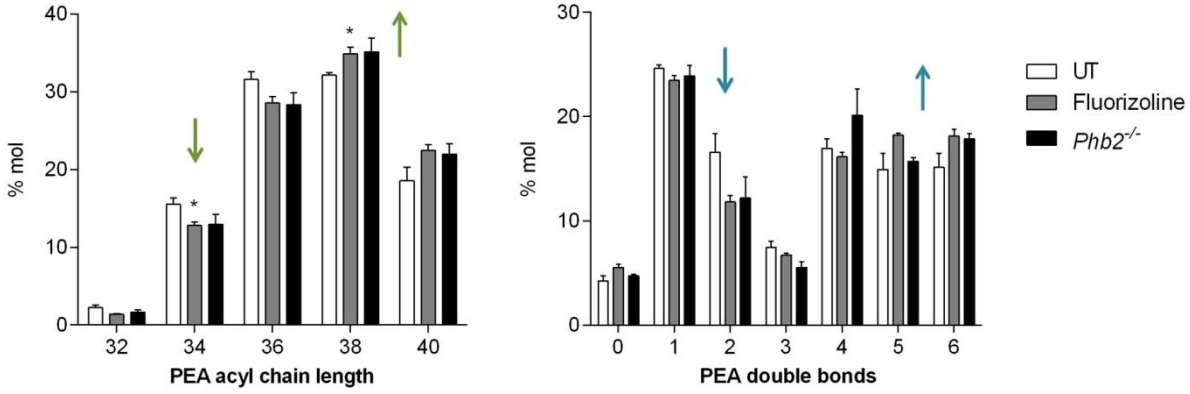

Figure 2.20. Lenght and saturation of PEA acyl chains. *Phb2*$^{fl/fl}$ MEFs were untreated (UT), treated with 20 μM fluorizoline for 24 hours, or Cre-transduced for 72 hours (*Phb2*$^{-/-}$). PEA acyl chains length and saturation were analyzed by quantitative mass spectrometry and are represented as the mean ± SEM (n=3) of the percentage of pmols relative to the total sum. Green arrows indicate statistically significant changes, blue arrows indicate a tendency. *p < 0.05.

CL was reported to have longer and less saturated acyl chains when PHBs were downregulated in HEK293 cells (Richter-Dennerlein et al. 2014). In contrast, the acyl chain length was shorter in fluorizoline-treated MEFs, while *Phb2*$^{-/-}$ MEFs did not show any significant modification. Both conditions tended to have more saturated acyl chains with no statistically significant difference (Fig. 2.21).

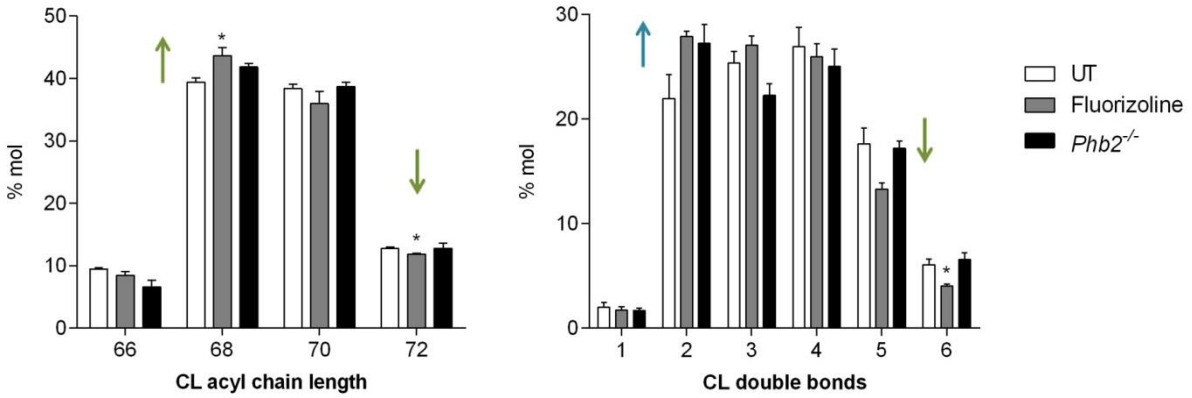

Figure 2.21. Lenght and saturation of CL acyl chains. *Phb2*$^{fl/fl}$ MEFs were untreated (UT), treated with 20 µM fluorizoline for 24 hours, or Cre-transduced for 72 hours (*Phb2*$^{-/-}$). CL acyl chains length and saturation were analyzed by quantitative mass spectrometry and are represented as the mean ± SEM (n=3) of the percentage of pmols relative to the total sum. Green arrows indicate fluorizoline-induced statistically significant changes, blue arrows indicate fluorizoline-induced tendency. *p < 0.05.

PC, PIN and PS presented longer acyl chains in PHBs-downregulated HEK293 cells (Richter-Dennerlein et al. 2014). Fluorizoline induced a significant increase in PC acyl chain length, and PIN, PS, PA, and PG showed a tendency to have longer chains as well (Fig. 2.22). In addition, PC double bonds were increased while PA double bonds were decreased upon fluorizoline treatment. Cre-mediated loss of PHBs only induced an increase in the length and unsaturation of PIN acyl cahins

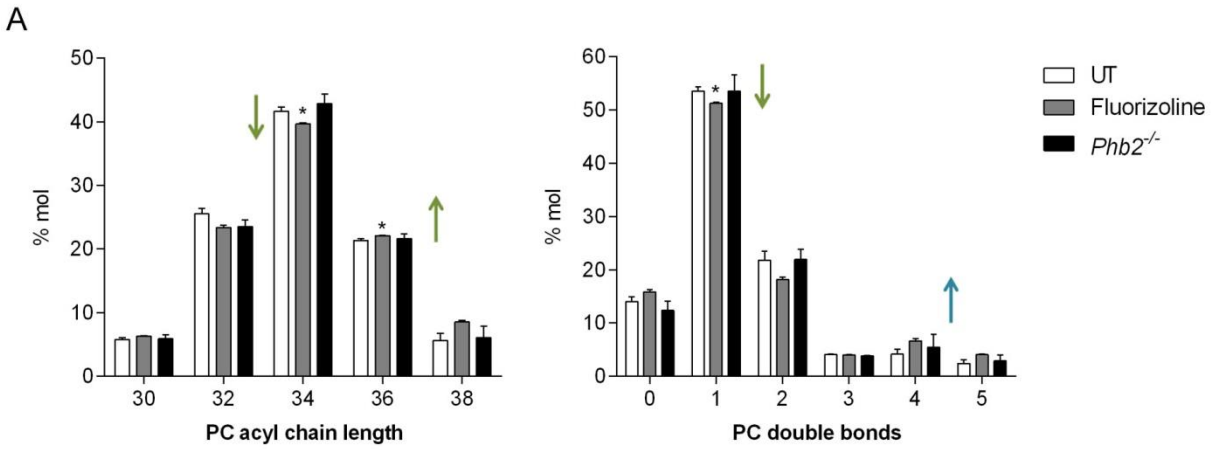

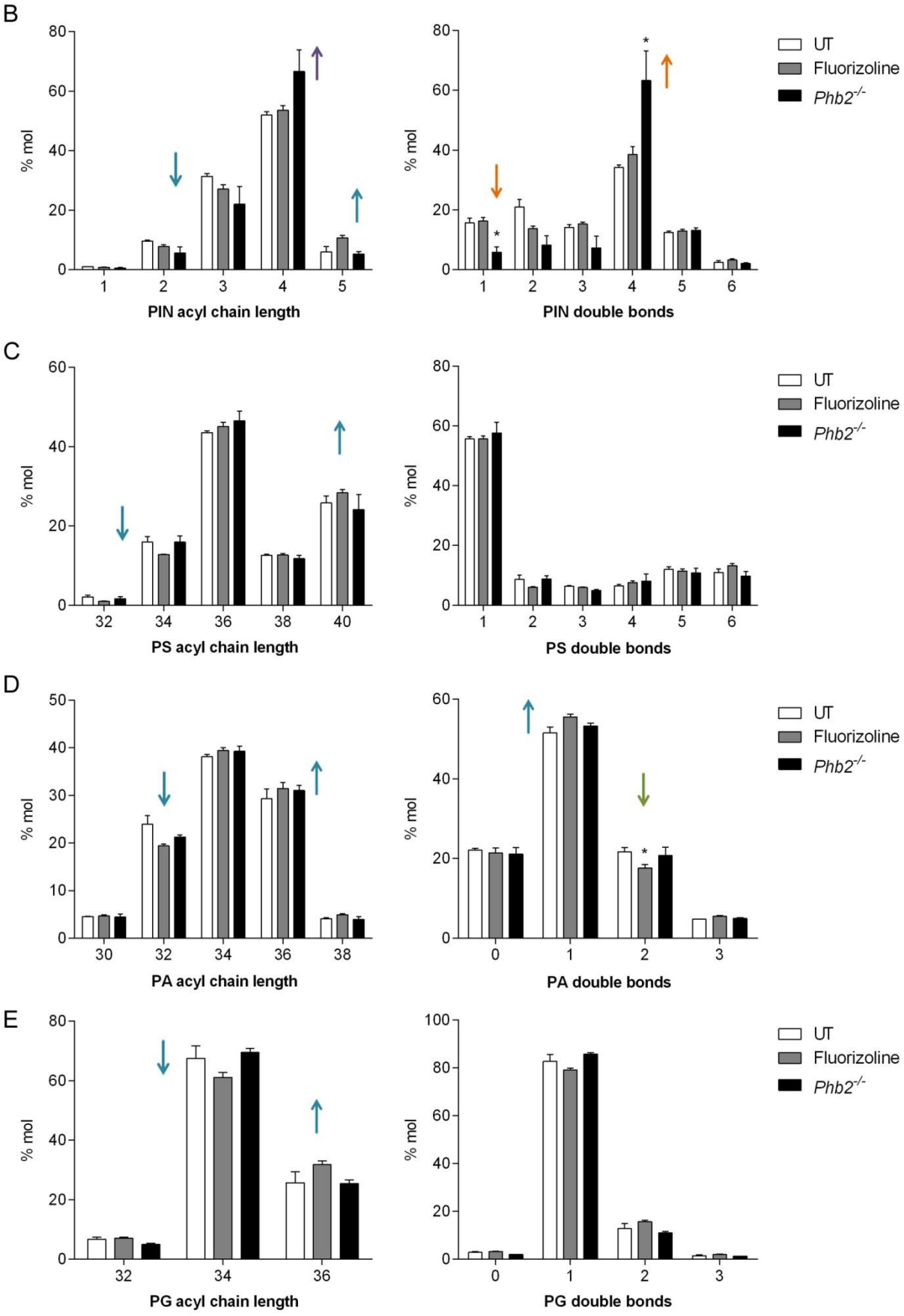

See next page for figure legend

Figure 2.22. Lenght and saturation of PC, PIN, PS, PA and PG acyl chains. *Phb2*$^{fl/fl}$ MEFs were untreated (UT), treated with 20 μM fluorizoline for 24 hours, or Cre-transduced for 72 hours (*Phb2*$^{-/-}$). PC **(A)**, PIN **(B)**, PS **(C)**, PA **(D)** and PG **(E)** acyl chains length and saturation were analyzed by quantitative mass spectrometry and are represented as the mean ± SEM (n=3) of the percentage of pmols relative to the total sum. Green arrows indicate fluorizoline-induced statistically significant changes, blue arrows indicate fluorizoline-induced tendency; orange arrows indicate Cre recombinase-induced changes, purple arrows indicate Cre recombinase-induced tendency. *$p < 0.05$.

To sum up, these data show that fluorizoline slightly increases the length of PEA and PC acyl chains but slightly decreases CL acyl chain length. Cre-mediated loss of PHBs increased PEA content as well as length and double bonds of PIN acyl chain length. On the whole, fluorizoline does not induce major changes in the whole cell phospholipid content.

2.8. PROHIBITINS MEDIATE THE MODULATION OF THE EXPRESSION OF DIFFERENT BCL-2 FAMILY MEMBERS UPON FLUORIZOLINE TREATMENT

Our group described that treatment with fluorizoline induces cytochrome *c* release and BAX/BAK dependent apoptosis (Pérez-Perarnau 2013, Pérez-Perarnau et al. 2014). These data suggest that fluorizoline triggers apoptosis through the mitochondrial apoptotic pathway. The execution of this apoptotic pathway depends on the balance between pro- and anti-apoptotic members of the BCL-2 family (Czabotar et al. 2014). To gain insight into the mechanism of apoptosis induction upon fluorizoline treatment, changes in the overall apoptosis mRNA expression profile were analyzed by reverse transcriptase multiplex ligation dependent probe amplification (RT-MLPA) in *Phb2*$^{fl/fl}$ MEFs. After 24 hours of treatment with 20 μM fluorizoline, upregulations of the pro-apoptotic members *Bim*, *Noxa*, *Bmf*, *Moap1* and *Smac* were observed, along with downregulations of the anti-apoptotic members *Bcl-2*, *Bcl-X*, *Hiap1* and *Survivin*; correlating with the apoptotic outcome. In addition, fluorizoline increased *Mcl-1*, *Flip* and *p21* and decreased *Bak* and *Htra2* mRNA levels (Fig. 2.23A). Although RT-MLPA includes probes for housekeeping genes, they were not included in the analysis as significant modulations were observed upon fluorizoline treatment.

As shown in figure 2.6, fluorizoline-induced decrease in viability requires the presence of PHBs. It is therefore conceivable that the modulations in apoptosis-related gene expression do not occur in cells lacking PHBs. To assess this, we transduced *Phb2*$^{fl/fl}$ MEFs with Cre recombinase for 72 hours and then treated them with 20 μM fluorizoline for 24 hours. Interestingly, Cre-mediated loss of PHBs abolished the modulations of mRNA levels triggered by fluorizoline (Fig. 2.23B). Therefore, the presence of PHBs is required for fluorizoline-induced changes in the apoptosis mRNA expression profile.

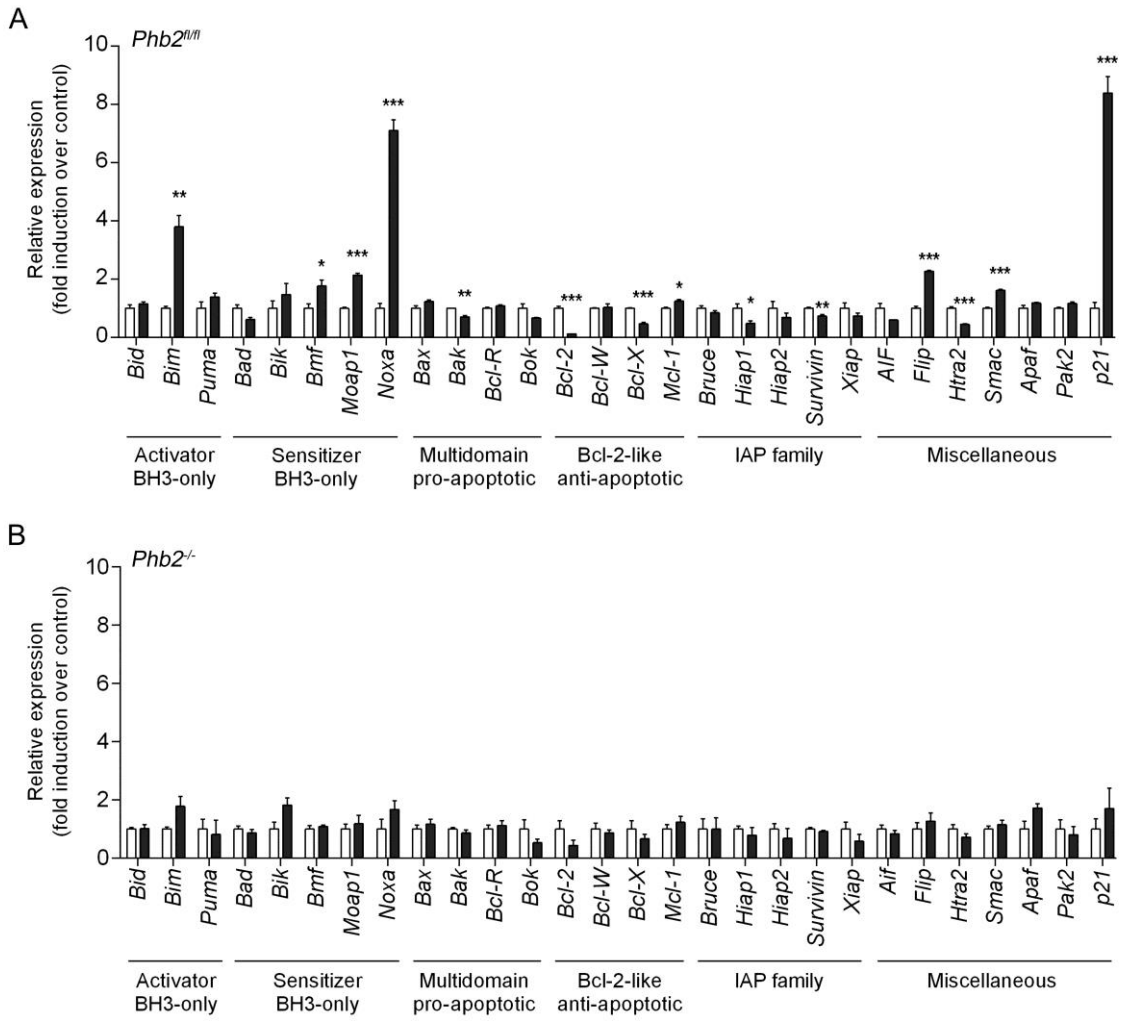

Figure 2.23. RT-MLPA analyses show PHB-dependent modulation of the expression of apoptosis related genes upon fluorizoline treatment. (A) *Phb2*$^{fl/fl}$ MEFs were untreated or treated with 20 μM fluorizoline for 24 hours. **(B)** *Phb2*$^{fl/fl}$ MEFs were transduced with Cre recombinase for 72 h and then untreated or treated with 20 μM fluorizoline for 24 hours. **(A, B)** mRNA levels were analyzed by RT-MLPA. White bars correspond to untreated cells, and grey bars to fluorizoline-treated cells. Data show the mean values of three independent experiments relative to the mean of the control. *$p < 0.05$, **$p < 0.01$, ***$p < 0.001$.

Interestingly, treatment with fluorizoline increased BIM protein levels in WT and *Phb2*$^{fl/fl}$ MEFs in the absence of Cre recombinase, while they were not modulated in Cre-transduced *Phb2*$^{fl/fl}$ MEFs, which lack PHBs (Fig. 2.24). Consistently, PARP was cleaved upon fluorizoline treatment in WT and *Phb2*$^{fl/fl}$ MEFs, but not in *Phb2*$^{-/-}$ MEFs. It would have been very interesting to study NOXA protein levels, but they could not be analyzed due to lack of proper antibodies detecting the mouse protein.

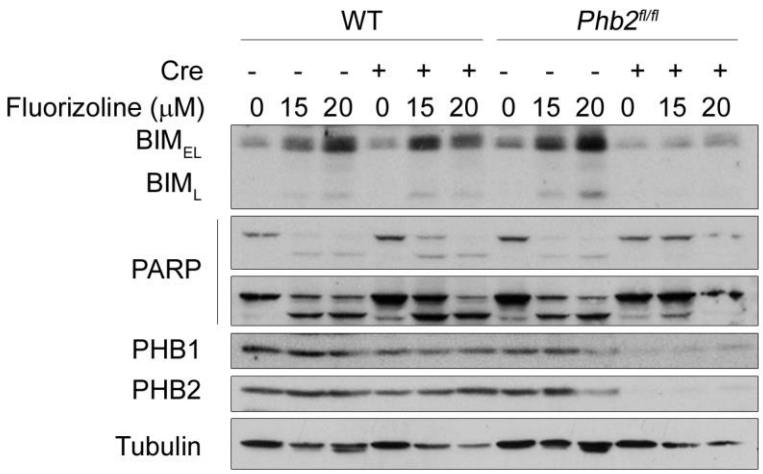

Figure 2.24. Fluorizoline induces BIM in a PHBs-dependent manner. WT and *Phb2*$^{fl/fl}$ MEFs were transduced or not with Cre recombinase for 72 hours and then untreated or treated with 15 or 20 μM fluorizoline for 24 hours. Protein levels were analyzed by western blot. This is a representative image of at least three independent experiments. Western blot analyses were performed by Dr. Iglesias-Serret.

There are more available antibodies to detect human BCL-2 family proteins, so we decided to further study fluorizoline-induced apoptosis by analyzing changes in the expression of BCL-2 family members in HeLa cells. To this end, we treated HeLa cells with 10 μM fluorizoline for 4, 8 and 24 hours and the apoptosis-related gene expression profile was examined by RT-MLPA. Interestingly, *BIM*, *PUMA*, *NOXA,* and *p21* mRNA levels were increased, while *BMF*, *AIF* and different IAP family members mRNA levels were downregulated after fluorizoline treatment (Fig. 2.25). *FLIP* mRNA levels are detected by two different probes; one of them increased yet the other one decreased upon fluorizoline treatment. Again, housekeeping genes were not included because fluorizoline significantly modulated their mRNA levels.

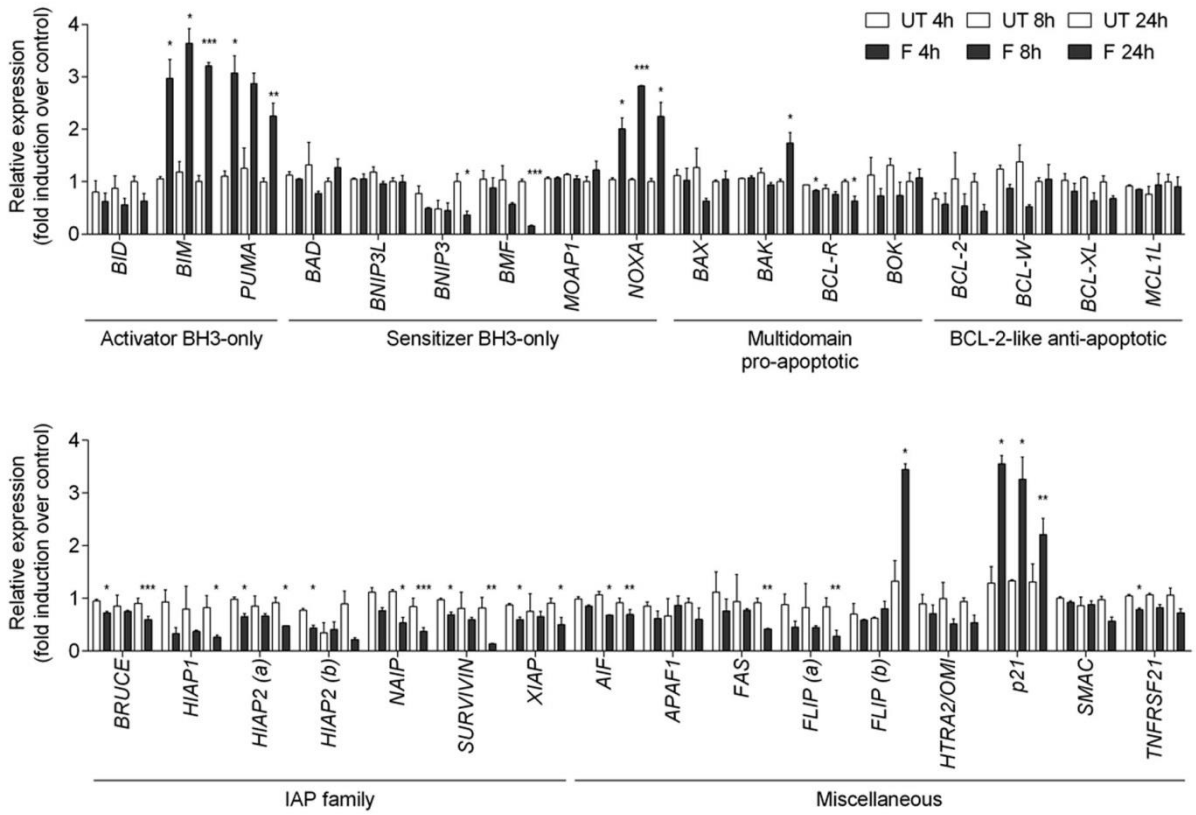

Figure 2.25. RT-MLPA analysis of apoptosis-related gene expression profile upon fluorizoline treatment in HeLa cells. HeLa cells were untreated (white bars) or treated with 10 μM fluorizoline (grey bars) for 4, 8 and 24 hours. mRNA levels were analyzed by RT-MLPA. Data show the mean ± SEM relative to the mean of the control (4 and 8 hours, n=2; 24 hours, n=3). *p < 0.05, **p < 0.01, ***p < 0.001.

Next, we sought to examine whether these modulations of the expression levels were leading to changes on the corresponding protein levels. We observed a time-dependent upregulation of BIM and NOXA protein levels as well as decreases in PUMA and MCL-1 (Fig. 2.26A). Despite dramatic decreases in *BCL-2* mRNA levels, fluorizoline did not significantly modulate its protein levels, in line with its long half-life (Merino et al. 1994). PHBs levels were not modified upon fluorizoline treatment, as described for other pro-apoptotic stimuli in different cell types (Coates et al. 2001). PARP cleavage was blotted as a control for apoptosis induction, which was pretty clear at 8 hours. Interestingly, OPA1 processing occurred within a time frame similar to PARP. Fluorizoline induced significant modulations of *Survivin* and *p21* mRNA levels. Nevertheless, after 24 hours of treatment, their protein levels were not modified (Fig. 2.26B).

It was important to assess whether these modulations were the cause or the consequence of apoptosis induction. To distinguish between these events, we incubated HeLa cells with pan-caspase inhibitor Q-VD-OPh and then treated them with fluorizoline for 24 hours. BIM and NOXA increases preceded caspase activation, as pre-incubation with Q-VD-OPh could not block their upregulation

(Fig. 2.26C). In contrast, caspase inhibition abolished MCL-1 and PUMA decrease mediated by fluorizoline treatment, which suggests that this event is downstream of caspase activation. This is in agreement with previous reports caspase-dependent proteolysis of these proteins (Herrant et al. 2002, 2004, Hadji et al. 2010).

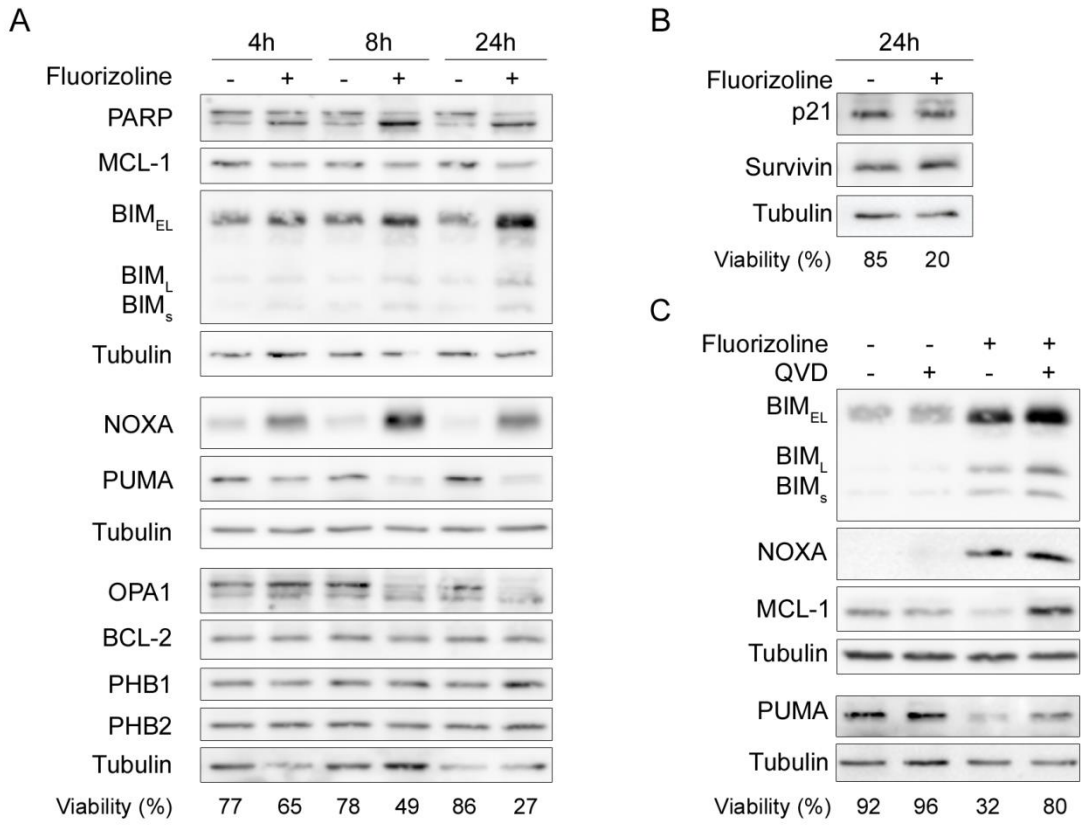

Figure 2.26. Fluorizoline induces changes in protein levels of various BCL-2 family members in HeLa cells. **(A)** HeLa cells were untreated or treated with 10 μM fluorizoline for 4, 8 and 24 hours. **(B)** HeLa cells were untreated or treated with 10 μM fluorizoline for 24 hours. **(C)** HeLa cells were pre-incubated with 20 μM caspase inhibitor Q-VD-OPh for 30 minutes and then treated with 10 μM fluorizoline for 24 hours. Viability was measured by flow cytometry and it is expressed as the percentage of non-apoptotic cells (annexin V-negative). Protein levels were analyzed by western blot. A and B, n≥3, except for p21 (n=1). C, n=3 except for PUMA (n=1).

DISCUSSION

1. CHARACTERIZATION OF AICAR-INDUCED APOPTOSIS

AICAR INDUCES ZMP-DEPENDENT BUT AMPK-INDEPENDENT APOPTOSIS IN MOUSE EMBRYONIC FIBROBLASTS

Our group has described AICAR-induced apoptosis in chronic lymphocytic leukemia (CLL) cells, though the exact mechanism of action remains unknown. CLL cells are difficult to transfect, which hinders the study of the mechanism at a molecular level. Here we propose mouse embryonic fibroblasts (MEFs) as an alternative model. AICAR induces cell cycle arrest and apoptosis in trisomic MEFs (Tang et al. 2011), while it inhibits proliferation without affecting the viability in primary WT MEFs (Jones et al. 2005). Our results show that AICAR induces ZMP-dependent but AMP-activated protein kinase (AMPK)-independent apoptosis in immortalized WT MEFs (also observed in González-Gironès 2012), consistent with the mechanism of action reported in CLL cells (Campàs et al. 2003, Santidrián et al. 2010). The reason why treatment with AICAR results in such different phenotypes in MEFs remains unknown.

AICAR is widely known as an activator of AMPK. This kinase has been historically perceived as anti-tumorigenic because it is the center of a signaling network that involves well-known tumor suppressors, such as LKB1 and TSC1/2. AMPK activation results in the inhibition of most of the metabolic changes that are necessary for rapidly proliferating cells (Hardie et al. 2012), which is consistent with an anti-tumorigenic role. Along the same lines, loss of AMPK induced the Warburg effect and accelerated MYC-induced lymphomagenesis (Faubert et al. 2013). Activation of the AMPK-mTOR pathway decreases MCL-1 protein levels, which leads to a sensitization to the extrinsic apoptosis (Pradelli et al. 2010a) or to ABT-737-induced apoptosis (Meynet et al. 2013). In addition, different drugs that activate AMPK, including AICAR, metformin or phenformin, can inhibit cancer cell growth and proliferation, which was initially understood as a proof that AMPK activation was indeed mediating the anti-tumorigenic effects (Hardie and Alessi 2013, Liang and Mills 2013, Faubert et al. 2015).

Nevertheless, our findings show that MEFs lacking AMPK are sensitive to AICAR treatment, proving an AMPK-independent mechanism for the induction of apoptosis. Recently, Vincent and colleagues studied the effect of AICAR in MEFs. Fully in keeping with our results, AICAR induced apoptosis and inhibited proliferation and glucose consumption in an AMPK-independent manner (Vincent et al. 2014). In addition, direct activation of AMPK failed to trigger apoptosis in MEFs (our results and Vincent et al. 2014), as observed in CLL cells (Santidrián et al. 2010), HEK293 cells (Vincent et al. 2014) and glioma cells (Liu et al. 2014). Other findings also point towards AMPK-independent effects of AICAR. First, follicular lymphoma cells are resistant to AICAR-induced apoptosis despite presenting activation of AMPK (Campàs et al. 2005). In Jurkat cells, AICAR

triggers apoptosis without inducing the phosphorylation of AMPK neither requiring ZMP accumulation (López et al. 2003). Furthermore, AICAR inhibits respiration in intact rat hepatocytes (Guigas et al. 2007), increases the radiosensitization of prostate cancer cell lines (Isebaert et al. 2011), inhibits autophagy (Meley et al. 2006, Viana et al. 2008), blocks phosphatidylcholine synthesis (Jacobs et al. 2007) and protects from heat-induced sudden death in RyR1 mutant mice (Lanner et al. 2012) independently of AMPK. Consistent with these AMPK-independent effects of AICAR, the anti-tumorigenic effects of other well-known AMPK activators, such as metformin, phenphormin or 2-deoxyglucose, were proved to be independent of AMPK in a wide range of cell types, including MEF and CLL cells (Santidrián et al. 2010, Liu et al. 2014, Vincent et al. 2014).

In fact, AMPK might be playing a survival role. We show that loss of AMPK sensitizes MEFs to AICAR-induced apoptosis, which was also observed by others in MEFs (Shaw et al. 2004, Vincent et al. 2014), as well as in mouse B lymphocytes (Santidrián et al. 2010, González-Gironès 2012), and in glioma cells (Liu et al. 2014). Consistently, it has been reported that AMPK promotes survival facing various stresses in MEFs (Jeon et al. 2012) and in other cell types (Ido et al. 2002, Lee et al. 2003, Liu et al. 2012, Estañ et al. 2012, Shackelford et al. 2013, Shao et al. 2014), although the exact mechanism remains unknown. It was proposed that AMPK promotes cell survival by redox regulation. AMPK activation maintains NADPH levels, which are critical for cell survival under energy stress conditions (Jeon et al. 2012). In this line, AMPK enhances SIRT1 activity by increasing NAD^+ levels, resulting in the deacetylation and the consequent degradation of SIRT1 target proteins, such as p53 (Cantó et al. 2009, Wang et al. 2012). Fully in keeping with the pro-survival role, AMPK has been linked to tumor development and progression (Hardie and Alessi 2013, Liang and Mills 2013, Faubert et al. 2015). Direct activation of AMPK by A769662 enhances cell proliferation under metabolic stress conditions (Vincent et al. 2014). Therefore, AMPK activation may facilitate tumor growth by providing cells the flexibility to adapt to the metabolic stresses that can occur along the tumor progression, such as anchorage-independent growth and glucose or oxygen limitation.

Interestingly, we have also shown that AICAR required ZMP but not AMPK to induce changes in the apoptosis-related gene expression profile in MEFs. Treatment with AICAR upregulated *Bim*, *Noxa*, and *Puma* mRNA levels, while decreased *Bcl-2* mRNA levels. The expression of BCL-2 family members was analyzed by RT-MLPA and RT-qPCR, being the latter more sensitive. In this regard, increases in *Bim* and *Puma* mRNA levels could only be detected by RT-qPCR but not by RT-MLPA. Despite increases in *Puma* mRNA levels, the lack of this BH3-only protein did not decrease the sensitivity to AICAR-induced apoptosis in MEFs. This result is consistent with the lack of resistance observed in $Bim^{-/-}/Puma^{-/-}$ B and T lymphocytes from mouse spleen and in $Noxa^{-/-}/Puma^{-/-}$ primary MEFs (González-Gironès 2012). Interestingly, MEFs lacking *Bim* and *Noxa* display high resistance to the pro-apoptotic effects of AICAR (González-Gironès 2012), in agreement with the role of these

BH3-only proteins in AICAR-induced cell death in CLL cells and mouse B lymphocytes (Santidrián et al. 2010).

Noxa expression is regulated by different transcription factors, including p53, p73, hypoxia-inducible factor 1α (HIF1α), E2F-1, c-Myc, cAMP response element (CRE)-binding proteins and SP-1 (Nikiforov et al. 2007, Ploner et al. 2008, Grande et al. 2012). Importantly, analysis of the regulation of *Noxa* promoter ruled out HIF, p53 and CRE as mediators of AICAR-induced increases of this gene (González-Gironès 2012). Regarding *Bim,* several transcriptional factors, including FOXO3a, E2F-1, and c-Jun, have been involved in its regulation (Piñon et al. 2008). Therefore, E2F-1 appears as the common factor regulating NOXA and BIM. However, E2F-1 seems not to be implicated here since AICAR induces apoptosis in wild-type and *E2F-1*$^{-/-}$ mouse lymphocytes alike (González-Gironès 2012). Further experiments are required to elucidate how AICAR treatment modulates the expression of *Bim* and *Noxa*. For this purpose, MEFs are a useful cellular system for the elucidation of the mechanism of action of AICAR, as the induction of apoptosis in MEFs, CLL cells and mouse B lymphocytes is highly similar.

THE ROLE OF p53 IN AICAR-INDUCED APOPTOSIS

Treatment with AICAR induces a cell cycle arrest through AMPK activation and p53 phosphorylation in primary MEFs (Jones et al. 2005). Similarly, p53 was proposed to mediate AICAR anti-proliferative effects in trisomic MEFs, although induction of apoptosis in trisomic cancer cell lines was independent of p53 mutational status (Tang et al. 2011). When we analyzed the role of p53 in AICAR-induced apoptosis, we observed that the pro-apoptotic effects after treatment with high doses of AICAR were p53-independent. Strikingly, our results also show that low doses of AICAR required an active p53 pathway to induce apoptosis. Different effects of AICAR depending on the dose were also observed in primary MEFs. Treatment with 0.5 mM AICAR induces an increase in the size of the cell, while 2 mM AICAR fails to modify it (Jones et al. 2005). Therefore, the range of doses of AICAR seems to activate different pathways which may have different consequences for MEFs.

Regardless of the dose-dependent differential effects, it is clear that the range of doses normally used in the rest of the experiments were inducing apoptosis independently of p53. This is consistent with previous results of our group, showing that AICAR efficiently triggers apoptosis in mouse lymphocytes lacking *p53* (González-Gironès 2012). In addition, the pro-apoptotic effects of AICAR do not induce p53 phosphorylation or accumulation in CLL cells, and do not depend on the mutational status of p53 (Campàs et al. 2003, Santidrián et al. 2010).

A p53-independent mechanism of action is crucial for the successful outcome of treatments for CLL. Mutations in p53 are frequent among patients with advanced and chemotherapy-resistant disease (Shindiapina et al. 2014). Hence, AICAR constitutes an interesting therapeutic strategy for CLL patients with defects in the p53 pathway.

PYRIMIDINE STARVATION AS A PUTATIVE MECHANISM OF ACTION OF AICAR

It was reported that AICAR triggered apoptosis in multiple myeloma (MM) cells by inhibiting uridine monophosphate synthase (UMPS), which leads to pyrimidine starvation. AICAR pro-apoptotic effects were blocked by addition of uridine and cytidine, and thymidine partially did it (Bardeleben et al. 2013). A similar mechanism of action has been reported for several anticancer agents, such as methotrexate, 5-fluorodeoxyuridine or IMP dehydrogenase inhibitors, which inhibit dNTP synthesis. This causes imbalances in the nucleotide pool that impair DNA synthesis and repair, leading to severe DNA damage and cell cycle arrest. These agents are frequently used to treat different solid and hematological malignancies, either alone or in combination treatment regimens (Wilson et al. 2014).

In CLL cells, we observed that addition of uridine and thymidine efficiently inhibited AICAR-induced apoptosis. Compared to MM cells, higher doses of pyrimidines were required to abolish the apoptotic effects upon AICAR treatment in CLL cells. Different activities or expression levels of the nucleoside transporters (NTs) in MM or CLL cells could explain the differences in the required doses for blocking AICAR-induced apoptosis depending on the model. AICAR influx is mediated by NBTI-sensitive NTs, which basically includes equilibrative NTs (ENTs) (Campàs et al. 2003). CLL cells are known to express both concentrative NTs (CNTs) and ENTs, whose expression or activity can be modulated by different stimuli, including nucleoside-derived drugs (Pastor-Anglada et al. 2004, Fernández-Calotti et al. 2011). On the other hand, NTs expression in MM cells has been less studied. Interestingly, AICAR entrance to a MM cell line (U266) could be inhibited by NBTI (Baumann et al. 2007), showing that at least NBTI-sensitive transporters are expressed. Uridine and thymidine can enter to the cell through both CNTs and ENTs (Young et al. 2013), while AICAR is mainly transported through ENTs (Campàs et al. 2003). As ENTs function according to the concentration of nucleosides at both sides of the membrane, addition of high doses of pyrimidines might saturate the NTs and thus block AICAR entrance to the cell. Considering that the cytotoxic activity of AICAR relies on its uptake (Campàs et al. 2003), it is conceivable that impaired uptake after pyrimidine addition may significantly modulate intracellular AICAR bioavailability, and therefore, its pro-apoptotic capacity. In agreement with this hypothesis, thymidine completely inhibited AICAR-induced acetyl-CoA carboxylase (ACC) phosphorylation and apoptosis at any of the time points that were studied, suggesting that it was blocking AICAR uptake. Bardeleben and collegues did not check

whether addition of pyrimidines was blocking AICAR entrance to the MM cells. Hence, it cannot be discarded that the rescue observed after pyrimidine addition in MM cells is caused by an impairement of AICAR uptake.

Strikingly, uridine delayed ACC phosphorylation in CLL cells, suggesting that it was somehow impairing AICAR entrance but not totally blocking it. Uridine is an intermediate in the *de novo* synthesis pathway of pyrimidines, which can be subsequently modified to generate UMP, TMP or CMP. Thus, addition of uridine alone may be able to counteract AICAR-induced pyrimidine starvation. Accordingly, patients with deficiencies in UMPS can be bypassed by treatment with uridine (Balasubramaniam et al. 2014).

Cytidine is incorporated to pyrimidine metabolism through deamination to uridine, a reaction carried out by cytidine deaminase. Therefore, cytidine could theoretically generate CMP, UMP and TMP and rescue AICAR-induced pyrimidine starvation as effectively as uridine does. Nevertheless, addition of cytidine did not inhibit AICAR-induced apoptosis in CLL cells. In fact, we observed that addition of cytidine was increasing the apoptosis induced after treatment with 2 mM AICAR. One possible cause of this effect is that CLL cells may have impaired cytidine deaminase activity, being unable to use cytidine for the rescue of AICAR-induced apoptosis. Excessive cytidine along with inhibition of *de novo* pyrimidine synthesis was reported to enhance cell death due to an unbalanced ratio between CTP and UTP (Chan and Howell 1989), which could explain the enhanced pro-apoptotic effects that we observed.

Other discrepancies have been observed comparing AICAR mechanism of action in CLL cells and MM cells. Adenosine abolished AICAR-mediated apoptosis in CLL cells (Campàs et al. 2003), but did not block it in MM cells (Bardeleben et al. 2013). In addition, treatment with AICAR results in the accumulation of ZMP and the consequent phosphorylation of AMPK and ACC in CLL cells (Campàs et al. 2003, Campàs 2004), though neither ZMP accumulation nor AMPK phosphorylation were observed upon AICAR treatment in two MM cell lines (Bardeleben et al. 2013).

RPMI 8226 cells were used as a control for our experiments, as it is a MM cell line that was studied by Bardeleben and collegues. Nevertheless, the percentage of apoptotic cells varied largely between the two groups. One could think that the differences could be attributed to the viability assay (measure of active caspase 3 *versus* phosphatidylserine exposure). Nevertheless, another manuscript reported a percentage of annexin V-positive cells similar to Bardeleben (Baumann et al. 2007). Hence, it is possible that RPMI 8226 clones have evolved differently and now show different responses to AICAR.

All in all, it is obvious that AICAR induces apoptosis in MM and CLL cells through very distinct mechanisms, which could explain that addition of pyrimidines have different effects on AICAR pro-apoptotic effects depending on the cell type analyzed.

REACTIVE OXYGEN SPECIES PRODUCTION IN AICAR-TREATED CLL CELLS

AICAR is an intermediate metabolite of the purine catabolism. Xanthine oxidase is involved in the last two steps, catalyzing hypoxanthine to xanthine and further to uric acid; generating reactive oxygen species (ROS). Allopurinol and febuxostat, two xanthine oxidase inhibitors, partially reverted AICAR-induced apoptosis and ROS production in CLL cells (González-Gironès 2012). Nevertheless, here we show that the generation of ROS is a caspase-dependent event, which discards it as a putative cause of induction of apoptosis. Xanthine oxidase inhibitors decreased ZMP accumulation and partially reverted ATP depletion induced by AICAR in CLL cells through an unknown mechanism (González-Gironès 2012). As ZMP accumulation is essential for AICAR-induced apoptosis (Campàs et al. 2003), it is conceivable that allopurinol and febuxostat abrogate the pro-apoptotic effects of AICAR by inhibiting the alterations in the nucleotide pool.

Taking our results together with the previous findings, we propose the following mechanism of apoptosis induction by AICAR (Fig. D.1). AICAR enters the cell through NBTI-sensitive transporters and is phosphorylated to ZMP by adenosine kinase. Through an unknown mechanism, BIM and NOXA are upregulated, which results in the release of cytochrome *c* to the cytosol and the subsequent induction of caspase-mediated apoptosis.ROS are produced as a consequence of caspase activation. The accumulation of ZMP leads to AMPK activation, though this event is not required for AICAR-induced apoptosis. In fact, AMPK seems to counteract the pro-apoptotic effects of AICAR. In addition, the mutational status of p53 and ATM does not influence the pro-apoptotic activity of AICAR.

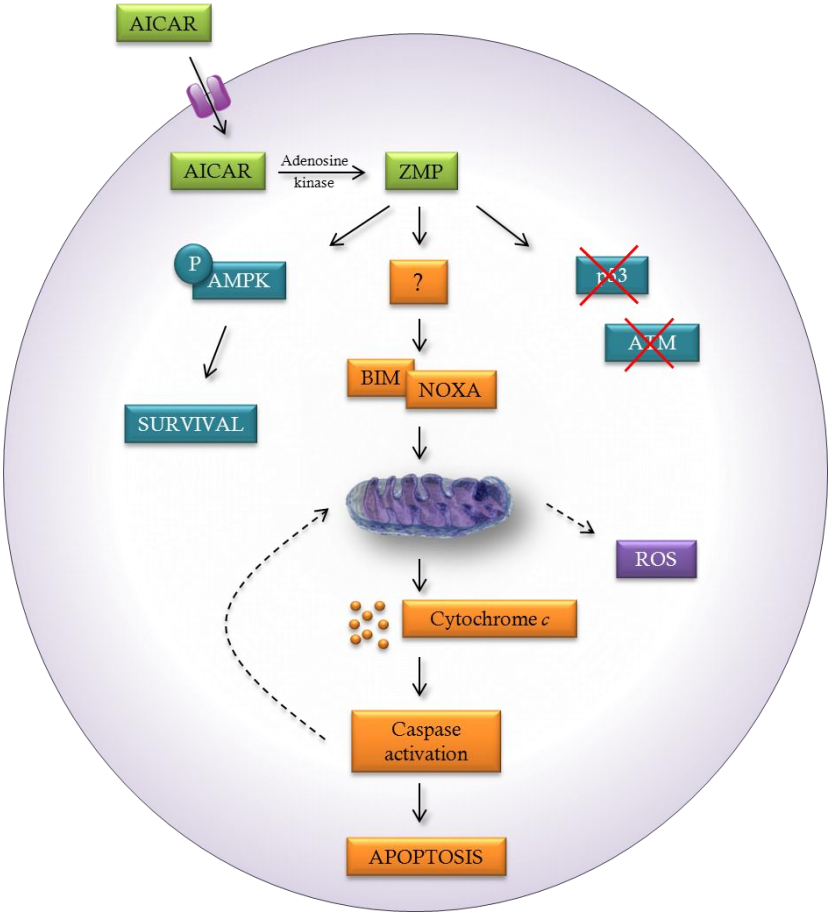

Figure D.1. Proposed mechanism of action of AICAR. ROS, reactive oxygen species. Caspase-dependent events are indicated in dashed arrows.

2. FLUORIZOLINE REQUIRES PROHIBITINS TO TRIGGER THE MITOCHONDRIAL APOPTOTIC PATHWAY

OPA1 PROCESSING UPON FLUORIZOLINE TREATMENT

Loss of prohibitins (PHBs) was reported to induce optic atrophy 1 (OPA1) processing, fragmentation of the mitochondrial network and cristae disorganization. These defects are caused by the loss of L-OPA1, as reexpression of a non-cleavable form of L-OPA reverts the phenotype (Merkwirth et al. 2008). In the same line, downregulation of OPA1 induces mitochondrial fragmentation and disorganization of the cristae (Olichon et al. 2003, Arnoult et al. 2005, Ishihara et al. 2006, Frezza et al. 2006). Interestingly, HeLa cells treated with fluorizoline also showed disappearance of L-OPA1, fragmentation of the mitochondrial network and cristae remodelling (Pérez-Perarnau 2013). This suggested that fluorizoline-induced apoptosis was indeed mediated by PHBs. OPA1 is known to have a crucial role in the maintenance of cristae structure in the inner mitochondrial membrane (IMM), where most of the cytochrome *c* resides. Upon treatment with various apoptotic stimuli, OPA1 complexes are disassembled (Frezza et al. 2006, Landes et al. 2010, Jiang et al. 2014), a step that is required for the reorganization of the mitochondrial cristae and the release of cytochrome *c* to the intermembrane space (Yamaguchi et al. 2008). Thus, bearing in mind the link between OPA1 and the induction of apoptosis, it was conceivable that other pro-apoptotic insults were also affecting OPA1 protein levels. Indeed, we observed that not only fluorizoline, but also ActD, STS and capsaicin induced the loss of L-OPA1. Importantly, inhibition of caspase activation blocked ActD- and fluorizoline-induced phosphatidylserine exposure but not the loss of L-OPA1, showing that it is an apoptotic event occurring upstream of caspase activation. These findings are in agreement with other reports describing OPA1 processing after treatment with various pro-apoptotic stimuli (Alaimo et al. 2014, Jiang et al. 2014), which could not be inhibited by the presence of the broad caspase inhibitor z-VAD.fmk (Ishihara et al. 2006). Along this line, BIM-induced apoptosis led to the disassembly OPA1 complexes and the release of OPA1 from the mitochondria, without requiring the activation of the caspases (Yamaguchi et al. 2008).

It is worth mentioning that various stresses, such as loss of membrane potential or heat stress, induce OPA1 processing and mitochondrial network fragmentation. Nevertheless, cytochrome *c* remains in the mitochondria, since the mitochondrial outer membrane remains intact (Duvezin-Caubet et al. 2006, Griparic et al. 2007, Baker et al. 2014). Hence, OPA1 processing does not always correlate with apoptosis induction; though apoptosis induction seems to imply OPA1 processing.

All in all, OPA1 processing cannot be only understood as a direct indicator of loss of PHBs functions, as other pro-apoptotic stimuli and stresses also result in the loss of L-OPA1. Therefore, it is not a valid proof-of-concept to demonstrate that fluorizoline induces apoptosis by targeting PHBs.

FLUORIZOLINE REQUIRES PROHIBITINS TO INDUCE APOPTOSIS

We sought to use another strategy in order to analyze whether PHBs were required for fluorizoline-induced apoptosis. Downregulation of PHBs in HeLa cells resulted in cell detachment without reduction in viability (Pérez-Perarnau 2013), in line with previous reports showing altered phenotypes upon loss of PHBs in HeLa cells (Rajalingam et al. 2005, Kasashima et al. 2006, Sievers et al. 2010, Sato et al. 2011). Consequently, we moved to *Phb2*$^{fl/fl}$ MEFs model, as it was reported that loss of PHBs blocked cell proliferation without inducing apoptosis (Merkwirth et al. 2008). We proved that PHBs mediate the pro-apoptotic effects of fluorizoline using two different approaches. First, *Phb2* was depleted by Cre recombinase transduction in *Phb2*$^{fl/fl}$ MEFs; and second, *Phb2* levels were downregulated by siRNA transfection in MEFs. In both cases, loss of PHBs conferred strong resistance to fluorizoline. Therefore, fluorizoline is as a new synthetic agent that reduces cell viability by specifically targeting PHBs.

We tried to carry out a genetic rescue by using two different cell lines that re-express PHB2. Nevertheless, their sensitivity to various apoptotic insults was lower than WT and *Phb2*$^{fl/fl}$ MEFs. This ruled them out as suitable genetic rescue models, as putative different sensitivity to fluorizoline would not be caused by the distinct levels of PHBs but by intrinsic resistance to pro-apoptotic stimuli.

PHBs have a key role in maintaining mitochondrial homeostasis. High expression of PHBs has been found in cells which heavily depend on mitochondrial function, notably proliferating cells. It is conceivable that these cells may be particularly susceptible to the lack of functional PHBs (Artal-Sanz and Tavernarakis 2009). In fact, downregulation of PHBs in various cell lines was reported to block cell proliferation (Merkwirth et al. 2008, Sievers et al. 2010, Jiang et al. 2015) as well as to induce apoptosis (Kasashima et al. 2006, Sánchez-Quiles et al. 2010, Kowno et al. 2014). Overexpression of PHBs protects cells from apoptosis induced by different stimuli (Fusaro et al. 2002, Zhou et al. 2013a, 2013b, Thuaud et al. 2013, Chowdhury et al. 2013, Han et al. 2014, Wang et al. 2014), consistent with the cytoprotective role of PHB1 (Thuaud et al. 2013). PHBs exert their anti-apoptotic function via OPA1 in MEFs, as the increased sensitivity to apoptosis observed in the absence of PHBs can be counteracted by re-expression of a non-cleavable variant of OPA1 (Merkwirth et al. 2008). In addition, it was reported that PHBs overexpression inhibited apoptosis through the induction of BCL-2 and BCL-X_L (Chowdhury et al. 2013), and downregulation of PHBs reduced BCL-X_L levels (Sripathi et al. 2011).

Importantly, PHBs therapeutic potential has been extensively discussed by many authors (Mishra et al. 2005, Thuaud et al. 2013). PHBs play a key role in regulating a diverse array of physiological processes and are amenable to modulation with small molecules. Hence, targeting PHBs would be a useful therapeutic approach for the treatment of a variety of diseases. In cancer, although some reports point to an anti-tumorigenic role of PHBs, most of the current data link PHBs to tumor development (Theiss and Sitaraman 2011, Thuaud et al. 2013, Han et al. 2014, Jiang et al. 2015, Ho et al. 2015). Fluorizoline was able to induce apoptosis in a wide range of cancer cell lines, including glioma or prostate cell lines (Pérez-Perarnau et al. 2014), in which PHBs were reported to be anti-tumorigenic (Dart et al. 2012, Qian et al. 2013). Considering the pro-apoptotic capacity of fluorizoline, this new agent with fluorinated thiazoline scaffold emerges as a potential new strategy for cancer treatment.

Stomatin-like protein 2 (SLP-2) is a member of the stomatin-prohibitin-flotilin-HflC/K (SPFH) superfamily. In the IMM, SLP-2 binds to cardiolipin and PHBs, forming membrane microdomains that facilitate mitochondrial biogenesis and function (Da Cruz et al. 2008, Christie et al. 2011). We observed that the loss of SLP-2 does not confer resistance to fluorizoline treatment. It was reported that shRNA-mediated downregulation of SLP-2 leads to a reduction of PHB1 protein levels, suggesting that SLP-2 is crucial for the stability of PHB1 (Da Cruz et al. 2008). However, PHBs protein levels in SLP-2 KO (SKO) MEFs were assessed by western blot by Hans Georg Sprenger (Dr. Langer's group) and no differences were found between *Phb2*$^{fl/fl}$ and SKO MEFs. Accordingly, total protein levels of PHB and the assembly of PHB complexes were not affected in T cells lacking SLP-2, although the compartmentalization of these proteins within the cell was abnormal (Christie et al. 2012, Mitsopoulos et al. 2015). Regardless of this controversy, SKO MEFs were sensitive to the pro-apoptotic effects of fluorizoline, proving that SLP-2 is not required for fluorizoline-induced apoptosis.

PROHIBITINS COMPLEXES IN THE INNER MITOCHONDRIAL MEMBRANE

It was reported that *Phb2*$^{-/-}$ MEFs have impaired cell proliferation (Merkwirth et al. 2008). Nevertheless, we observed some cell proliferation in *Phb2*$^{-/-}$ MEFs and therefore we tried to generate a stable *Phb2*$^{-/-}$ cell line. Among 83 clones that were analyzed, none of them presented both *Phb2* alleles depleted. As PHBs are crucial for cell proliferation, the absence of *Phb2*$^{-/-}$ clones may be due to their reduced proliferation rate. Those cells with PHBs grow faster, while the *Phb2*-depleted clones have a clear disadvantage and grow more slowly. This is in agreement with a previous report in which shRNA-mediated PHB1 silencing was performed in various cancer cell lines. Prolonged culture of these cells led to a loss of shRNA-expressing cells, which was not due to increased apoptosis of this

population but due to faster growth of the non-transduced one (Sievers et al. 2010). A high percentage of the analyzed clones were heterozygous (*Phb2*$^{fl/-}$), and we further studied their response to fluorizoline compared to homozygous clones (*Phb2*$^{fl/fl}$). Interestingly, the heterozygous clones had lower protein levels of PHB 1 and 2, which were not enough to maintain the balance of L-OPA1 and S-OPA1 forms. However, the heterozygous and homozygous clones displayed similar sensitivity to fluorizoline-induced apoptosis.

PHBs are found in very large complexes that presumably act as lipid and protein scaffolds, creating functional microdomains within the IMM. These platforms may be limiting the access of proteases to their substrates (Osman et al. 2009b, McBride and Soubannier 2010). OMA1 is a protease that cleaves OPA1 upon loss of membrane potential, heat stress or apoptosis induction (McBride and Soubannier 2010, Zhang et al. 2014, Richter-Dennerlein et al. 2014, Jiang et al. 2014). Importantly, downregulation of PHBs reduces L-OPA1 levels in HEK293 cells, which are restored through OMA1 downregulation (Richter-Dennerlein et al. 2014). These results suggest that OMA1 is the protease responsible for OPA1 processing upon loss of PHBs (Fig. D.2).

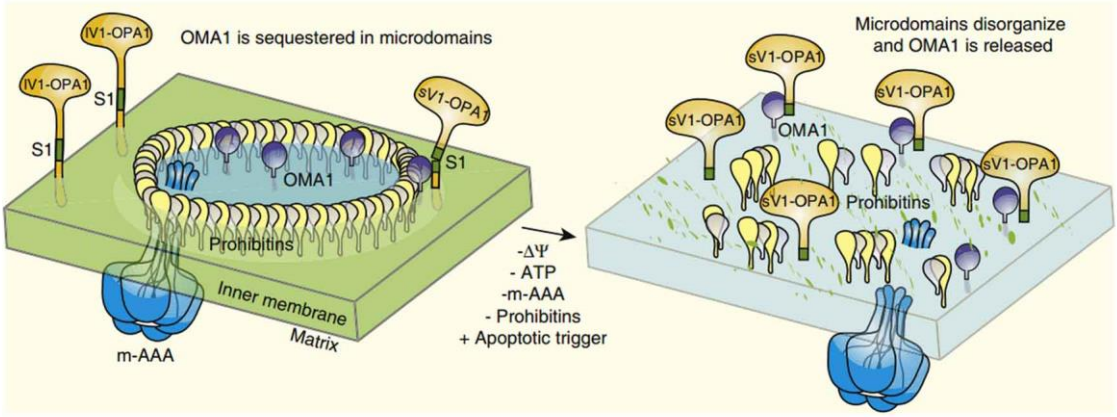

Figure D.2. Model of PHBs microdomains in the IMM that may control OPA1 processing. PHBs supercomplexes would form a microdomain sequestring OMA1 from OPA1. Mitochondrial dysfunction, loss of PHBs or pro-apoptotic stimuli would lead to the destabilization and/or disassembly of these platforms, allowing OMA1 to access OPA1 and accelerate processing of L-OPA1 to S-OPA1 forms. Adapted from McBride and Soubannier 2010.

In *Phb2*$^{fl/-}$ MEFs, the reduced protein levels of PHBs may lead to the disruption of the microdomains in the IMM, allowing OMA1 to reach and cleave OPA1. The fact that fluorizoline is still capable of inducing apoptosis in *Phb2*$^{fl/-}$ MEFs suggests that its mechanism of action may not be based on the disruption of PHBs megacomplexes in the IMM.

Accordingly, BN-PAGE analysis revealed that PHBs complex and prohibitin/mAAA protease (PMA) supercomplexes are maintained in spite of fluorizoline treatment. In addition, western blot analyses show stable steady state levels of PHBs even after incubation with fluorizoline. The loss of either PHB1 or PHB2 might destabilize PHBs mitochondrial complex, leading to the activation of quality control mechanisms which would degrade the other partner (Browman et al. 2007, Osman et al. 2009b). Therefore, all these results suggest that fluorizoline may not be inducing apoptosis by massively affecting the assembly of PHBs complex and PMA supercomplexes.

Of note, PHBs complexes have a huge molecular weight. Subtle changes in the composition of the complexes, e.g. loss or incorporation of small proteins, would not be detected by BN-PAGE. One possible mechanism of action of fluorizoline is affecting the specific binding of PHBs to other interacting partners, without grossly altering the complexes in the IMM. Thus, further experiments would be necessary to characterize more precisely fluorizoline-induced changes in PHBs complexes. In this sense, *Phb2*$^{fl/fl}$*::CNAP-Phb2* MEFs could be a very useful tool to study PHBs interactome in the presence or absence of fluorizoline.

The proposed scaffold function of PHBs in the IMM contributes to the homeostasis of different phospholipids (Osman et al. 2009b, Richter-Dennerlein et al. 2014). Downregulation of PHBs in HEK293 cells resulted in a decrease in the amounts of cardiolipin (CL) and phosphatidylethanolamine (PEA) as well as an increase in phosphatidylinositol (PIN). Furthermore, PEA, CL, PIN, phosphatidylcholine (PC), phosphatidylserine (PS), phosphatidic acid (PA), and phosphatidylglycerol (PG) showed longer and less saturated acyl chains in PHB-depleted cells (Richter-Dennerlein et al. 2014). Our analysis of the phospholipid composition of fluorizoline-treated or Cre-transduced *Phb2*$^{fl/fl}$ MEFs did not reveal major changes. Fluorizoline slightly increased the length of PEA and PC acyl chains but slightly decreased CL acyl chain length. Cre-mediated loss of PHBs increased PEA content as well as length and double bonds of PIN acyl chain length.

There is an obvious disagreement between the reported alterations in the phospholipidome and our results. There are several experimental differences that could explain this incoherence: the analyzed cell line (human HEK293 *versus* MEFs), the technique used for reducing PHBs levels (siRNA transfection *versus* Cre recombinase transduction) and the analyzed cellular fraction (isolated mitochondria *versus* whole cell extract).

Taken together, the sensitivity to fluorizoline of clones that cannot maintain L-OPA1 forms, the proper assembly of PHBs complex and PMA and the unaltered phospholipidome upon fluorizoline treatment strongly suggest that fluorizoline does not induce apoptosis by massively affecting the assembly PHBs complexes in the IMM.

PROHIBITINS MEDIATE FLUORIZOLINE-INDUCED CHANGES IN THE EXPRESSION OF BCL-2 FAMILY MEMBERS

Treatment with fluorizoline induced changes in the mRNA expression of various BCL-2 family members in *Phb2*$^{fl/fl}$ MEFs, including *Bim* and *Noxa* mRNA levels. Importantly, these changes required the presence of PHBs, which proves that PHBs mediate fluorizoline-induced transcriptional modulations. Accordingly, BIM protein levels were increased in WT and *Phb2*$^{fl/fl}$ MEFs, while loss of PHBs blocked it in *Phb2*$^{-/-}$ MEFs. *Noxa* mRNA levels were significantly modulated upon fluorizoline treatment, though their protein levels could not be detected due to lack of proper antibodies. Therefore, we moved to HeLa cells as there are more available antibodies detecting human BCL-2 family proteins. Treatment with fluorizoline upregulated *BIM* and *NOXA* mRNA and protein levels, in a time- and dose-dependent manner. Interestingly, protein increases preceded caspase activation, which could explain the apoptotic outcome. In contrast, caspase activation was required for fluorizoline-induced decreases in MCL-1 and PUMA protein levels, consistent with their known caspase-dependent proteolysis (Herrant et al. 2002, 2004, Hadji et al. 2010).

In addition to their role in mitochondria, PHBs also localize in other cellular compartments, including the nucleus and the plasma membrane, in a wide range of cell types (Mishra et al. 2010, Thuaud et al. 2013). In the plasma membrane, PHBs have been involved in the activation of the signaling pathways Ras-Raf-MAPK and the tyrosine kinase Syk (Rajalingam et al. 2005, Chiu et al. 2013, Kim et al. 2013, Chowdhury et al. 2014). In the nucleus, PHBs were reported to regulate the activity of various transcription factors such as p53, E2F1, and estrogen receptor (Thuaud et al. 2013). Whether the fluorizoline-induced transcriptional modulations are directly mediated by nuclear PHBs or indirectly mediated by PHBs in other cellular compartments requires further analysis.

Other members of our group (Dr. Pérez Perarnau, José Saura and Sonia Núñez) analyzed the response to fluorizoline treatment of MEF and HeLa cells lacking *Bim* and *Noxa*, observing cell type differences. BIM and NOXA played a key role in fluorizoline-induced apoptosis in MEFs, while NOXA had a major role in HeLa cells. This is in agreement with the reported differences in the apoptotic potential of NOXA depending on the cell type (Ploner et al. 2008). Specifically, NOXA overexpression induced significant apoptosis in HeLa cells (Oda et al. 2000), but in MEFs it proved to be poorly apoptotic (Chen et al. 2005, Shibue et al. 2006). Fluorizoline-induced increases in *NOXA* mRNA levels were observed in 10 cancer cell lines from various tissues, including cervix, hematopoietic system or brain (Pérez-Perarnau 2013). This argues in favor of a major role of NOXA in fluorizoline-induced apoptosis, while other BCL-2 family members may also contribute to apoptosis induction in certain cell types. Further experiments are aimed at characterizing the mechanism by which fluorizoline upregulates *Noxa*. As mentioned before, *Noxa* expression is regulated by several transcription factors, including p73, HIF1α, E2F-1, CRE-binding proteins and

SP-1 (Nikiforov et al. 2007, Ploner et al. 2008, Grande et al. 2012). In MEFs, E2F-1 emerges as an interesting protein to analyze, as it is the transcription factor that regulates both *Noxa* and *Bim* (Piñon et al. 2008, Ploner et al. 2008).

Taken together, these findings show that PHBs are required for fluorizoline-induced apoptosis. PHBs mediate the upregulation of *Noxa* and *Bim*, which are crucial for the pro-apoptotic effects of fluorizoline. Moreover, our findings demonstrate that PHBs are amenable to modulation with small molecules to ultimately induce apoptosis, and thus further contribute to highlight the suitability of PHBs as promising therapeutic targets for cancer treatment.

CONCLUSIONS

1. AICAR triggers ZMP-dependent but p53- and AMPK-independent apoptosis in MEFs. This mechanism is highly similar to the effects observed in CLL cells, and thus MEFs emerge as an alternative cellular system for the elucidation of the mechanism of apoptosis induction by AICAR.

2. Addition of thymidine and uridine blocks AICAR-induced apoptosis, presumably by preventing AICAR entrance into the cell.

3. Generation of ROS in AICAR-treated CLL cells is a caspase-dependent event and thus it is discarded as the responsible for the pro-apoptotic effects of this compound.

4. Fluorizoline requires the presence of prohibitins to trigger the mitochondrial apoptotic pathway. Prohibitins mediate fluorizoline-induced changes in the expression of various BCL-2 family members, notably increases in *Bim* and *Noxa*.

5. Fluorizoline and other pro-apoptotic stimuli trigger the loss of L-OPA1 upstream of caspases activation. This event is not a valid proof-of-concept to demonstrate that fluorizoline induces apoptosis by targeting prohibitins.

6. Prohibitin complexes in the inner mitochondrial membrane and the phospholipid composition are not grossly altered upon fluorizoline treatment.

PATIENTS, MATERIALS AND METHODS

INDEX OF PATIENTS, MATERIALS AND METHODS

1. SAMPLES COLLECTION FROM CLL PATIENTS

Chronic lymphocytic leukemia (CLL) patients were diagnosed by clinicians at the Hospital Universitari de Bellvitge following clinical, morphological, molecular, and immunophenotypic criteria, as proposed by the World Health Organization. Peripheral blood samples of CLL patients were collected in Servei d'Hematologia of Hospital Universitari de Bellvitge in tubes with anticoagulant EDTA. The information of the sample was collected in an internal database which scored diagnosis, date of collection, lymphocyte count and percentage of lymphocytes, as well as any information of interest, such as genetic anomalies, aggressiveness, treatment or chemoresistance. Each sample and each patient was assigned with an identification number, which was linked to the clinical history number given by Institut Català de la Salut. In addition, the database informs whether there are cryopreserved samples. We do not include any personal patient information as it is established by Universitat de Barcelona and Hospital de Bellvitge Ethical Committees. Written informed consent was obtained from all patients in accordance with Hospital de Bellvitge Ethical Committee.

2. MONONUCLEAR CELLS ISOLATION FROM PERIPHERAL BLOOD OF CLL PATIENTS

Mononuclear cells from peripheral blood samples were isolated by centrifugation on a Ficoll-Hypaque (Seromed) gradient (Fig. M.1). Blood was diluted in phosphate buffered saline (PBS) to a final volume of 8 mL. This mixture was gently added above 4 mL of Ficoll solution (density = 1.077 g/mL) trying to maintain the interface. The preparation was centrifuged for 20 min at 850 g at room temperature (RT). The centrifuge stop was conducted without brake to avoid breaking the gradient. In the resulting separation, erythrocytes and polimorphonucleated leukocytes are at the bottom of the tube due to their higher density; mononuclear cells form a ring above Ficoll, and plasma and platelets remain at the top, diluted in PBS. The ring of mononuclear cells was collected with a glass Pasteur pipette and deposited on 40 mL of PBS. A wash centrifugation was performed for 10 min at 480 g at RT and cell count was performed. Pellets were resuspended in complete medium and viability and percentage of B and T cells were analyzed by flow cytometry (see section 7). If the percentage of B cells was higher than 75%, samples were used to perform RNA and protein extractions, as well as annexin V and propidium iodide (PI) double staining viability analyses. If the percentage was below 75%, samples were only used for viability analyses by triple staining with anti-CD19 antibody (for B cells), anti-CD3 antibody (for T cells) and annexin V. Cells were used right after the purification or cells were cryopreserved for later use. Table M.1 summarizes the characteristics of the CLL samples that were used.

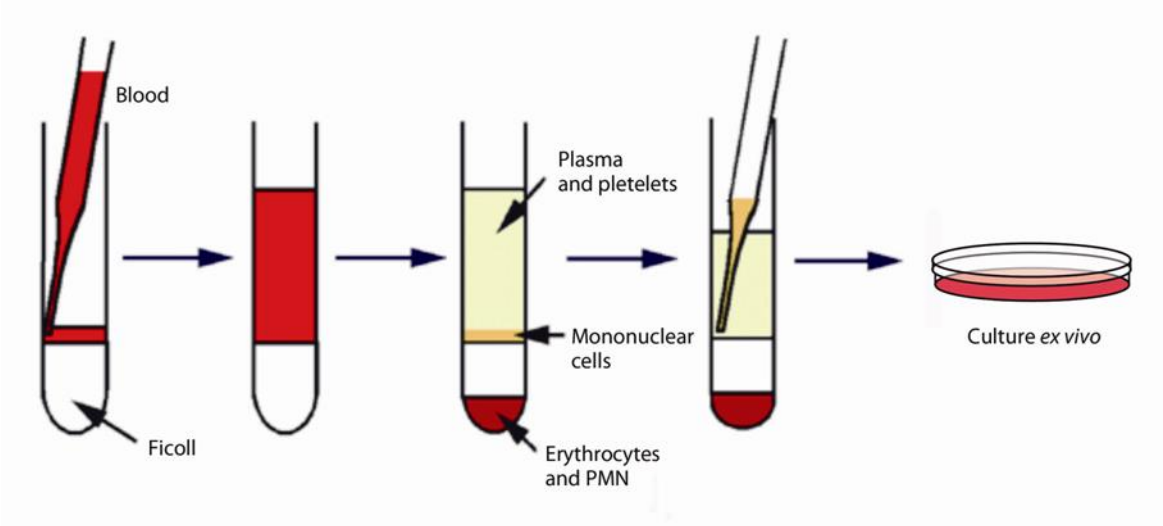

Figure M.1. Purification of mononuclear cells from peripheral blood and *ex vivo* culture. Polymorphonucleated cells (PMN). Taken from Pérez-Perarnau 2013.

Patient	Sample	Gender	Date	WBC	% L	% B	% T	Cytogenetics
69	55/08	F	27/03/2008	65,3	88	87.37	3.96	ND
108	56/13	M	02/10/2013	314	75	94.52	1.88	Normal
188	124/08	F	19/09/2008	87,7	89	91.67	5.16	Normal
320	192/05	M	14/10/2005	129	92	93.64	1.83	Del13q 20%
342	27/11	F	21/11/2011	21,9	89	72.24	4.92	ND
414	47/05	F	01/04/2005	111	93	93.04	3.33	Del 17p
432	127/08	M	25/09/2008	52,2	91	85.81	4.18	ND
815	1/13	M	28/01/2013	69	95	95.91	1.22	Del 13q11q
818	15/11	F	16/06/2011	90,5	95	78.88	5.49	ND
866	71/13	M	28/10/2013	77,8	87	73.36	10.48	ND
884	94/13	F	12/12/2013	62	81	72.31	10	ND

Table M.1. Characteristics of the samples of CLL patients. Female (F), male (M), date indicates the day of sample collection, white blood cell (WBC) count (10^9/L), percentage of lymphocytes (% L), percentage of B cells (% B), percentage of T cells (% T), not determined (ND), deletion (del). Genomic alterations were determined by fluorescent in situ hybridization or by multiplex ligation-dependent probe amplification for genomic alterations.

3. CELL LINES

- WT mouse embryonic fibroblasts (MEFs) were generated at Dr. Korsmeyer's laboratory (Wei et al. 2001), kindly provided by Dr. Jacint Boix (Universitat de Lleida) or by Dr. Cristina Muñoz (IDIBELL, Barcelona). The former were used in Figures 1.1, 1.3, 1.4, 1.5, 1.7 and 1.8; and the latter were used in Figure 1.8.

- WT and *Ampkα1*$^{-/-}$/*Ampkα2*$^{-/-}$ (DKO) MEFs were provided by Dr. Benoit Viollet's laboratory (Laderoute et al. 2006), and by Dr. Aramburu (Universitat Pompeu Fabra, Barcelona).

- WT and *Puma*$^{-/-}$ MEFs were a kind gift of Dr. Andreas Villunger (Medical University Innsbruck, Austria).

- *p53*$^{-/-}$ MEFs were a kind gift of Dr. Guillermina Lozano (McMasters et al. 1996).

- WT, *Phb2*$^{fl/fl}$, *Phb2*$^{fl/fl}$*::Phb2*, *Phb2*$^{fl/fl}$*::CNAP-Phb2* and *SLP-2* KO (SKO) MEFs were kindly provided by Dr. Thomas Langer (Institute for Genetics, CECAD, Cologne, Germany) (Merkwirth et al. 2008, Richter-Dennerlein et al. 2014).

- HeLa cells: epithelial cell line derived from human cervix adenocarcinoma. It was supplied by the European Collection of Cell Culture.

4. CELL CULTURE

CLL cells were cultured at a concentration of 0.5 to 4x10^6 cells/mL in RPMI 1640 culture medium supplemented with 10% heat-inactivated fetal bovine serum (FBS), 2 mM L-glutamine, 100 U/mL penicillin, and 100 ng/mL streptomycin (all from Biological Industries).

MEF and HeLa cells were cultured in DMEM (Biological Industries) supplemented with 10% FBS, 2 mM L-glutamine, 100 U/mL penicillin, and 100 ng/mL streptomycin. Growing cells were not maintained for more than 1-2 months since many lines easily mutate in culture, being genetically unstable and changing their characteristics after several passages.

Manipulation of the human primary samples was carried out in a flow laminar cabin of biosafety stage IIA, whereas cell lines were manipulated in a vertical laminar flow bench with an HEPA filter. CLL cells were grown in incubators for exclusive use for primary cells of human origin, and cell lines were grown in incubators only used for human or mouse cell lines, at 37ºC in a humidified atmosphere containing 5% carbon dioxide.

5. DETECTION OF MYCOPLASMA

Mycoplasma is a prokaryotic organism that is a frequent and occult contaminant of cell cultures. Mycoplasma lacks a cell wall and thus it is unaffected by common antibiotics. This organism can modify many aspects of cell physiology, so the results obtained with contaminated cells may not be trustful (Young et al. 2010, Geraghty et al. 2014). All new cell lines entering to the laboratory were tested for the presence of mycoplasma by PCR or by DAPI staining.

5.1. PCR-BASED DETECTION OF MYCOPLASMA

Protocol

Grow the cells for 5-7 days in a 60 mm plate in antibiotic-free medium. Get 1.5 mL of the medium and centrifuge at 300 g for 10 min at 4ºC. Transfer the supernatant to a new sterile tube and centrifuge at 13,000 g for 10 min at 4ºC. Remove the supernatant, resuspend the pellet with 50 μL of sterile H_2O and heat at 95ºC for 10 min. Samples can be immediately used or frozen for later analysis. The PCR analysis was performed by the responsible of the cell cultures. PCR conditions: 95ºC, 5 min. [94ºC, 1 min. 60ºC, 1 min. 72ºC, 1 min 30 s.] 30-35 cycles. 72ºC, 7 min. 4ºC, ∞.

5.2. DAPI STAINING

Protocol

Grow the cells on a sterile glass coverslip in antibiotic-free medium for 2 days. Remove the cell culture medium and incubate cells for 15 min with 4% paraformaldehid at RT. Wash the cells twice with PBS. Incubate cells with DAPI solution for 5 min. Wash the cells 2-3 times with PBS. Carefully remove the coverslips from the wells and blot to remove any excess water. Dispense 1 drop of anti-fade mounting medium (ProLong™ Gold Antifade Mountant, Life Technologies) onto the microscope slide per coverslip. Mount the coverslip with the cells facing towards the microscope slide. Visualize using a fluorescence microscope (e.g. Nikon Eclipse E800).

In case contamination was observed, cells were cultured in isolated laminar cabin and incubator to avoid cross-contamination to other cell lines. For decontamination, cells were treated with 1:100 or 1:200 Baycip® Ótico (Ciprofloxacin, Bayer. 1 mg/0.5 mL) for three weeks and then Mycoplasma detection test was repeated to confirm the decontamination.

6. FREEZING AND THAWING CELLS

Cryopreservation allows the storage of cells for later use as they maintain their characteristics and viability. Regarding cell lines, it is recommended to freeze cell lines right after thawing a tube and expanding the line in order to avoid changes occurring during the culture. The cryopreservation procedure is performed in cold DMSO as a membrane stabilizer.

Protocol for cryopreserving primary CLL cells

Resuspend the pellet of mononuclear cells in cold FBS (previously inactivated by heat for 30 min at 56°C) so that there are 20-30x10^6 cells/0.75 mL FBS/tube. Maintain the suspension of cells in ice. Add slowly an equal volume of cold cryopreservation solution, prepared with RPMI 1640, inactivated FBS and DMSO in ratio 3:1:1. Finally, there will be 20-30x10^6 cells/1.5 mL/tube in 10% DMSO. Get the 1.5 mL sample into 2 mL cryopreservation tubes. Keep tubes at -80ºC for 12-24 hours in an isopropanol freezer or in polystyrene so that temperature decreases gradually. Then, move the tubes into a liquid nitrogen tank.

Protocol for cryopreserving MEF and HeLa cells

Collect cells in exponential growth phase and pellet down by centrifugation for 5 min at 480 g. On the basis of a 60 cm^2 confluent plate we obtain 4 tubes. Resuspend the pellet in cold FBS so that cells are in 0.90 mL FBS/tube. Maintain the suspension of cells in Hospital Universitari de Bellvitge zice. Slowly add to the previous suspension 100 μL cold DMSO/tube. Get the final 1 mL sample into 2 mL cryopreservation tubes. Keep tubes at -80ºC for 12-24 hours in an isopropanol freezer or in polystyrene so that temperature decreases gradually. Then, move the tubes into a liquid nitrogen tank.

Protocol for thawing primary CLL cells

Place the cryopreserved tube in a bath at 37ºC unless its content is partially unfrozen. Pour the tube content on 40 mL of RPMI 1640 medium supplemented with 20% of inactivated FBS, previously heated at 37ºC, so that frozen cells thaw in a volume at least 10 times higher. Clean cells from DMSO by centrifugation to 480 g for 10 min. Resuspend the pellet of cells in culture medium.

Protocol for thawing MEF and HeLa cells

Place the cryopreserved tube in a bath at 37ºC until its content is partially unfrozen. Pour the tube content on 40 mL of DMEM medium supplemented with 20% FBS, previously heated at 37ºC, so that frozen cells thaw in a volume at least 10 times higher. Clean cells from DMSO by centrifugation to 480 g for 5 min. Resuspend the pellet of cells in culture medium.

7. ANALYSIS OF CELL VIABILITY BY FLOW CYTOMETRY

The cell membrane is composed of a lipid bilayer of asymmetrical distribution. Phosphatidylserine (PS) is a phospholipid entirely located on the inner monolayer surface of the plasma membrane. When a cell undergoes apoptosis, PS is no longer restricted to the cytosolic part of the membrane, but becomes exposed to the surface of the cell, which plays an important role in the recognition and removal of apoptotic cells by macrophages. The translocation of PS to the outer layer is considered an initial event in the apoptotic process and it has become a marker of apoptosis in mammalian cells. The protein annexin V binds with great affinity to PS in a calcium-dependent manner (Fig. M.2). Annexin V is conjugated to fluorochromes such as fluorescein isothiocyanate (FITC) or allophycocyanin (APC) so that cells that expose PS can be detected by flow cytometry. On the other hand, plasma membrane integrity is lost during advanced apoptosis and necrosis so that it becomes permeable to substances like propidium iodide (PI), while it is excluded by viable cells. PI is a fluorescent molecule that intercalates between the bases of double-stranded nucleic acid with little or no sequence preference.

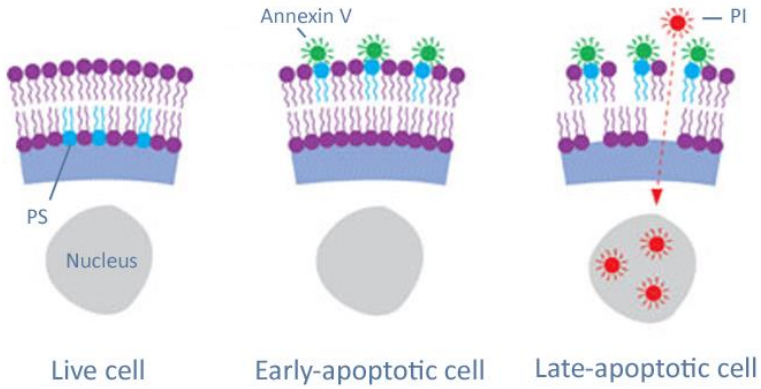

Figure M.2. Staining of apoptotic cells. Phosphatidylserine (PS) translocates to the outer layer in early-apoptotic cells, which is recognized by annexin V. In late-apoptotic cells, the integrity of the plasma membrane is compromised, allowing the entrance of propidium iodide (PI). Modified from http://www.biomol.de.

In this way, cell viability was determined by measuring PS exposure and membrane integrity. This was determined by double staining with annexin V conjugated with a fluorochrome and PI. Flow cytometry analysis generally show three cell populations: one cell population which does not emit any fluorescence (living cells), another population positive for annexin V (cells at an early stage of apoptosis) and another with double positivity staining (cells at a later stage of apoptosis). These three populations are characteristic of a typical apoptosis. There is the possibility of the emergence of a fourth population only stained with PI, which defines necrosis (Fig. M.3).

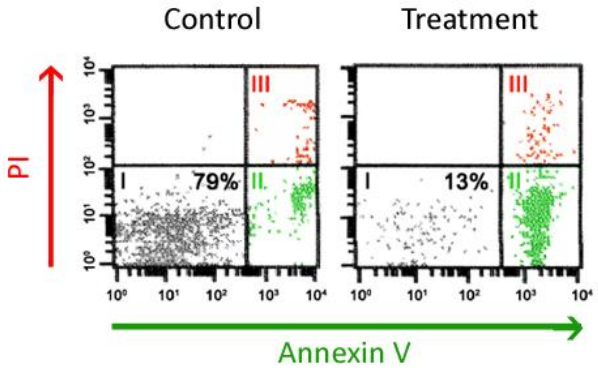

Figure M.3. Cell viability analysis by flow cytometry with annexin V-FITC/PI staining. Cells were untreated (control) or treated with a pro-apoptotic compound. Cell viability was analyzed by flow cytometry using a FACSCalibur. Viable cells are annexin V/PI double-negative (I); early-apoptotic cells are annexin V-positive (II) and late-apoptotic cells are annexin V/PI double-positive (III). Adapted from Cosialls 2011.

Cell viability was measured as the percentage of annexin V-FITC/PI-negative cell population, and it is expressed as the percentage of non-apoptotic cells. In cases where cells were treated with fluorizoline, we used annexin V-APC to avoid interference. Then, cell viability was measured as the percentage of annexin V-APC negative cell population, and it is expressed as the percentage of non-apoptotic cells. Cell viability analysis was performed using a FACSCalibur flow cytometer (Becton Dickinson) and CellQuest Pro Software for data acquisition and analysis (Becton Dickinson).

Protocol for annexin V-FITC / PI staining of CLL cells

Incubate CLL cells with the indicated drugs for a specific period of time according to the experiment setup. Collect $0.25x10^6$ cells in a flow cytometry tube on annexin-binding buffer (ABB). Wash by centrifugation for 10 min at 480 g. Resuspend the cell pellet in 100 µL of ABB with 1 µL annexin V-FITC. Incubate for 20 min at RT and in the dark. Add 50 µL of ABB with PI to a final concentration of 0.5 µg/mL. In the flow cytometer, acquire 10,000 events (cells) and analyze the data.

Protocol for annexin V-FITC / PI staining or annexin V-APC staining of MEFs

Incubate cells with the indicated drugs for a specific period of time according to the experiment setup. Collect around $0.25x10^6$ cells in a flow cytometry tube on ABB. Wash by centrifugation for 5 min at 480 g. Resuspend the cell pellet in 100 µL of ABB with 4 µL annexin V-APC or -FITC. Incubate for 20 min at RT and in the dark. Add 100 µL of ABB (for annexin V-APC staining) or 100 µL of ABB with PI to a final concentration of 0.5 µg/mL (for annexin V-FITC / PI staining). In the flow cytometer, acquire 10,000 events (cells) and analyze the data.

1X Annexin Binding Buffer, pH 7.4	
HEPES-NaOH	10 mM
NaCl	140 mM
$CaCl_2$	2.5 mM

Table M.2. Composition of the annexin binding buffer used for viability analysis.

Purified mononuclear leukocytes contain B cells, T cells and monocytes in various proportions according to the patient and the stage of the disease. The annexin V/PI protocol is suitable when the purity of B cell population in CLL samples is above 80%. When the percentage was lower, cell viability of each of population was analyzed separately using specific antibodies conjugated with fluorochromes, which are specifically directed against surface markers. In this case, we used CD19 conjugated with phycoerythrin (PE) for human B cells, and CD3 conjugated with APC for human T cells (Becton Dickinson). By adding annexin V conjugated with FITC we can determine cell viability of both populations without sorting (Fig. M.4).

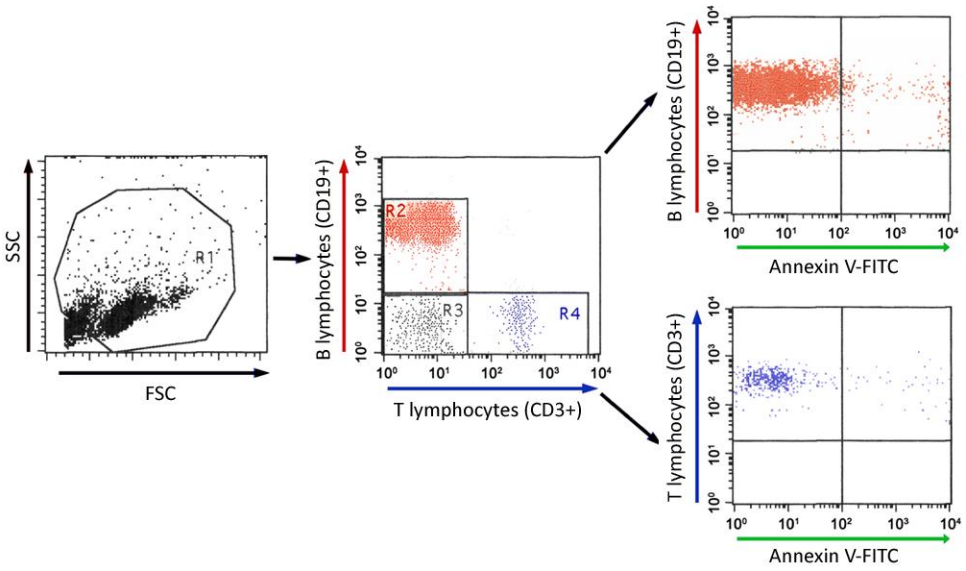

Figure M.4. Cell viability analysis with triple staining. B cells are stained with anti-CD19 antibody (R2) while T cells are stained with anti-CD3 (R4). R3 shows double-negative population. The addition of annexin V enables the measurement of cell viability of each cell population. Adapted from Cosialls 2011.

Protocol for triple staining with anti-CD19/anti-CD3/annexin V of CLL cells

Incubate mononuclear cells with the indicated drugs for a specific period of time according to the experiment setup. Collect $0.5x10^6$ cells in a flow cytometry tube on ABB. Wash by centrifugation for 10 min at 480 g. Resuspend the cell pellet in 50 μL of ABB with 2 μL anti-CD19-PE (for human B cells) and 2 μL of anti-CD3-APC (for human T cells). Incubate for 10 min at RT and in the dark. Add 100 μL of ABB with 1 μL annexin V-FITC. Incubate for 15 min at RT and in the dark. In the flow cytometer, acquire 30,000 events (cells) and analyze the data.

8. NUCLEIC ACID EXTRACTION AND ANALYSIS

8.1. MEFs GENOTYPE ANALYSIS

Protocol

Pellet down MEFs by centrifugation for 5 min, 1,200 rpm at 4ºC. Remove the supernatant and resuspend in 480 μL lysis buffer and 400 μg/mL proteinase K. Shake overnight at 1,400 rpm, at 56ºC at the thermal cycler. Centrifuge for 10 min, 13,000 rpm at RT to pellet unsoluble debris. Transfer the supernatant to a new tube and add 500 μL isopropanol to precipitate DNA. Mix gently by inverting the tube 6-8 times until a viscous texture can be observed, do not vortex. Centrifuge for 30 min, 13,000 rpm at RT to pellet chromosomal DNA. Discard the supernatant and add 500 μL 70% ethanol. Centrifuge for 30 min, 13,000 rpm at RT to wash the pellet. Discard the ethanol completely with a pipette and dry the pellet for 30 min at RT under a light or at the thermal cycler at 90ºC. Resuspend in 100 μL H_2O (DNAse free) and store at 4ºC. PCR analysis for determining the genotype of MEFs was performed as previously described (Merkwirth et al. 2008).

DNA ISOLATION BUFFER		
Lysis buffer (1X)	Tris	100 mM, pH=8.5
	EDTA	5 mM
	Sodium dodecyl sulfate	0.2%
	NaCl	200 mM

Table M.3. DNA isolation buffer.

8.2. GENE EXPRESSION ANALYSIS

The study of gene expression was performed using two different techniques: quantitative PCR and retrotranscriptase multiplex ligation-dependent probe amplification.

8.2.1. RNA EXTRACTION

Total RNA was extracted from cells by using the RNeasy Micro Kit (QIAGEN). 2-5x10^6 cells were collected for each condition. Cells were centrifuged for 5-10 min at 480 g and proceeded according to the manufacturer's instructions while maintaining the samples at RT (as opposed to other methods of purification of RNA). Total RNA samples were quantified in the Nanodrop® spectrophotometer. To obtain and work with RNA solutions, all material used was sterile and RNAse free.

8.2.2. QUANTITATIVE REAL-TIME PCR (RT-qPCR) ANALYSIS

cDNA quantification by real-time PCR relies on measuring the Taqman probes-derived fluorescence, which is proportional to the amount of sample amplified. The fluorescence increases exponentially until it reaches a saturation phase at the end of the reaction. During the exponential amplification phase, the sequence of the cDNA target doubles every cycle. A threshold for detection of cDNA-based fluorescence is automatically set. The number of cycles at which the fluorescence exceeds the threshold and the exponential phase begins is called the cycle threshold, C_t. The C_t value allows to estimate the amount of mRNA present in our samples. The normalization procedure is commonly called the $\Delta\Delta C_t$-method and permits comparison of expression of a particular gene among different samples, relative to the C_t values of a housekeeping gene in the same sample.

Protocol

First, 0.5-2 μg of total RNA were reverse-transcribed using a Ready-To-Go You-Prime First-Strand Beads Kit (GE Healthcare) and Random Hexamers (Applied Biosystems). The reaction was performed at 37ºC for 2 hours using a thermocycler.

RT-qPCRs were performed to measure the amount of amplified product in real time. These experiments were carried out using an ABI Prism 7900 HT Fast Real-Time PCR System, and pre-designed human TaqMan assays (Applied Biosystems) were used to quantify gene expression of *Bim* (Mm00437796_m1), *Noxa* (Mm00451763_m1), *Puma* (Mm00519268_m1) and *Bcl-2* (Mm00477631_m1) according to the manufacturer's guidelines. The housekeeping gene *Gapdh* (Mm99999915_ g1) was used as a control for RNA quality and for normalization. PCR data were

captured and analyzed using the Sequence Detector Software (SDS version 2.2.2, Applied Biosystems). Each reaction was prepared as follows (Table M.4):

RT-qPCR 384 wells reaction mix

Sterile ultrapure Water	8.2 µL
Taqman Universal Master Mix	10 µL
cDNA (50 ng)	0.8 µL
Gene Expression Assay	1 µL

Table M.4. RT-qPCR reaction mix composition per well.

8.2.3. RETROTRANSCRIPTASE MULTIPLEX LIGATION-DEPENDENT PROBE AMPLIFICATION

RNA content was analyzed by reverse transcriptase multiplex ligation–dependent probe amplification (RT-MLPA) using the SALSA MLPA KIT (R011-C1 human; RM002-B1 mouse) Apoptosis mRNA from MRC-Holland for the simultaneous detection of 40 messenger RNA molecules (Eldering et al. 2003). In brief, RNA samples (200 ng total RNA) were first reverse transcribed using a gene-specific primer mix. The resulting cDNA was annealed overnight at 60°C to the MLPA probe mix. Annealed oligonucleotides were ligated by adding Ligase-65 (MRC-Holland) and incubated at 54°C for 15 min. Ligation products were amplified by PCR (35 cycles, 30 seconds at 95°C; 30 seconds at 60°C, and 1 minute at 72°C) with one unlabeled and one FAM labeled primer. PCR fragments were separated by capillary electrophoresis on a 48-capillary ABI-Prism 3730 Genetic Analyzer (Applied Biosystems). Peak area and height were measured using the GeneScan analysis software (Applied Biosystems) (Fig. M.5 and Table M.5). Housekeeping genes were not used for normalizing as they were statistically modulated upon AICAR and fluorizoline treatment. The sum of all peak data was set to 100% to normalize for fluctuations in total signal between samples, and individual peaks were calculated relative to the 100% value. For fluorizoline experiments, data are shown as relative expression (fold induction over the control), which was calculated as the mean expression of treated conditions referred to the mean of the untreated conditions.

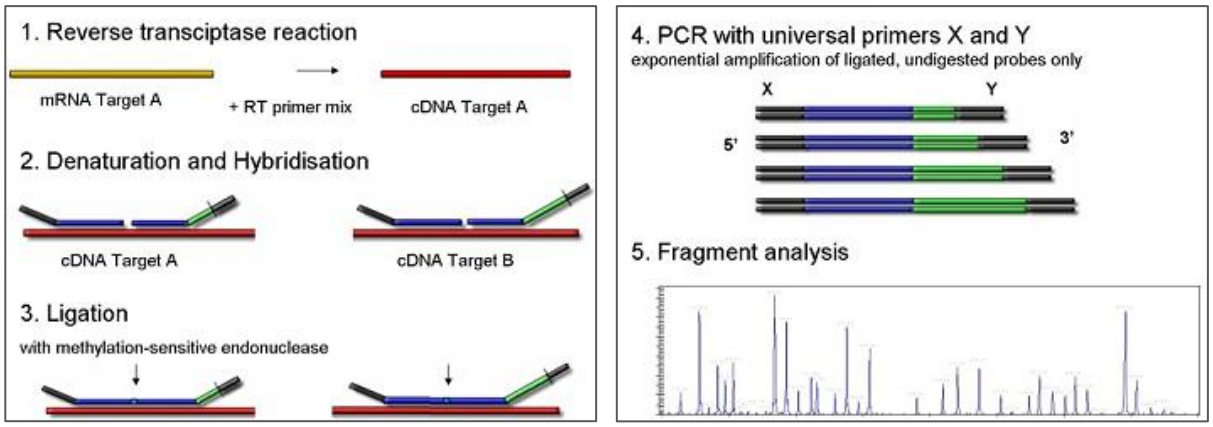

Figure M.5. RT-MLPA steps. Adapted from www.mlpa.com.

HUMAN (R011-C1)				**MOUSE** (RM002-B1)			
GENE	**bp**	**GENE**	**bp**	**GENE**	**bp**	**GENE**	**bp**
TNFRSF21	116	*HIAP1*	310	*BOK*	130	*XIAP*	301
CDKN1A	130	*XIAP*	321	*SERPINB9*	136	*SURVIVIN*	310
HTRA2	136	*SURVIVIN*	328	*BCL2-W*	142	*NAIP*	319
BCLW	142	*BRUCE*	337	*BCL2-X*	148	*LIVIN*	328
FLIP (1)	148	*LIVIN*	346	*FLIP*	154	*HIAP2*	337
BCLX	154	*SERPINA*	355	*GUSB*	160	*HIAP1*	346
NOXA	160	*PUMA*	362	*BCL2*	166	*NOXA*	355
BCL2	166	*PARN*	373	*BFL1*	172	*PUMA*	364
BFL1	172	*AIF*	382	*MCL1 L*	178	*BRUCE*	373
FLIP (2)	178	*MOAP1*	391	*BAX*	184	*HTRA2*	382
MCL1 L	184	*GUSB*	400	*BAK*	190	*B2M*	391
B2M	193	*BNIP3L*	409	*BCLG*	196	*TBP*	400
BAD	202	*APAF*	418	*BCL2-R*	202	*P21*	409
BAX	211	*GZMB*	427	*BID*	211	*GZMB*	418
BOK	216	*PRF1*	436	*BAD*	220	*PRF1*	427
BAK	229	*BNIP3*	445	*BIK*	229	*SMAC*	436
BIM	238	*SMAC*	454	*BIM*	238	*PAK2*	445
BID	247	*BMF*	463	*BMF*	254		
BCL-R	256	*BIK*	474	*HRK*	252		
BCL-G	265	*BOO/DIVA*	481	*MOAP1*	265		
HRK	274	*HIAP2* (2)	488	*APAF*	274		
NAIP	292	*FAS*	496	*AIF*	283		
HIAP2 (1)	298			*BOO/DIVA*	292		

Table M.5. List of apoptosis-related genes analyzed by human and mouse RT-MLPA. Sizes of each PCR product (in base pairs, bp) are indicated according to the manufacturer specifications. Adapted from www.mlpa.com.

9. TRANSIENT TRANSFECTION

MEFs were transfected with scramble (12935-300) or *Phb2* siRNA (MSS236022) using the Lipofectamine RNAiMax Reagent (all from Life Technologies). MEFs were used in experiments 72 hours after siRNA transfection, and the efficiency of the downregulation was assessed by western blot.

Protocol

Seed MEFs in two 10 cm plates, one for scramble siRNA and the other one for *Phb2* siRNA, to be 30% confluence at transfection. Prepare the following mix for each plate:

A) 1 mL OptiMEM + 9 μL Lipofectamine RNAiMAX
B) 1 mL OptiMEM + 10 μL siRNA

Incubate the mix for 5 min at RT. Add the solution B into the solution A. Incubate for 20 min at RT. Meanwhile, aspirate the medium from the plates and add 5 mL complete medium without antibiotics. Add the complexes dropwise to the cells and incubate for 24 hours. Then, wash with PBS and add fresh DMEM for 24 hours. Split the cells to 10 cm plates, taking into account that si*Phb2*-transfected cells grow much slower than the scramble-transfected ones. Wait 24 hours for cells to attach. Incubate MEFs with the indicated drugs and harvest for further analysis.

10. PROTEIN ANALYSIS

10.1. TOTAL LYSIS EXTRACTION

Lysing cells with reducing Laemmli Sample Buffer (SB) is a quick, simple and potent denaturing lysis procedure. It contains 2% sodium dodecyl sulfate (SDS), which ensures the total cell lysis by disrupting the membrane lipid bilayer, including the nucleus that results in the extraction of genomic DNA.

Protocol

Incubate cells with the indicated drugs for a specific period of time according to the experiment setup. Collect cells and wash with PBS by centrifugation for 5 min at 480 g. Resuspend the pellet with PBS and wash it again by centrifugation for 5 min at 480 g. Add on the pellet 50-100 μL of SB buffer and heat samples to 95°C for 10 min. Check the efficiency of lysis by various cycles of heating, vortex and centrifugation to dissolve the pellet. If the lysis process is not total, freeze samples at -20°C and repeat the cycles of heating at 95°C for 10 min and assess whether more SB buffer is required. Samples can be stored frozen at -20°C.

10.2. RIPA EXTRACTION

RIPA buffer enables protein extraction from cytoplasmic, membrane and nuclear proteins. Protease or phosphatase inhibitors have to be added right before its use. RIPA extraction has been used for protein analysis of phospho-AMPK or phospho-ACC in MEF and CLL cells.

Protocol

Incubate cells with the indicated drugs for a specific period of time according to the experiment setup. Collect cells and wash by centrifugation at 480 g for 5 min (MEFs) or 10 min (CLL cells). Discard the supernatant. Resuspend the pellet with PBS and wash again by centrifugation. Discard the supernatant. Resuspend the pellet with 100 µL RIPA buffer. Pipette the mixture up and down to suspend the pellet. Gently shake the mixture for 15 min on ice. Centrifuge the mixture at 14,000 g for 15 min to pellet the cell debris. Transfer the supernatant to a new tube for further analysis. Store the cell extracts at -20°C and keep them always cold. Before loading the gel, add sufficient volume of SB 4X to make the final concentration of SB 1X in order to get completely denaturated proteins. Once added, heat samples for 10 min at 95°C.

10.3. PROTEIN QUANTIFICATION BY BCA ASSAY

To analyze proteins by western blot, it is necessary to quantify the protein concentration of the samples in order to load the same amount of protein for each sample. Protein quantification was conducted with the kit Micro BCA Protein Assay Reagent (Thermo Scientific), using a plate reader of 550 nm. This kit is based on a colorimetric quantitative determination with bicinchoninic acid (BCA) to detect Cu^{2+} reduction to Cu^{+} due to the basic pH of the proteins. It is compatible with the presence of various detergents, including 1% SDS. Two molecules of BCA chelate one Cu^{+} molecule and the resulting complex present color, which is directly proportional to the amount of protein in the sample.

10.4. PROTEIN ANALYSIS BY WESTERN BLOT

Western blot allows the analysis of proteins, which become separated according to their molecular weight. Once proteins are transferred to a membrane, protein levels can be detected by specific antibodies.

10.4.1. PROTEIN SEPARATION BY SDS-PAGE ELECTROPHORESIS

Prepare protein extracts with the same protein amount (10-50 μg) and final volume (20-35 μL) according to the quantification. Add SB buffer (contains SDS detergent which denatures and negatively charge all proteins), 100 mM dithiothreitol (breaks disulphide bridges) and bromophenol blue (indicates the progress of the protein front in the electrophoresis). Heat samples for 10 min at 95ºC to completely denature the proteins before loading on the gel. Prepare the SDS-PAGE gel. The gel is formed by a concentrating/stacking gel (3% acrylamide) and a separating/running part which, on the basis of the proteins which you want to analyze, the percentage of acrylamide can vary from 5-15% of 37.5:1, acrilamyde:bisacrylamide. Lower molecular weight protein analysis requires higher percentage of acrylamide. Load the samples and the molecular weight marker. Submerge the gel in appropriate buckets with electrophoresis buffer and apply an electric current of 125 V.

10.4.2. PROTEINS TRANSFER TO PVDF MEMBRANES

Activate a polyvinyl difluoride (PVDF) membrane Immobilon-P (Millipore) with methanol, and hydrate with water. Prepare a sandwich where we place the separating gel, the membrane, and several drying papers, avoiding the formation of bubbles. Apply an electric current of 400 mA for 1 hour with transfer buffer, in cold conditions and continuous agitation to avoid excessive heating. After the transfer, wash the membrane with TBS-T for 5 min.

10.4.3. IMMUNOBLOT

Incubate the membrane for one hour in blocking solution (TBS-T with 5% low-fat milk) to avoid non-specific bindings of the primary antibody. Incubate the membranes with the primary antibody against the protein of interest under the conditions recommended for each case (Table M.6). Wash 3 times for 5 min with TBS-T. Incubate for 1½ hour with the secondary antibody prepared in blocking solution. The secondary antibody recognizes the primary antibody constant region. Wash 3 times for 5 min with TBS-T and the last 10 min with TBS (optional). For the detection of the secondary antibody, enhanced chemiluminescence solution is used. When this solution contacts with the Horse Raddish Peroxidase (HRP) enzyme of the secondary antibody, it gets oxidized and emits chemiluminescence. Acquire the data by using the Las-3000 detection system (Fujifilm).

Antibody	Source	Dilution	Reference	Company
ACC-P Ser-79	Rabbit	1:1000	3661	Upstate Biotechnology
AMPK	Rabbit	1:1000	2532	Cell Signaling
AMPK-P Thr 172	Rabbit	1:1000	2531	Cell Signaling
BCL-2 (human)	Mouse	1:1000	M0887	Dako
BCL-2 (mouse)	Rabbit	1:1000	554279	BD Biosciences
BIM	Rabbit	1:1000	2933	Cell Signaling
Cleaved caspase 3	Rabbit	1:1000	9661	Cell Signaling
ERK2	Mouse	1:500	1B3B9	Upstate Biotechnology
MCL-1	Rabbit	1:1000	S-19, sc-819	Santa Cruz Biotechnology
NOXA	Mouse	1:500	Ab13654	Abcam
OPA1	Mouse	1:1000	612607	BD Biosciences
p21	Rabbit	1:1000	C-19, SC-397	Santa Cruz Biotechnology
PARP	Rabbit	1:1000	9542	Cell Signaling
Prohibitin 1	Rabbit	1:1000	H-80	Santa Cruz Biotechnology
Prohibitin 2	Rabbit	1:1000	07-234	Upstate Biotechnology
PUMA	Rabbit	1:1000	4976	Cell Signaling
Survivin	Rabbit	1:1000	2803	Cell Signaling
Tubulin	Rabbit	1:1000	CP06	Millipore – Calbiochem
β- Actin	Mouse	1:5000	A5441	Sigma-Aldrich
Anti-rabbit IgG, HRP linked	Donkey	1:5000	NA934	GE Healthcare
Anti-mouse IgG, HRP linked	Sheep	1:5000	NA931	GE Healthcare

Table M.6. List of primary antibodies.

PROTEIN ANALYSIS BUFFERS		
SB (Laemmli sample buffer) (1X)	Tris-HCl pH 6.8	80 mM
	SDS	2%
	Glycerol	10%
	DTT	0.1 M
RIPA lysis buffer (1X)	Tris-HCl pH 7.5	50 mM
	Triton X-100	1%
	Na_3VO_4	1 mM
	NaF	50 mM
	EDTA	5 mM
	β-Glycerophosphate	40 mM
	NaCl	100 mM
	PMSF	1 mM
	Pepstatin	1 μg/mL
	Leupeptin	1 μg/mL
	Aprotinin	1 μg/mL
	Benzamidin	1 mM
Upper buffer for electrophoresis pH=6.8	Tris	0,5 M
	SDS	0.4%
Lower buffer for electrophoresis pH=8.8	Tris	1.5 M
	SDS	0.4%
Electrophoresis buffer (1X) pH=8.3	Tris	25 mM
	Glycine	192 mM
	SDS	0.1%
Transfer buffer (1X) pH=8.3	Tris	25 mM
	Glycine	192 mM
	Methanol	10% for >30kDa proteins
		20% for <30 kDa proteins
TBS (Tris Buffered Saline) (1X) pH=7.4	Tris-HCl	20 mM
	NaCl	137 mM
TBS-T pH=7.4	TBS 1x	1X
	Tween-20	0.1%
Blocking solution	TBS-T	1X
	Non-fat dry milk	5%
Loading buffer (6X)	Glycerol	30%
	Bromophenol blue	0.25%

Table M.7. Buffers used for protein analysis.

10.4.4. TRIS-ACETATE GRADIENT GELS

Gradient gels were used to separate and analyze proteins with very high and very low molecular weight in the same electrophoresis gel. The protocol was previously described by the group headed by Dr. Rosa, in our department (Cubillos-Rojas et al. 2010, 2012).

Protocol

Prepare two solutions with different percentage of acrylamide in separated tubes (Table M.8).

	3%	**15%**
3M Tris-acetate pH 7.0 (15X)	0.4 mL	0.4 mL
40% Acrylamide solution	0.45 mL	2.25 mL
mQ water	5.15 mL	3.35 mL
TOTAL VOLUME	6 mL	6 mL
TEMED	7.5 µL	7.5 µL
APS 10%	28.5 µL	28.5 µL

Table M.8. Composition of the solutions for preparing tris-acetate gels.

Get a gradient maker (Hoefer®) and connect it to the glass plates through a thin cannula. Place the gradient maker on the right height so that the solution goes into the plates in a suitable speed. Add the 3% acrylamide solution in the left chamber, and the 15% one in the right chamber with a magnetic stir bar. First open the right valve in order to allow the 15% solution reaches the bottom of the glass plates. Then, open the left valve so that the 3% solution gets into the right chamber. It may be necessary to force its entrance by applying air pressure. This step allows the mixture of the 3% solution with the 15% one, generating the gradient. Let the solutions get into the glass plates until the top of the inner one and add the comb (Fig. M.6).

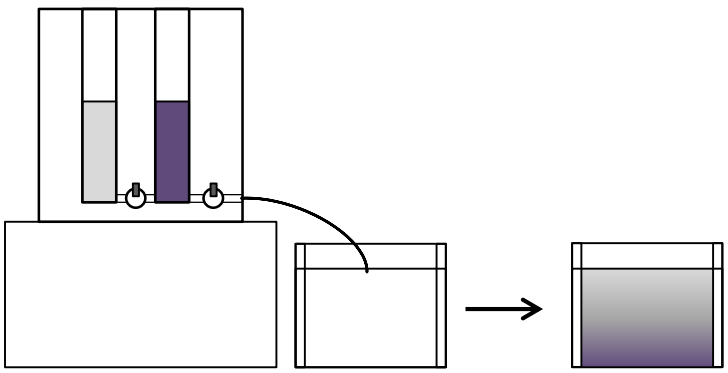

Figure M.6. Schematic representation of the preparation of a gradient gel.

Load the samples and the molecular weight marker. Submerge the gel in appropriate buckets with the gradient electrophoresis buffer and apply an electric current of 30-40 mA/gel (125 V). Transference was done at 200 mA for 2 hours at 4ºC using the gradient transference buffer.

TRIS-ACETATE GRADIENT GELS BUFFERS		
Tris-acetate gel buffer (15X) pH=7, adjust with acetic acid Store at 4ºC	Tris acetate	3 M
Running buffer (1X) pH=8.2, not necessary to adjust Store at 4ºC	Tricine Tris SDS Sodium bisulfite	50 mM 50 mM 0.1% 1.3 mM
Transfer buffer (1X) pH=7.2, not necessary to adjust Store at 4ºC	Methanol Bicine Bis-Tris EDTA Sodium bisulfite	20% 25 mM 25 mM 1 mM 1.3 mM

Table M.9. Buffers used for tris-acetate gradient gels.

11. DETERMINATION OF INTRACELLULAR SUPEROXIDE

Dihydroethidium (DHE, Life Techonologies) is extensively used to monitor superoxide production. DHE reacts with superoxide anions and forms a red fluorescent product 2-hydroxyethidium which intercalates with DNA.

Protocol

Incubate cells with the indicated drugs for a specific period of time according to the experiment setup. At the time of interest, collect $2.5x10^5$ cells in flow cytometry tubes, add 2 μM DHE (make the dilution in PBS right before its use, trying to protect DHE from light) and incubate for 30 min at 37ºC in the dark. Wash cells with PBS, centrifuge and resuspend in 150 μL of PBS. Analyze 10,000 cells by flow cytometry and measure the mean fluorescence intensity.

12. CRE RECOMBINASE SYNTHESIS

Expression and purification of HTNC Cre recombinase, a fusion protein formed by Histidines for protein purification, TAT peptide for celular absorption, Nuclear localization signal (NLS) and the enzyme Cre recombinase. Its synthesis was described (Peitz et al. 2002), and the following protocol is based on Dr. Langer's laboratory one.

12.1. HTNC EXPRESSION IN BACTERIAL CULTURE

Pre-culture

Add 1% glucose, 50 μg/mL carbenecillin and 34 μg/mL chloramphenicol to 250 mL lysogeny broth (LB). Inoculate the growing medium with bacteria from the glycerol stock (TUNER (DE3)pLacI E.coli transformed with HTNC plasmid, (Peitz et al. 2002)). Shake overnight at 37°C, 160 U/min.

Expression culture

Prepare 12 L of LB, split 2 L in 6 sterile 5 L Erlenmeyer flasks and autoclave. Add 1% sterile glucose, 100 μg/mL ampicillin and 34 μg/mL chloramphenicol. Inoculate each flask with 40 mL (1:50) of the overnight culture. Shake at 37°C at 160 U/min until an OD_{600} of 0.8 is reached (2.5 – 3.5 h). Get 100 μL of the culture for later electrophoresis analysis (centrifuge 5 min, 6,000 rpm and resuspend the pellet with 100 μL SB 1X).

Protein expression induction

Induce protein expression by adding 0.5 mM Isopropyl β-D-1-thiogalactopyranoside (IPTG). After 3 or 4 hours of incubation, get 100 μL culture for later electrophoresis analysis (centrifuge 5 min, 6,000 rpm and resuspend the pellet with 100 μL SB 1X). Centrifuge the rest of the culture in 1 L beakers at 6,000 g for 20 min at 4°C. Discard supernatants except 50 mL in which the pellet is resuspended by vortexing. Pool the suspensions and centrifuge in a 500 mL beaker (10 min, 6,000 g, 4°C in Beckman Avanti J-20 AP; Rotor JA10). Discard supernatant completely. Shockfreeze the beaker containing the cell pellet in liquid nitrogen and store at -20°C. The protocol can be stopped at this step.

12.2. HTNC PURIFICATION

HTNC purification was performed by using nickel-nitrilotriacetic acid (Ni-NTA) agarose (Qiagen), an affinity chromatography matrix for purifying recombinant proteins carrying a Histidine tag. Cleared cell lysates are loaded onto the columns, histidine residues bind to immobilized nickel ions with high specificity and affinity, while most of the non-tagged proteins flow through. Residual contaminants and unspecific bound proteins are removed by washing with buffers of slightly reduced pH or with buffers containing a low concentration of imidazole. His-tagged proteins are eluted by adding a higher concentration of imidazole, which binds with more affinity to nickel and displaces His-tagged proteins.

Lysis

Resuspend frozen cell pellet in 10 mL lysis buffer (PTB 1X) per litre flask culture in a beaker (120 mL). Add 1 mg lysozyme per mL suspension (120 mg), mix for 20 min at RT in a 250 mL beaker using a magnetic shaker. Add 120 µL benzonase (purity > 90%; Novagen) and mix for 15 min at RT (120 µL).

Sonicate 2 min with 0.5 sec pulses on ice (output 8, duty cycle 50). Change to a new beaker in order to get rid of the bubbles. Important: Add 1 mL cold TSB buffer per mL suspension (120 mL), mix gently and incubate for 5 min on ice (crucial step to avoid protein precipitation in the glycerol stock).

Distribute in 50 mL Beckman centrifuge bottles, balance them precisely and centrifuge for 30 min at 17,000 rpm (35,000 g), at 4°C (Beckman Avanti J-20 AP; Rotor JA25.50). The supernatant contains the soluble fraction; and the pellet, the insoluble one. Carefully transfer cleared supernatant into a clean 250 mL beaker without any residuals from the pellet. Get 100 µL of the supernatant and add 100 µL SB 2X; get pellet sample and add SB 1X; and freeze both samples.

Purification

Ni-NTA agarose is provided as a 50% solution. For HTNC purification, 2 mL 50% Ni-NTA agarose per liter expression culture are needed (in total, 24 mL). Before using it, it is necessary to equilibrate with lysis buffer. Get 24 mL 50% Ni-NTA agarose and centrifuge at 800 rpm for 1 min. Ni-NTA agarose remains at the lower fraction (12 mL), get rid of the supernatant and resuspend the agarose in 12 mL lysis buffer.

Get the 250 mL beaker with the supernatant and add the 24 mL of equilibrated 50% Ni-NTA agarose. Shake gently for 60 min at 4°C in 250 mL glass flask by using a magnetic shaker.

The approximate volume at this point is 264 mL (120 mL PTB + 120 mL TSB + 24 mL 50% Ni-NTA). Apply the suspension carefully onto three 10 mL columns (BioRad), 88 mL per column, and let it flow through by gravity.

Next, it is necessary to wash twice in order to get rid of unspecific proteins that bound to the resin. The volume of washing buffer is 5X of the resin volume. We used 24 mL 50% Ni-NTA that contain 12 mL resin, which are divided into three columns, so 4 mL resin are in each column. Thus, use 20 mL washing buffer for each column.

Three columns → 4 mL resin/column → 2 times x 20 mL wash buffer/column.

Finally, the specific His-tagged protein that is bound to the resin has to be eluted. The volume of elution buffer is 3X of the resin volume. Then, use 12 mL of elution buffer per column.

Three columns → 4 mL resin/column → 12 mL elution buffer/column.

After each washing and elution step, get 100 μL supernatant for later electrophoresis analysis, add 100 μL SB 2X and freeze.

Because of its high protein concentration, the solution mostly gets turbid. In this case, add some more elution buffer and mix gently to clear the solution.

The Ni-NTA resin and the columns can be reused up to 6 times. Get the Ni-NTA resin that is stacked in the columns with a spatula, add mQ H_2O (1:2 dilution, so as to have again 50% Ni-NTA solution) and store at 4ºC.

12.3. HTNC CONCENTRATION

HTNC stock concentration can be increased in other to minimize the total volume needed for Cre recombinase transduction and the imidazole content, which is important for HTNC application to cell cultures. To this end, the eluted protein is dialyzed in high salt buffer and glycerol salt buffer.

Protocol

Get a dialysis membrane (SnakeSkin Pleated Dialysis Tubing, Life Technologies), and make knot at one end. Add the eluted protein into the membrane and make a knot at the other end, trying to avoid bubbles inside. Reinforce the knots with two sealing clips. Put the high salt dialysis buffer in a 2 L beaker, place the dialysis membrane floating at the top and dialyze 24 hours with continuous stirring with a magnetic shaker at 4ºC. Remove the high salt buffer, add glycerol salt buffer and dialyze 24 hours with continuous stirring with a magnetic shaker at 4ºC. Important: in all steps, the buffer/sample ratio should be at least 50. Get 100 μL of the dialyzed protein, add 100 μL SB 2X and freeze.

Determine protein concentration of the dialyzed Cre protein using the Nanodrop® spectrophotometer (sample diluted 1:100 in PBS; blank: glycerol salt buffer diluted 1:100 in PBS). Measure the A_{260} and the A_{280} and calculate the protein concentration by using the Warburg formula:

$$\text{Protein concentration } (\mu g/mL) = [\ (1.55 * A_{280}) - (0.76 * A_{260})\ ] * 100 \text{ (dilution correction)}$$

$$\text{Molarity } (\mu M) = \text{concentration } (mg/mL) / 0.043$$

HTNC stocks can be stored at -20 or -80°C for several months without loss of activity.

12.4. ELECTROPHORESIS ANALYSIS OF HTNC EXPRESSION AND PURIFICATION

Run a standard SDS electrophoresis gel (12% acrylamide) with 10 μL of all the samples obtained along the HTNC synthesis and purification steps. Stain the gel with Bio-Safe Coomassie (Bio-Rad) and discolor it with mQ water. Ideally, it should be observed that IPTG induces the expression of the protein (~41 kDa), soluble fraction contains the protein of interest, washing buffers do not elute big amounts of protein, the protein was eluted as pure as possible and it is preserved after dialysis.

HTNC EXPRESSION BUFFERS			
LB (per 12 L) pH= 7.0	Bacto-tryptone NaCl Bacto-yeast extract	120 g 120 g 60 g	
HTNC PURIFICATION BUFFERS			
Lysis buffer (PTB) (10X) pH=7.8 Prepare 250 mL PTB 1X	$NaH_2PO_4 \cdot 2\ H_2O$ Tris	500 mM 50 mM	
Tartaric salt buffer (TSB) (1X) Prepare 120 mL freshly Store at 4ºC	$NaH_2PO_4 \cdot 2\ H_2O$ Tris Sodium tartaric dibasic dihydrate* Imidazole	50 mM 5 mM 2 M 20 mM	PTB 1X
Washing buffer (1X) pH=7.4 Prepare 200 mL freshly Store at 4ºC	$NaH_2PO_4 \cdot 2\ H_2O$ Tris NaCl Imidazole	50 mM 5 mM 500 mM 20 mM	PTB 1X
Elution buffer (1X) pH=7.4 Prepare 100 mL freshly Store at 4ºC	$NaH_2PO_4 \cdot 2\ H_2O$ Tris NaCl Imidazole	50 mM 5 mM 500 mM 250 mM	PTB 1X
HTNC CONCENTRATION BUFFERS			
High salt buffer (1X) pH=7.4 Prepare 2 L the day before	NaCl HEPES	600 mM 20 mM	
Glycerol salt buffer (1X) pH=7.4 Prepare 2 L the day before	NaCl HEPES Glycerol	600 mM 20 mM 50%	

* Sodium tartaric dibasic dehydrate is soluble at 0.1 M in H_2O at 20ºC. To prepare 2 M sodium tartaric salt, heat it up to 95ºC. Once diluted, bring it to the cold room, stir it with a magnetic shaker and add PTB and imidazole. Otherwise, tartaric salt precipitates.

Table M.10. Buffers used for HTNC synthesis.

13. CRE RECOMBINASE TRANSDUCTION

Protocol

Day 1

For a complete experiment including RNA, protein and viability analysis, plate MEFs at ~40% of density in a 15 cm plate ($2x10^6$ cells). Let them attach for 4-5 hours. The final concentration of Cre recombinase to be used should be determined every time that a newly synthetized Cre recombinase was used for the first time (see results, section 2). Dilute the amount of Cre recombinase in a 1:1 mixture of DMEM/PBS (without FBS, P/S nor glutamine), and use 12-15 mL for a 15cm plate. Remove the medium from the plate, and apply Cre recombinase solution by filtering it using a syringe and a 0.22 μm filter and incubate for 20 hours.

Day 2

Remove the Cre recombinase solution and add complete medium. Let MEFs grow for 24 hours.

Day 3

Split the cells into 10 cm plates, so that the following day the confluence is suitable for fluorizoline treatment. After Cre recombinase transduction, *Phb2*$^{fl/fl}$ MEFs grow more slowly than WT MEFs due to the lack of PHBs.

Days 4 and 5

Treat cells with fluorizoline for different times according to the experiment and collect the cells in a suitable manner for RNA, protein and viability analysis. It is highly recommendable to have at least viability analysis at 24 hours as a control for fluorizoline-induced pro-apoptotic effects.

14. GENERATION OF A STABLE *Phb2*$^{-/-}$ CELL LINE

Phb2$^{fl/fl}$ MEFs were transduced with Cre recombinase for 20 hours and further grown for 72 hours. Cells in a confluent 10 cm dish were resuspended in 1 mL PBS and single cells were sorted individually in each well of two 96-well plate (containing 200 μL complete medium/well) by using the FACSAria cell sorter (Becton Dickinson). Cells were then grown for several days until they reached confluence. Clones were selected and split to a 24-well plate, and then to a 6-well plate. At this point, some cells were collected for PCR analysis. The selection and amplification steps were repeated for four different days to ensure including clones with different proliferating rates.

15. ANALYSIS OF MITOCHONDRIAL PROTEIN COMPLEXES

15.1. MITOCHONDRIAL ISOLATION

Mitochondria from *Phb2*$^{fl/fl}$ MEFs were isolated in order to study PHB complexes. This protocol is based on the one written by Simon Troeder (Institute for Genetics, CECAD, Cologne, Germany).

Protocol

Incubate cells with the indicated drugs for a specific period of time according to the experiment setup. Use one 15 cm plate of MEFs for control conditions, and two 15 cm plates for fluorizoline-treated conditions. Scrape cells from plate in cold PBS, wash once with cold PBS (600 g, 5 min, 4°C) and take up in appropriate volume of homogenization buffer (2 mL/15 cm plate). Incubate on ice for 15 min to facilitate swelling. Homogenize the tissue by 15 strokes with Teflon® homogenizer, avoiding bubbles. Centrifuge the homogenate (1,000 g, 10 min, 4°C). Optional: Repeat the homogenization with pellet and pool the supernatant (containing mitochondria). Centrifuge the supernatant once again (1,000 g, 10 min, 4°C).
Isolate mitochondrial fraction from supernatant by centrifugation (8,000 g, 10 min, 4°C, in 2 mL eppendorf tubes) and carefully resuspend the pellets all together in 100 µL of isolation buffer. Determine the protein concentration using the Bradford assay (Bio-Rad) according to the manufacturer's instructions. Dilute the mitochondrial suspension to 10 mg protein/mL with isolation buffer. Mitochondria can be frozen and stored at -80°C, though freezing will severely retard the activity of mitochondria. To freeze mitochondria, isolate mitochondria by centrifugation (8,000 g, 10 min, 4°C) and resuspend the pellet carefully in freezing buffer at 10 mg/mL. Freeze in small aliquots slowly at -80°C.

MITOCHONDRIAL ISOLATION BUFFERS

Homogenization buffer (1X)	Mannitol	220 mM
pH=7.4	Sucrose	70 mM
Prepare freshly	EGTA	2 mM
	Fatty acid free BSA	0.1% (w/v)
	HEPES-KOH	20 mM
	Protease inhibitor complete EDTA-free	1X (Roche)
Isolation buffer (1X)	Mannitol	220 mM
pH=7.4	Sucrose	70 mM
Prepare freshly	EGTA	2 mM
	HEPES-KOH	20 mM
	Protease inhibitor complete EDTA-free	1X (Roche)

Freezing buffer (1X) pH=7.4, sterile filtered Store at -20ºC	Sucrose HEPES-KOH	500 mM 10 mM

Table M.11. Buffers used for mitochondrial isolation.

15.2. BLUE NATIVE-PAGE

BLUE NATIVE-PAGE (BN-PAGE) is suitable for separation of water soluble or membrane-bound protein complexes in the range from 10 to 1,000 kDa. A charge shift on the proteins is induced by negatively charged Coomassie dye instead of SDS, so the separated protein complexes are in their native conformation and therefore mantain their enzymatic activity and oligomeric state. This method can be used for determining the subunit composition and degree of homogeneity of protein complexes. This protocol is based on the one written by Anne Korwitz (Institute for Genetics, CECAD, Cologne, Germany).

Protocol for gels preparation

Assemble glass plates and keep them cold. Prepare the gel solutions and make a gradient gel at 4°C using a Hoefer® gradient mixer. Do not fill the plates until the top. Once polymerized, add stacking gel solution on top of the separation gel, insert the comb and let the gel polymerize at 4°C.

	3%	**13%**	**Stacking**
AB mix (49.5% T, 3% C)	0.48 mL	2.08 mL	0.36 mL
3X gel buffer	2.67 mL	2.67 mL	2 mL
Glycerol 50%	0.32 mL		
Glycerol 87%		2.76 mL	
H_2O	4.45 mL	0.5 mL	3.64 mL
APS (per gel)	20 µL	10 µL	10 µL
TEMED (per gel)	2 µL	1 µL	1 µL

Table M.12. Composition of the solutions for the preparation of 3 mini-gels for blue native-PAGE.

Protocol for samples preparation

Spin down 100 µg mitochondria per lane for 5 min at 16,100 g and 4°C to get rid of the freezing buffer. Discard supernatant, resuspend pellet in solubilization buffer with digitionin (20 µL solubilization buffer 2X + 14 µL H_2O + 6 µL digitonin 10%). Shake samples for 30 min at 4°C.

Centrifuge samples for 30 min at 20,000 rpm to get rid of cell debris. Transfer the supernatant to new tube and add Coomassie Brilliant Blue (CBB) (36 µL sample + 4 µL CBB per lane → 45 µg).

Protocol for gel running

Fill the chamber with anode and deep blue cathode buffers. Wash slots with deep blue cathode buffer. Load marker (12.5 µL) and samples, and fill empty slots with 1X CBB. Let the gel run at 100 V until the samples have entered the separation gel (~2 hours). Exchange deep blue cathode buffer with slightly blue cathode buffer and switch voltage to 300 V.

Marker Mix: 2.5 µL Thioglobulin 25 mg/Ml, 2.5 µL Ferritin 25 mg/mL, 5 µL ADH 25 mg/mL, 2.5 µL BSA 25 mg/mL, 5 µL Catalase 50 mg/mL. Add up to 100 µL with solubilization buffer

Protocol for blotting

Equilibrate the gel in blot buffer for 30 min. Cut PVDF membrane and shortly equilibrate it in methanol. Perform semi-dry blotting for 3h at 400 mA. Destain membrane with methanol and stain with Ponceau-S solution. Block the membrane with 5% dry milk in TBS-T for 1 hour.

BLUE NATIVE PAGE BUFFERS		
Anode buffer (1X) pH=7	Imidazole/HCl	25 mM
Deep blue cathode buffer (1X)	Tricine Imidazole Coomassie G250	50 mM 7.5 mM 0.02%
Slightly blue cathode buffer (1X)	Tricine Imidazole Coomassie G250	50 mM 7.5 mM 0.002%
3X gel buffer (1X)	Imidazole/HCl, pH=7 6-aminohexanoic acid	75 mM 1.5 M
Solubilization buffer (1X)	NaCl 6-aminohexanoic acid Imidazole/HCl, pH=7 Glycerol KPi-buffer, pH=7.4	50 mM 5 mM 50 mM 10% 50 mM
CBB (1X)	Coomassie G250	1%
Blot buffer (1X)	Methanol SDS Tris Glycine	20% 0.02% 20 mM 0.15 mM

Table M.13. Buffers used for BN-PAGE.

16. MASS SPECTOMETRIC ANALYSIS OF THE PHOSPHOLIPIDOME IN MEFs

Phb2$^{fl/fl}$ MEFs were untreated, treated with 20 μM fluorizoline for 24 hours, or Cre-transduced for 72 hours (*Phb2*$^{-/-}$). Phospholipidome analysis was performed by Dr. Takashi Tatsuta (Institute for Genetics, CECAD, Cologne, Germany) as previously described (Richter-Dennerlein et al. 2014). One milion cells were resuspended in 40 μL H_2O and mixed with 360 μL chloroform/methanol/25% HCl (40:80:0.6 [v/v]). Cells were disrupted by vortexing 30 sec and 200 μL were taken for lipid extracts. H_2O (0.4 mL) was added and vortexing was repeated. Next, 0.5 mL H_2O and 0.5 mL chloroform were added, followed by vortexing and centrifugation at 800 g for 2 min to separate the phases. The lower chloroform phase was moved to a second tube, and the upper phase was washed with 0.5 mL chloroform and 0.8 mL H_2O. The washed chloroform phase of the second tube was transferred to a third tube, and the chloroform phase of the initial tube was combined with the upper phase of the second tube, followed by re-extraction. Upon phase separation, the chloroform phases were merged and evaporated by a gentle stream of argon at 37ºC. HCl was removed from the extraction solution to suppress the deacylation of cardiolipin. Lipids were dissolved in 5 mM ammonium acetate and 0.05% piperidine in methanol and analyzed on a 4000 QTrap® triple quadrupole mass spectrometer (Applied Biosystems) equipped with a Turbo V™ electrospray ion source. Identification and quantification of the lipids were done using the LipidView™ Software Version 2.0 (AB Sciex). Lipid amounts (pmol) were corrected for response differences between internal standards and endogenous lipids. The length and saturation profile of the acyl chains in a phospholipid was calculated by summing the amounts of phospholipid species carrying acyl chains with the same number of total carbons or of double bonds and represented relative to the total amount of lipids.

17. LICENSE AGREEMENT FOR REPRINTING FIGURES

Figures from manuscripts by other authors are reprinted with written permission from the different publishers (Nature publishing group, Elsevier and Company of Biologists Ltd).

18. STATISTICAL ANALYSIS

The results are shown as the mean ± standard error of the mean (SEM) of values obtained in a number of independent experiments indicated in each figure legend. Statistical analysis was determined using two-tailed unpaired Student's *t* test by using the GraphPad Prism® 6.0 Software Inc. The *p* values below 0.05 were considered statistically significant (*$p < 0.05$; **$p < 0.01$; ***$p < 0.001$).

REFERENCES

A

Adams, J. M., and S. Cory. 2007. The Bcl-2 apoptotic switch in cancer development and therapy. Oncogene 26:1324–37.

Alaimo, A., R. M. Gorojod, J. Beauquis, M. J. Muñoz, F. Saravia, and M. L. Kotler. 2014. Deregulation of mitochondria-shaping proteins Opa-1 and Drp-1 in manganese-induced apoptosis. PloS one 9:e91848.

Arnoult, D., A. Grodet, Y.-J. Lee, J. Estaquier, and C. Blackstone. 2005. Release of OPA1 during apoptosis participates in the rapid and complete release of cytochrome c and subsequent mitochondrial fragmentation. The Journal of biological chemistry 280:35742–50.

Artal-Sanz, M., and N. Tavernarakis. 2009. Prohibitin and mitochondrial biology. Trends in endocrinology and metabolism: TEM 20:394–401.

Artal-Sanz, M., W. Y. Tsang, E. M. Willems, L. A. Grivell, B. D. Lemire, H. van der Spek, L. G. J. Nijtmans, and M. A. Sanz. 2003. The mitochondrial prohibitin complex is essential for embryonic viability and germline function in Caenorhabditis elegans. The Journal of biological chemistry 278:32091–9.

B

Bae, J., C. P. Leo, S. Y. Hsu, and A. J. Hsueh. 2000. MCL-1S, a splicing variant of the antiapoptotic BCL-2 family member MCL-1, encodes a proapoptotic protein possessing only the BH3 domain. The Journal of biological chemistry 275:25255–61.

Baker, M. J., P. A. Lampe, D. Stojanovski, A. Korwitz, R. Anand, T. Tatsuta, and T. Langer. 2014. Stress-induced OMA1 activation and autocatalytic turnover regulate OPA1-dependent mitochondrial dynamics. The EMBO journal 33:578–93.

Balasubramaniam, S., J. A. Duley, and J. Christodoulou. 2014. Inborn errors of pyrimidine metabolism: clinical update and therapy. Journal of inherited metabolic disease 37:687–98.

Balmanno, K., and S. J. Cook. 2009. Tumour cell survival signalling by the ERK1/2 pathway. Cell death and differentiation 16:368–77.

Bardeleben, C., S. Sharma, J. R. Reeve, S. Bassilian, P. Frost, B. Hoang, Y. Shi, and A. Lichtenstein. 2013. Metabolomics identifies pyrimidine starvation as the mechanism of 5-aminoimidazole-4-carboxamide-1-β-riboside-induced apoptosis in multiple myeloma cells. Molecular cancer therapeutics 12:1310–21.

Baumann, P., S. Mandl-Weber, B. Emmerich, C. Straka, and R. Schmidmaier. 2007. Activation of adenosine monophosphate activated protein kinase inhibits growth of multiple myeloma cells. Experimental cell research 313:3592–603.

Bellosillo, B., N. Villamor, D. Colomer, G. Pons, E. Montserrat, and J. Gil. 1999. In vitro evaluation of fludarabine in combination with cyclophosphamide and/or mitoxantrone in B-cell chronic lymphocytic leukemia. Blood 94:2836–43.

Vanden Berghe, T., A. Linkermann, S. Jouan-Lanhouet, H. Walczak, and P. Vandenabeele. 2014. Regulated necrosis: the expanding network of non-apoptotic cell death pathways. Nature reviews. Molecular cell biology 15:135–47.

Boise, L. H., M. González-García, C. E. Postema, L. Ding, T. Lindsten, L. A. Turka, X. Mao, G. Nuñez, and C. B. Thompson. 1993. bcl-x, a bcl-2-related gene that functions as a dominant regulator of apoptotic cell death. Cell 74:597–608.

Bratton, S. B., and G. S. Salvesen. 2010. Regulation of the Apaf-1-caspase-9 apoptosome. Journal of cell science 123:3209–14.

Browman, D. T., M. B. Hoegg, and S. M. Robbins. 2007. The SPFH domain-containing proteins: more than lipid raft markers. Trends in cell biology 17:394–402.

Byrd, J. C., S. Stilgenbauer, and I. W. Flinn. 2004. Chronic lymphocytic leukemia. Hematology / the Education Program of the American Society of Hematology. American Society of Hematology. Education Program:163–83.

C

Campàs, C. 2004. Bases moleculars de la teràpia de la leucèmia limfàtica crònica de cèl·lules B. Recerca de nous agents inductors d'apoptosi. PhD Thesis, Universitat de Barcelona.

Campàs, C., J. M. Lopez, A. F. Santidrián, M. Barragán, B. Bellosillo, D. Colomer, and J. Gil. 2003. Acadesine activates AMPK and induces apoptosis in B-cell chronic lymphocytic leukemia cells but not in T lymphocytes. Blood 101:3674–80.

Campàs, C., A. F. Santidrián, A. Domingo, and J. Gil. 2005. Acadesine induces apoptosis in B cells from mantle cell lymphoma and splenic marginal zone lymphoma. Leukemia 19:292–4.

Cantó, C., Z. Gerhart-Hines, J. N. Feige, M. Lagouge, L. Noriega, J. C. Milne, P. J. Elliott, P. Puigserver, and J. Auwerx. 2009. AMPK regulates energy expenditure by modulating NAD+ metabolism and SIRT1 activity. Nature 458:1056–60.

Chan, T. C., and S. B. Howell. 1989. Unexpected synergy between N-phosphonacetyl-L-aspartate and cytidine against human tumor cells. European journal of cancer & clinical oncology 25:721–7.

Chander, H., M. Halpern, L. Resnick-Silverman, J. J. Manfredi, and D. Germain. 2010. Skp2B attenuates p53 function by inhibiting prohibitin. EMBO reports 11:220–5.

Chen, J., and N. A. J. McMillan. 2008. Molecular basis of pathogenesis, prognosis and therapy in chronic lymphocytic leukaemia. Cancer biology & therapy 7:174–9.

Chen, L., S. N. Willis, A. Wei, B. J. Smith, J. I. Fletcher, M. G. Hinds, P. M. Colman, C. L. Day, J. M. Adams, and D. C. S. Huang. 2005. Differential targeting of prosurvival Bcl-2 proteins by their BH3-only ligands allows complementary apoptotic function. Molecular cell 17:393–403.

Chiorazzi, N. 2007. Cell proliferation and death: forgotten features of chronic lymphocytic leukemia B cells. Best practice & research. Clinical haematology 20:399–413.

Chiorazzi, N., K. R. Rai, and M. Ferrarini. 2005. Chronic lymphocytic leukemia. The New England journal of medicine 352:804–15.

Chiu, C.-F., M.-Y. Ho, J.-M. Peng, S.-W. Hung, W.-H. Lee, C.-M. Liang, and S.-M. Liang. 2013. Raf activation by Ras and promotion of cellular metastasis require phosphorylation of prohibitin in the raft domain of the plasma membrane. Oncogene 32:777–87.

Chowdhury, I., A. Branch, M. Olatinwo, K. Thomas, R. Matthews, and W. E. Thompson. 2011. Prohibitin (PHB) acts as a potent survival factor against ceramide induced apoptosis in rat granulosa cells. Life sciences 89:295–303.

Chowdhury, I., W. E. Thompson, and K. Thomas. 2014. Prohibitins role in cellular survival through Ras-Raf-MEK-ERK pathway. Journal of cellular physiology 229:998–1004.

Chowdhury, I., W. E. Thompson, C. Welch, K. Thomas, and R. Matthews. 2013. Prohibitin (PHB) inhibits apoptosis in rat granulosa cells (GCs) through the extracellular signal-regulated kinase 1/2 (ERK1/2) and the Bcl family of proteins. Apoptosis : an international journal on programmed cell death 18:1513–25.

Chowdhury, I., W. Xu, J. K. Stiles, A. Zeleznik, X. Yao, R. Matthews, K. Thomas, and W. E. Thompson. 2007. Apoptosis of rat granulosa cells after staurosporine and serum withdrawal is suppressed by adenovirus-directed overexpression of prohibitin. Endocrinology 148:206–17.

Christie, D. A., C. D. Lemke, I. M. Elias, L. A. Chau, M. G. Kirchhof, B. Li, E. H. Ball, S. D. Dunn, G. M. Hatch, and J. Madrenas. 2011. Stomatin-like protein 2 binds cardiolipin and regulates mitochondrial biogenesis and function. Molecular and cellular biology 31:3845–56.

Christie, D. A., P. Mitsopoulos, J. Blagih, S. D. Dunn, J. St-Pierre, R. G. Jones, G. M. Hatch, and J. Madrenas. 2012. Stomatin-like protein 2 deficiency in T cells is associated with altered mitochondrial respiration and defective CD4+ T cell responses. Journal of immunology (Baltimore, Md. : 1950) 189:4349–60.

Coates, P. J., R. Nenutil, A. McGregor, S. M. Picksley, D. H. Crouch, P. A. Hall, and E. G. Wright. 2001. Mammalian prohibitin proteins respond to mitochondrial stress and decrease during cellular senescence. Experimental cell research 265:262–73.

Corton, J. M., J. G. Gillespie, S. A. Hawley, and D. G. Hardie. 1995. 5-aminoimidazole-4-carboxamide ribonucleoside. A specific method for activating AMP-activated protein kinase in intact cells? European journal of biochemistry / FEBS 229:558–65.

Cosialls, A. M. 2011. Estudio de la respuesta a inhibidores de proteínas reguladoras de la apoptosis, análisis de la mutación en la treonina 169 de BAX y validación del ensayo ex vivo y del método MS-MLPA en células leucémicas. PhD Thesis, Universitat de Barcelona.

Creagh, E. M. 2014. Caspase crosstalk: integration of apoptotic and innate immune signalling pathways. Trends in immunology 35:631–640.

Da Cruz, S., P. A. Parone, P. Gonzalo, W. V Bienvenut, D. Tondera, A. Jourdain, M. Quadroni, and J.-C. Martinou. 2008. SLP-2 interacts with prohibitins in the mitochondrial inner membrane and contributes to their stability. Biochimica et biophysica acta 1783:904–11.

Cubillos-Rojas, M., F. Amair-Pinedo, I. Tato, R. Bartrons, F. Ventura, and J. L. Rosa. 2010. Simultaneous electrophoretic analysis of proteins of very high and low molecular mass using Tris-acetate polyacrylamide gels. Electrophoresis 31:1318–21.

Cubillos-Rojas, M., F. Amair-Pinedo, I. Tato, R. Bartrons, F. Ventura, and J. L. Rosa. 2012. Tris-acetate polyacrylamide gradient gels for the simultaneous electrophoretic analysis of proteins of very high and low molecular mass. Methods in molecular biology (Clifton, N.J.) 869:205–13.

Czabotar, P. E., G. Lessene, A. Strasser, and J. M. Adams. 2014. Control of apoptosis by the BCL-2 protein family: implications for physiology and therapy. Nature reviews. Molecular cell biology 15:49–63.

D

Dart, D. A., G. N. Brooke, A. Sita-Lumsden, J. Waxman, and C. L. Bevan. 2012. Reducing prohibitin increases histone acetylation, and promotes androgen independence in prostate tumours by increasing androgen receptor activation by adrenal androgens. Oncogene 31:4588–98.

Duvezin-Caubet, S., R. Jagasia, J. Wagener, S. Hofmann, A. Trifunovic, A. Hansson, A. Chomyn, M. F. Bauer, G. Attardi, N.-G. Larsson, W. Neupert, and A. S. Reichert. 2006. Proteolytic processing of OPA1 links mitochondrial dysfunction to alterations in mitochondrial morphology. The Journal of biological chemistry 281:37972–9.

E

Eldering, E., C. A. Spek, H. L. Aberson, A. Grummels, I. A. Derks, A. F. de Vos, C. J. McElgunn, and J. P. Schouten. 2003. Expression profiling via novel multiplex assay allows rapid assessment of gene regulation in defined signalling pathways. Nucleic acids research 31:e153.

Estañ, M. C., E. Calviño, E. de Blas, M. del C. Boyano-Adánez, M. L. Mena, M. Gómez-Gómez, E. Rial, and P. Aller. 2012. 2-Deoxy-D-glucose cooperates with arsenic trioxide to induce apoptosis in leukemia cells: involvement of IGF-1R-regulated Akt/mTOR, MEK/ERK and LKB-1/AMPK signaling pathways. Biochemical pharmacology 84:1604–16.

F

Fadok, V. A., and P. M. Henson. 2003. Apoptosis: giving phosphatidylserine recognition an assist--with a twist. Current biology : CB 13:R655–7.

Faubert, B., G. Boily, S. Izreig, T. Griss, B. Samborska, Z. Dong, F. Dupuy, C. Chambers, B. J. Fuerth, B. Viollet, O. A. Mamer, D. Avizonis, R. J. DeBerardinis, P. M. Siegel, and R. G. Jones. 2013. AMPK is a negative regulator of the Warburg effect and suppresses tumor growth in vivo. Cell metabolism 17:113–24.

Faubert, B., E. E. Vincent, M. C. Poffenberger, and R. G. Jones. 2015. The AMP-activated protein kinase (AMPK) and cancer: many faces of a metabolic regulator. Cancer letters 356:165–70.

Fernald, K., and M. Kurokawa. 2013. Evading apoptosis in cancer. Trends in cell biology 23:620–33.

Fernández-Calotti, P. X., D. Colomer, and M. Pastor-Anglada. 2011. Translocation of nucleoside analogs across the plasma membrane in hematologic malignancies. Nucleosides, nucleotides & nucleic acids 30:1324–40.

Fletcher, C. E., D. A. Dart, A. Sita-Lumsden, H. Cheng, P. S. Rennie, and C. L. Bevan. 2012. Androgen-regulated processing of the oncomir miR-27a, which targets Prohibitin in prostate cancer. Human molecular genetics 21:3112–27.

Frezza, C., S. Cipolat, O. Martins de Brito, M. Micaroni, G. V Beznoussenko, T. Rudka, D. Bartoli, R. S. Polishuck, N. N. Danial, B. De Strooper, and L. Scorrano. 2006. OPA1 controls apoptotic cristae remodeling independently from mitochondrial fusion. Cell 126:177–89.

Fulda, S., and D. Vucic. 2012. Targeting IAP proteins for therapeutic intervention in cancer. Nature reviews. Drug discovery 11:109–24.

Fusaro, G., P. Dasgupta, S. Rastogi, B. Joshi, and S. Chellappan. 2003. Prohibitin induces the transcriptional activity of p53 and is exported from the nucleus upon apoptotic signaling. The Journal of biological chemistry 278:47853–61.

Fusaro, G., S. Wang, and S. Chellappan. 2002. Differential regulation of Rb family proteins and prohibitin during camptothecin-induced apoptosis. Oncogene 21:4539–48.

G

Galluzzi, L., J. M. Bravo-San Pedro, I. Vitale, S. A. Aaronson, J. M. Abrams, D. Adam, E. S. Alnemri, L. Altucci, D. Andrews, M. Annicchiarico-Petruzzelli, E. H. Baehrecke, N. G. Bazan, M. J. Bertrand, K. Bianchi, M. V Blagosklonny, K. Blomgren, C. Borner, D. E. Bredesen, C. Brenner, M. Campanella, et al. 2014. Essential versus accessory aspects of cell death: recommendations of the NCCD 2015. Cell death and differentiation 22:58–73.

Gamble, S. C., D. Chotai, M. Odontiadis, D. A. Dart, G. N. Brooke, S. M. Powell, V. Reebye, A. Varela-Carver, Y. Kawano, J. Waxman, and C. L. Bevan. 2007. Prohibitin, a protein downregulated by androgens, represses androgen receptor activity. Oncogene 26:1757–68.

Geraghty, R. J., A. Capes-Davis, J. M. Davis, J. Downward, R. I. Freshney, I. Knezevic, R. Lovell-Badge, J. R. W. Masters, J. Meredith, G. N. Stacey, P. Thraves, and M. Vias. 2014. Guidelines for the use of cell lines in biomedical research. British Journal of Cancer 111:1021–1046.

González-Gironès, D. M. 2012. AICAR and new therapeutic agents for chronic lymphocytic leukemia: Mechanism of apoptosis induction. PhD thesis, Universitat de Barcelona.

Gonzalvez, F., and A. Ashkenazi. 2010. New insights into apoptosis signaling by Apo2L/TRAIL. Oncogene 29:4752–65.

Grande, L., G. Bretones, M. Rosa-Garrido, E. M. Garrido-Martin, T. Hernandez, S. Fraile, L. Botella, E. de Alava, A. Vidal, X. Garcia del Muro, A. Villanueva, M. D. Delgado, and J. L. Fernandez-Luna. 2012. Transcription factors Sp1 and p73 control the expression of the proapoptotic protein NOXA in the response of testicular embryonal carcinoma cells to cisplatin. The Journal of biological chemistry 287:26495–505.

Green, D. R., and G. Kroemer. 2004. The pathophysiology of mitochondrial cell death. Science (New York, N.Y.) 305:626–9.

Gregory-Bass, R. C., M. Olatinwo, W. Xu, R. Matthews, J. K. Stiles, K. Thomas, D. Liu, B. Tsang, and W. E. Thompson. 2008. Prohibitin silencing reverses stabilization of mitochondrial integrity and chemoresistance in ovarian cancer cells by increasing their sensitivity to apoptosis. International journal of cancer. Journal international du cancer 122:1923–30.

Griparic, L., T. Kanazawa, and A. M. van der Bliek. 2007. Regulation of the mitochondrial dynamin-like protein Opa1 by proteolytic cleavage. The Journal of cell biology 178:757–64.

Guigas, B., N. Taleux, M. Foretz, D. Detaille, F. Andreelli, B. Viollet, and L. Hue. 2007. AMP-activated protein kinase-independent inhibition of hepatic mitochondrial oxidative phosphorylation by AICA riboside. The Biochemical journal 404:499–507.

Gyrd-Hansen, M., and P. Meier. 2010. IAPs: from caspase inhibitors to modulators of NF-κB, inflammation and cancer. Nature Reviews Cancer 10:561–574.

H

Hadji, A., C. Clybouw, M.-T. Auffredou, C. Alexia, K. Poalas, A. Burlion, O. Feraud, G. Leca, and A. Vazquez. 2010. Caspase-3 triggers a TPCK-sensitive protease pathway leading to degradation of the BH3-only protein puma. Apoptosis : an international journal on programmed cell death 15:1529–39.

Hallek, M. 2015. Chronic lymphocytic leukemia: 2015 Update on diagnosis, risk stratification, and treatment. American Journal of Hematology 90:446–460.

Han, J., C. Yu, R. F. Souza, and A. L. Theiss. 2014. Prohibitin 1 modulates mitochondrial function of Stat3. Cellular signalling 26:2086–95.

Hanahan, D., and R. A. Weinberg. 2011. Hallmarks of cancer: the next generation. Cell 144:646–74.

Hardie, D. G., and D. R. Alessi. 2013. LKB1 and AMPK and the cancer-metabolism link - ten years after. BMC biology 11:36.

Hardie, D. G., F. A. Ross, and S. A. Hawley. 2012. AMPK: a nutrient and energy sensor that maintains energy homeostasis. Nature reviews. Molecular cell biology 13:251–62.

Hayden, R. E., G. Pratt, C. Roberts, M. T. Drayson, and C. M. Bunce. 2012. Treatment of chronic lymphocytic leukemia requires targeting of the protective lymph node environment with novel therapeutic approaches. Leukemia & lymphoma 53:537–49.

He, B., Q. Feng, A. Mukherjee, D. M. Lonard, F. J. DeMayo, B. S. Katzenellenbogen, J. P. Lydon, and B. W. O'Malley. 2008. A repressive role for prohibitin in estrogen signaling. Molecular endocrinology (Baltimore, Md.) 22:344–60.

Hermansson, M., K. Hokynar, and P. Somerharju. 2011. Mechanisms of glycerophospholipid homeostasis in mammalian cells. Progress in lipid research 50:240–57.

Herrant, M., A. Jacquel, S. Marchetti, N. Belhacène, P. Colosetti, F. Luciano, and P. Auberger. 2004. Cleavage of Mcl-1 by caspases impaired its ability to counteract Bim-induced apoptosis. Oncogene 23:7863–73.

Herrant, M., F. Luciano, A. Loubat, and P. Auberger. 2002. The protective effect of phorbol esters on Fas-mediated apoptosis in T cells. Transcriptional and postranscriptional regulation. Oncogene 21:4957–68.

Hishikawa, D., T. Hashidate, T. Shimizu, and H. Shindou. 2014. Diversity and function of membrane glycerophospholipids generated by the remodeling pathway in mammalian cells. Journal of lipid research 55:799–807.

Ho, M.-Y., C.-M. Liang, and S.-M. Liang. 2015. MIG-7 and phosphorylated prohibitin coordinately regulate lung cancer invasion/metastasis. Oncotarget 6:381–93.

Hotchkiss, R. S., A. Strasser, J. E. McDunn, and P. E. Swanson. 2009. Cell death. The New England journal of medicine 361:1570–83.

I

Ido, Y., D. Carling, and N. Ruderman. 2002. Hyperglycemia-induced apoptosis in human umbilical vein endothelial cells: inhibition by the AMP-activated protein kinase activation. Diabetes 51:159–67.

Isebaert, S. F., J. V Swinnen, W. H. McBride, A. C. Begg, and K. M. Haustermans. 2011. 5-aminoimidazole-4-carboxamide riboside enhances effect of ionizing radiation in PC3 prostate cancer cells. International journal of radiation oncology, biology, physics 81:1515–23.

Ishihara, N., Y. Fujita, T. Oka, and K. Mihara. 2006. Regulation of mitochondrial morphology through proteolytic cleavage of OPA1. The EMBO journal 25:2966–77.

Ising, C., S. Koehler, S. Brähler, C. Merkwirth, M. Höhne, O. R. Baris, H. Hagmann, M. Kann, F. Fabretti, C. Dafinger, W. Bloch, B. Schermer, A. Linkermann, J. C. Brüning, C. E. Kurschat, R.-U. Müller, R. J. Wiesner, T. Langer, T. Benzing, and P. T. Brinkkoetter. 2015. Inhibition of insulin/IGF-1 receptor signaling protects from mitochondria-mediated kidney failure. EMBO molecular medicine 7:275–87.

J

Jackson, S. P., and J. Bartek. 2009. The DNA-damage response in human biology and disease. Nature 461:1071–8.

Jacobs, R. L., S. Lingrell, J. R. B. Dyck, and D. E. Vance. 2007. Inhibition of hepatic phosphatidylcholine synthesis by 5-aminoimidazole-4-carboxamide-1-beta-4-ribofuranoside is independent of AMP-activated protein kinase activation. The Journal of biological chemistry 282:4516–23.

Jeon, S.-M., N. S. Chandel, and N. Hay. 2012. AMPK regulates NADPH homeostasis to promote tumour cell survival during energy stress. Nature 485:661–5.

Jiang, L., P. Dong, Z. Zhang, C. Li, Y. Li, Y. Liao, X. Li, Z. Wu, S. Guo, S. Mai, D. Xie, Z. Liu, and F. Zhou. 2015. Akt phosphorylates Prohibitin 1 to mediate its mitochondrial localization and promote proliferation of bladder cancer cells. Cell death & disease 6:e1660.

Jiang, X., H. Jiang, Z. Shen, and X. Wang. 2014. Activation of mitochondrial protease OMA1 by Bax and Bak promotes cytochrome c release during apoptosis. Proceedings of the National Academy of Sciences of the United States of America 111:14782–7.

Jones, R. G., D. R. Plas, S. Kubek, M. Buzzai, J. Mu, Y. Xu, M. J. Birnbaum, and C. B. Thompson. 2005. AMP-activated protein kinase induces a p53-dependent metabolic checkpoint. Molecular cell 18:283–93.

K

Kasahara, A., and L. Scorrano. 2014. Mitochondria: from cell death executioners to regulators of cell differentiation. Trends in Cell Biology 24:761–70.

Kasashima, K., E. Ohta, Y. Kagawa, and H. Endo. 2006. Mitochondrial functions and estrogen receptor-dependent nuclear translocation of pleiotropic human prohibitin 2. The Journal of biological chemistry 281:36401–10.

Keating, M. J. 1993. Immunosuppression with purine analogues--the flip side of the gold coin. Annals of oncology : official journal of the European Society for Medical Oncology / ESMO 4:347–8.

Kelly, P. N., and A. Strasser. 2011. The role of Bcl-2 and its pro-survival relatives in tumourigenesis and cancer therapy. Cell death and differentiation 18:1414–24.

Kim, D. K., H. S. Kim, A.-R. Kim, G. H. Jang, H. W. Kim, Y. H. Park, B. Kim, Y. M. Park, M. A. Beaven, Y. M. Kim, and W. S. Choi. 2013. The scaffold protein prohibitin is required for antigen-stimulated signaling in mast cells. Science signaling 6:ra80.

Kim, J.-W., M. Akiyama, J.-H. Park, M.-L. Lin, A. Shimo, T. Ueki, Y. Daigo, T. Tsunoda, T. Nishidate, Y. Nakamura, and T. Katagiri. 2009. Activation of an estrogen/estrogen receptor signaling by BIG3 through its inhibitory effect on nuclear transport of PHB2/REA in breast cancer. Cancer science 100:1468–78.

Ko, K. S., M. L. Tomasi, A. Iglesias-Ara, B. A. French, S. W. French, K. Ramani, J. J. Lozano, P. Oh, L. He, B. L. Stiles, T. W. H. Li, H. Yang, M. L. Martínez-Chantar, J. M. Mato, and S. C. Lu. 2010. Liver-specific deletion of prohibitin 1 results in spontaneous liver injury, fibrosis, and hepatocellular carcinoma in mice. Hepatology (Baltimore, Md.) 52:2096–108.

Kowno, M., K. Watanabe-Susaki, H. Ishimine, S. Komazaki, K. Enomoto, Y. Seki, Y. Y. Wang, Y. Ishigaki, N. Ninomiya, T. K. Noguchi, Y. Kokubu, K. Ohnishi, Y. Nakajima, K. Kato, A. Intoh, H. Takada, N. Yamakawa, P.-C. Wang, M. Asashima, and A. Kurisaki. 2014. Prohibitin 2 regulates the proliferation and lineage-specific differentiation of mouse embryonic stem cells in mitochondria. PloS one 9:e81552.

Kumar, V., A. Abbas, and J. Aster. 2014. Robbins & Cotran Pathologic Basis of Disease. Page 1472. 9th editio. Elsevier.

Kuramori, C., M. Azuma, K. Kume, Y. Kaneko, A. Inoue, Y. Yamaguchi, Y. Kabe, T. Hosoya, M. Kizaki, M. Suematsu, and H. Handa. 2009. Capsaicin binds to prohibitin 2 and displaces it from the mitochondria to the nucleus. Biochemical and biophysical research communications 379:519–25.

Kvansakul, M., H. Yang, W. D. Fairlie, P. E. Czabotar, S. F. Fischer, M. A. Perugini, D. C. S. Huang, and P. M. Colman. 2008. Vaccinia virus anti-apoptotic F1L is a novel Bcl-2-like domain-swapped dimer that binds a highly selective subset of BH3-containing death ligands. Cell death and differentiation 15:1564–71.

L

Labi, V., and M. Erlacher. 2015. How cell death shapes cancer. Cell death & disease 6:e1675.

Labi, V., M. Erlacher, S. Kiessling, and A. Villunger. 2006. BH3-only proteins in cell death initiation, malignant disease and anticancer therapy. Cell death and differentiation 13:1325–38.

Laderoute, K. R., K. Amin, J. M. Calaoagan, M. Knapp, T. Le, J. Orduna, M. Foretz, and B. Viollet. 2006. 5'-AMP-activated protein kinase (AMPK) is induced by low-oxygen and glucose deprivation conditions found in solid-tumor microenvironments. Molecular and cellular biology 26:5336–47.

Landes, T., L. J. Emorine, D. Courilleau, M. Rojo, P. Belenguer, and L. Arnauné-Pelloquin. 2010. The BH3-only Bnip3 binds to the dynamin Opa1 to promote mitochondrial fragmentation and apoptosis by distinct mechanisms. EMBO reports 11:459–65.

Lanner, J. T., D. K. Georgiou, A. Dagnino-Acosta, A. Ainbinder, Q. Cheng, A. D. Joshi, Z. Chen, V. Yarotskyy, J. M. Oakes, C. S. Lee, T. O. Monroe, A. Santillan, K. Dong, L. Goodyear, I. I. Ismailov, G. G. Rodney, R. T. Dirksen, and S. L. Hamilton. 2012. AICAR prevents heat-induced sudden death in RyR1 mutant mice independent of AMPK activation. Nature medicine 18:244–51.

Lee, M., J.-T. Hwang, H.-J. Lee, S.-N. Jung, I. Kang, S.-G. Chi, S.-S. Kim, and J. Ha. 2003. AMP-activated protein kinase activity is critical for hypoxia-inducible factor-1 transcriptional activity and its target gene expression under hypoxic conditions in DU145 cells. The Journal of biological chemistry 278:39653–61.

Liang, J., and G. B. Mills. 2013. AMPK: a contextual oncogene or tumor suppressor? Cancer research 73:2929–35.

Linkermann, A., and D. R. Green. 2014. Necroptosis. The New England journal of medicine 370:455–65.

Liu, L., J. Ulbrich, J. Müller, T. Wüstefeld, L. Aeberhard, T. R. Kress, N. Muthalagu, L. Rycak, R. Rudalska, R. Moll, S. Kempa, L. Zender, M. Eilers, and D. J. Murphy. 2012. Deregulated MYC expression induces dependence upon AMPK-related kinase 5. Nature 483:608–12.

Liu, T., H. Tang, Y. Lang, M. Liu, and X. Li. 2009. MicroRNA-27a functions as an oncogene in gastric adenocarcinoma by targeting prohibitin. Cancer letters 273:233–42.

Liu, X., R. R. Chhipa, S. Pooya, M. Wortman, S. Yachyshin, L. M. L. Chow, A. Kumar, X. Zhou, Y. Sun, B. Quinn, C. McPherson, R. E. Warnick, A. Kendler, S. Giri, J. Poels, K. Norga, B. Viollet, G. A. Grabowski, and B. Dasgupta. 2014. Discrete mechanisms of mTOR and cell cycle regulation by AMPK agonists independent of AMPK. Proceedings of the National Academy of Sciences of the United States of America 111:E435–44.

Lomonosova, E., and G. Chinnadurai. 2008. BH3-only proteins in apoptosis and beyond: an overview. Oncogene 27 Suppl 1:S2–19.

López, J. M., A. F. Santidrián, C. Campàs, and J. Gil. 2003. 5-Aminoimidazole-4-carboxamide riboside induces apoptosis in Jurkat cells, but the AMP-activated protein kinase is not involved. The Biochemical journal 370:1027–32.

M

Mahmood, Z., and Y. Shukla. 2010. Death receptors: targets for cancer therapy. Experimental cell research 316:887–99.

Martelli, A. M., F. Chiarini, C. Evangelisti, A. Ognibene, D. Bressanin, A. M. Billi, L. Manzoli, A. Cappellini, and J. A. McCubrey. 2012. Targeting the liver kinase B1/AMP-activated protein kinase pathway as a therapeutic strategy for hematological malignancies. Expert opinion on therapeutic targets 16:729–42.

McBride, H., and V. Soubannier. 2010. Mitochondrial function: OMA1 and OPA1, the grandmasters of mitochondrial health. Current biology : CB 20:R274–6.

McMasters, K. M., R. Montes de Oca Luna, J. R. Peña, and G. Lozano. 1996. mdm2 deletion does not alter growth characteristics of p53-deficient embryo fibroblasts. Oncogene 13:1731–6.

Meley, D., C. Bauvy, J. H. P. M. Houben-Weerts, P. F. Dubbelhuis, M. T. J. Helmond, P. Codogno, and A. J. Meijer. 2006. AMP-activated protein kinase and the regulation of autophagic proteolysis. The Journal of biological chemistry 281:34870–9.

Merino, R., L. Ding, D. J. Veis, S. J. Korsmeyer, and G. Nuñez. 1994. Developmental regulation of the Bcl-2 protein and susceptibility to cell death in B lymphocytes. The EMBO journal 13:683–91.

Merkwirth, C., S. Dargazanli, T. Tatsuta, S. Geimer, B. Löwer, F. T. Wunderlich, J.-C. von Kleist-Retzow, A. Waisman, B. Westermann, and T. Langer. 2008. Prohibitins control cell proliferation and apoptosis by regulating OPA1-dependent cristae morphogenesis in mitochondria. Genes & development 22:476–88.

Merkwirth, C., and T. Langer. 2009. Prohibitin function within mitochondria: essential roles for cell proliferation and cristae morphogenesis. Biochimica et biophysica acta 1793:27–32.

Merkwirth, C., P. Martinelli, A. Korwitz, M. Morbin, H. S. Brönneke, S. D. Jordan, E. I. Rugarli, and T. Langer. 2012. Loss of prohibitin membrane scaffolds impairs mitochondrial architecture and leads to tau hyperphosphorylation and neurodegeneration. PLoS genetics 8:e1003021.

Meynet, O., B. Zunino, L. Happo, L. A. Pradelli, J. Chiche, M. A. Jacquin, L. Mondragón, J.-F. Tanti, B. Taillan, G. Garnier, J. Reverso-Meinietti, N. Mounier, J.-F. Michiels, E. M. Michalak, M. Carles, C. L. Scott, and J.-E. Ricci. 2013. Caloric restriction modulates Mcl-1 expression and sensitizes lymphomas to BH3 mimetic in mice. Blood 122:2402–11.

Mishra, S., S. R. Ande, and B. L. G. Nyomba. 2010. The role of prohibitin in cell signaling. The FEBS journal 277:3937–46.

Mishra, S., L. C. Murphy, B. L. G. Nyomba, and L. J. Murphy. 2005. Prohibitin: a potential target for new therapeutics. Trends in molecular medicine 11:192–7.

Mitsopoulos, P., Y.-H. Chang, T. Wai, T. König, S. D. Dunn, T. Langer, and J. Madrenas. 2015. Stomatin-like Protein-2 is Required for In vivo Mitochondrial Respiratory Chain Supercomplex Formation and Optimal Cell Function. Molecular and cellular biology.

Moldoveanu, T., A. V. Follis, R. W. Kriwacki, and D. R. Green. 2014. Many players in BCL-2 family affairs. Trends in biochemical sciences 39:101–11.

Montraveta, A., S. Xargay-Torrent, M. López-Guerra, L. Rosich, P. Pérez-Galán, I. Salaverria, S. Beà, S. G. Kalko, M. de Frias, C. Campàs, G. Roué, and D. Colomer. 2014. Synergistic anti-tumor activity of acadesine (AICAR) in combination with the anti-CD20 monoclonal antibody rituximab in in vivo and in vitro models of mantle cell lymphoma. Oncotarget 5:726–39.

N

Nabhan, C., and S. T. Rosen. 2014. Chronic Lymphocytic Leukemia. JAMA 312:2265.

Van Den Neste, E., G. Van den Berghe, and F. Bontemps. 2010. AICA-riboside (acadesine), an activator of AMP-activated protein kinase with potential for application in hematologic malignancies. Expert opinion on investigational drugs 19:571–8.

Van Den Neste, E., B. Cazin, A. Janssens, E. González-Barca, M. J. Terol, V. Levy, J. Pérez de Oteyza, P. Zachee, A. Saunders, M. de Frias, and C. Campàs. 2013. Acadesine for patients with relapsed/refractory chronic lymphocytic leukemia (CLL): a multicenter phase I/II study. Cancer chemotherapy and pharmacology 71:581–91.

Nikiforov, M. A., M. Riblett, W.-H. Tang, V. Gratchouck, D. Zhuang, Y. Fernandez, M. Verhaegen, S. Varambally, A. M. Chinnaiyan, A. J. Jakubowiak, and M. S. Soengas. 2007. Tumor cell-selective regulation of NOXA by c-MYC in response to proteasome inhibition. Proceedings of the National Academy of Sciences of the United States of America 104:19488–93.

O

Oda, E., R. Ohki, H. Murasawa, J. Nemoto, T. Shibue, T. Yamashita, T. Tokino, T. Taniguchi, and N. Tanaka. 2000. Noxa, a BH3-only member of the Bcl-2 family and candidate mediator of p53-induced apoptosis. Science (New York, N.Y.) 288:1053–8.

Olichon, A., L. Baricault, N. Gas, E. Guillou, A. Valette, P. Belenguer, and G. Lenaers. 2003. Loss of OPA1 perturbates the mitochondrial inner membrane structure and integrity, leading to cytochrome c release and apoptosis. The Journal of biological chemistry 278:7743–6.

Osman, C., M. Haag, C. Potting, J. Rodenfels, P. V. Dip, F. T. Wieland, B. Brügger, B. Westermann, and T. Langer. 2009a. The genetic interactome of prohibitins: coordinated control of cardiolipin and phosphatidylethanolamine by conserved regulators in mitochondria. The Journal of cell biology 184:583–96.

Osman, C., C. Merkwirth, and T. Langer. 2009b. Prohibitins and the functional compartmentalization of mitochondrial membranes. Journal of cell science 122:3823–30.

P

Pacher, P., A. Nivorozhkin, and C. Szabó. 2006. Therapeutic effects of xanthine oxidase inhibitors: renaissance half a century after the discovery of allopurinol. Pharmacological reviews 58:87–114.

Park, S.-E., J. Xu, A. Frolova, L. Liao, B. W. O'Malley, and B. S. Katzenellenbogen. 2005. Genetic deletion of the repressor of estrogen receptor activity (REA) enhances the response to estrogen in target tissues in vivo. Molecular and cellular biology 25:1989–99.

Pastor-Anglada, M., M. Molina-Arcas, F. J. Casado, B. Bellosillo, D. Colomer, and J. Gil. 2004. Nucleoside transporters in chronic lymphocytic leukaemia. Leukemia 18:385–93.

Pastor-Anglada, M., and S. Pérez-Torras. 2015. Nucleoside transporter proteins as biomarkers of drug responsiveness and drug targets. Frontiers in pharmacology 6:13.

Patel, N., S. K. Chatterjee, V. Vrbanac, I. Chung, C. J. Mu, R. R. Olsen, C. Waghorne, and B. R. Zetter. 2010. Rescue of paclitaxel sensitivity by repression of Prohibitin1 in drug-resistant cancer cells. Proceedings of the National Academy of Sciences of the United States of America 107:2503–8.

Peitz, M., K. Pfannkuche, K. Rajewsky, and F. Edenhofer. 2002. Ability of the hydrophobic FGF and basic TAT peptides to promote cellular uptake of recombinant Cre recombinase: a tool for efficient genetic engineering of mammalian genomes. Proceedings of the National Academy of Sciences of the United States of America 99:4489–94.

Pérez-Perarnau, A. 2013. Histone deacetylase inhibitors and diaryl (mono and bis)thiazoles: new strategies independent of p53 pathway for cancer treatment. PhD thesis, Universitat de Barcelona.

Pérez-Perarnau, A., S. Preciado, C. M. Palmeri, C. Moncunill-Massaguer, D. Iglesias-Serret, D. M. González-Gironès, M. Miguel, S. Karasawa, S. Sakamoto, A. M. Cosialls, C. Rubio-Patiño, J. Saura-Esteller, R. Ramón, L. Caja, I. Fabregat, G. Pons, H. Handa, F. Albericio, J. Gil, and R. Lavilla. 2014. A Trifluorinated Thiazoline Scaffold Leading to Pro-apoptotic Agents Targeting Prohibitins. Angewandte Chemie International Edition 53:10150–10154.

Piñon, J. D., V. Labi, A. Egle, and A. Villunger. 2008. Bim and Bmf in tissue homeostasis and malignant disease. Oncogene 27 Suppl 1:S41–52.

Ploner, C., R. Kofler, and A. Villunger. 2008. Noxa: at the tip of the balance between life and death. Oncogene 27 Suppl 1:S84–92.

Polager, S., and D. Ginsberg. 2009. p53 and E2f: partners in life and death. Nature reviews. Cancer 9:738–48.

Polier, G., J. Neumann, F. Thuaud, N. Ribeiro, C. Gelhaus, H. Schmidt, M. Giaisi, R. Köhler, W. W. Müller, P. Proksch, M. Leippe, O. Janssen, L. Désaubry, P. H. Krammer, and M. Li-Weber.

2012. The natural anticancer compounds rocaglamides inhibit the Raf-MEK-ERK pathway by targeting prohibitin 1 and 2. Chemistry & biology 19:1093–104.

Pop, C., and G. S. Salvesen. 2009. Human caspases: activation, specificity, and regulation. The Journal of biological chemistry 284:21777–81.

Pradelli, L. A., M. Bénéteau, C. Chauvin, M. A. Jacquin, S. Marchetti, C. Muñoz-Pinedo, P. Auberger, M. Pende, and J.-E. Ricci. 2010a. Glycolysis inhibition sensitizes tumor cells to death receptors-induced apoptosis by AMP kinase activation leading to Mcl-1 block in translation. Oncogene 29:1641–52.

Pradelli, L. A., M. Bénéteau, and J.-E. Ricci. 2010b. Mitochondrial control of caspase-dependent and -independent cell death. Cellular and molecular life sciences : CMLS 67:1589–97.

Puente, X. S., M. Pinyol, V. Quesada, L. Conde, G. R. Ordóñez, N. Villamor, G. Escaramis, P. Jares, S. Beà, M. González-Díaz, L. Bassaganyas, T. Baumann, M. Juan, M. López-Guerra, D. Colomer, J. M. C. Tubío, C. López, A. Navarro, C. Tornador, M. Aymerich, et al. 2011. Whole-genome sequencing identifies recurrent mutations in chronic lymphocytic leukaemia. Nature 475:101–5.

Q

Qian, X., P. Zhao, W. Li, Z.-M. Shi, L. Wang, Q. Xu, M. Wang, N. Liu, L.-Z. Liu, and B.-H. Jiang. 2013. MicroRNA-26a promotes tumor growth and angiogenesis in glioma by directly targeting prohibitin. CNS neuroscience & therapeutics 19:804–12.

Quesada, V., L. Conde, N. Villamor, G. R. Ordóñez, P. Jares, L. Bassaganyas, A. J. Ramsay, S. Beà, M. Pinyol, A. Martínez-Trillos, M. López-Guerra, D. Colomer, A. Navarro, T. Baumann, M. Aymerich, M. Rozman, J. Delgado, E. Giné, J. M. Hernández, M. González-Díaz, et al. 2012. Exome sequencing identifies recurrent mutations of the splicing factor SF3B1 gene in chronic lymphocytic leukemia. Nature genetics 44:47–52.

R

Raemy, E., and J.-C. Martinou. 2014. Involvement of cardiolipin in tBID-induced activation of BAX during apoptosis. Chemistry and physics of lipids 179:70–4.

Rajalingam, K., C. Wunder, V. Brinkmann, Y. Churin, M. Hekman, C. Sievers, U. R. Rapp, and T. Rudel. 2005. Prohibitin is required for Ras-induced Raf-MEK-ERK activation and epithelial cell migration. Nature cell biology 7:837–43.

Reed, J. C. 2003. Apoptosis-targeted therapies for cancer. Cancer cell 3:17–22.

Renault, T. T., and J. E. Chipuk. 2014. Death upon a kiss: mitochondrial outer membrane composition and organelle communication govern sensitivity to BAK/BAX-dependent apoptosis. Chemistry & biology 21:114–23.

Renshaw, S. A., C. E. Dempsey, F. A. Barnes, S. M. Bagstaff, S. K. Dower, C. D. Bingle, and M. K. B. Whyte. 2004. Three novel Bid proteins generated by alternative splicing of the human Bid gene. The Journal of biological chemistry 279:2846–55.

Ribeiro, N., F. Thuaud, Y. Bernard, C. Gaiddon, T. Cresteil, A. Hild, E. C. Hirsch, P. P. Michel, C. G. Nebigil, and L. Désaubry. 2012. Flavaglines as potent anticancer and cytoprotective agents. Journal of medicinal chemistry 55:10064–73.

Ricci, J.-E., C. Muñoz-Pinedo, P. Fitzgerald, B. Bailly-Maitre, G. A. Perkins, N. Yadava, I. E. Scheffler, M. H. Ellisman, and D. R. Green. 2004. Disruption of mitochondrial function during apoptosis is mediated by caspase cleavage of the p75 subunit of complex I of the electron transport chain. Cell 117:773–86.

Richter-Dennerlein, R., A. Korwitz, M. Haag, T. Tatsuta, S. Dargazanli, M. Baker, T. Decker, T. Lamkemeyer, E. I. Rugarli, and T. Langer. 2014. DNAJC19, a mitochondrial cochaperone associated with cardiomyopathy, forms a complex with prohibitins to regulate cardiolipin remodeling. Cell metabolism 20:158–71.

Robert, G., I. Ben Sahra, A. Puissant, P. Colosetti, N. Belhacene, P. Gounon, P. Hofman, F. Bost, J.-P. Cassuto, and P. Auberger. 2009. Acadesine Kills Chronic Myelogenous Leukemia (CML) Cells through PKC-Dependent Induction of Autophagic Cell Death. PLoS ONE 4:e7889.

S

Samatar, A. A., and P. I. Poulikakos. 2014. Targeting RAS–ERK signalling in cancer: promises and challenges. Nature Reviews Drug Discovery 13:928–942.

Sánchez-Quiles, V., E. Santamaría, V. Segura, L. Sesma, J. Prieto, and F. J. Corrales. 2010. Prohibitin deficiency blocks proliferation and induces apoptosis in human hepatoma cells: molecular mechanisms and functional implications. Proteomics 10:1609–20.

Sanford, D. S., W. G. Wierda, J. A. Burger, M. J. Keating, and S. M. O'Brien. 2015. Three Newly Approved Drugs for Chronic Lymphocytic Leukemia: Incorporating Ibrutinib, Idelalisib, and Obinutuzumab into Clinical Practice. Clinical lymphoma, myeloma & leukemia.

Santidrián, A. F., D. M. González-Gironès, D. Iglesias-Serret, L. Coll-Mulet, A. M. Cosialls, M. de Frias, C. Campàs, E. González-Barca, E. Alonso, V. Labi, B. Viollet, A. Benito, G. Pons, A. Villunger, and J. Gil. 2010. AICAR induces apoptosis independently of AMPK and p53 through up-regulation of the BH3-only proteins BIM and NOXA in chronic lymphocytic leukemia cells. Blood 116:3023–32.

Sato, S., A. Murata, T. Orihara, T. Shirakawa, K. Suenaga, H. Kigoshi, and M. Uesugi. 2011. Marine natural product aurilide activates the OPA1-mediated apoptosis by binding to prohibitin. Chemistry & biology 18:131–9.

Schleicher, M., B. R. Shepherd, Y. Suarez, C. Fernandez-Hernando, J. Yu, Y. Pan, L. M. Acevedo, G. S. Shadel, and W. C. Sessa. 2008. Prohibitin-1 maintains the angiogenic capacity of endothelial

cells by regulating mitochondrial function and senescence. The Journal of cell biology 180:101–12.

Schug, Z. T., and E. Gottlieb. 2009. Cardiolipin acts as a mitochondrial signalling platform to launch apoptosis. Biochimica et biophysica acta 1788:2022–31.

Scorrano, L., M. Ashiya, K. Buttle, S. Weiler, S. A. Oakes, C. A. Mannella, and S. J. Korsmeyer. 2002. A distinct pathway remodels mitochondrial cristae and mobilizes cytochrome c during apoptosis. Developmental cell 2:55–67.

Seiffert, M., S. Dietrich, A. Jethwa, H. Glimm, P. Lichter, and T. Zenz. 2012. Exploiting biological diversity and genomic aberrations in chronic lymphocytic leukemia. Leukemia & lymphoma 53:1023–31.

Shackelford, D. B., E. Abt, L. Gerken, D. S. Vasquez, A. Seki, M. Leblanc, L. Wei, M. C. Fishbein, J. Czernin, P. S. Mischel, and R. J. Shaw. 2013. LKB1 inactivation dictates therapeutic response of non-small cell lung cancer to the metabolism drug phenformin. Cancer cell 23:143–58.

Shalini, S., L. Dorstyn, S. Dawar, and S. Kumar. 2014. Old, new and emerging functions of caspases. Cell death and differentiation 22:526–39.

Shao, D., S.-I. Oka, T. Liu, P. Zhai, T. Ago, S. Sciarretta, H. Li, and J. Sadoshima. 2014. A redox-dependent mechanism for regulation of AMPK activation by Thioredoxin1 during energy starvation. Cell metabolism 19:232–45.

Shaw, R. J., M. Kosmatka, N. Bardeesy, R. L. Hurley, L. A. Witters, R. A. DePinho, and L. C. Cantley. 2004. The tumor suppressor LKB1 kinase directly activates AMP-activated kinase and regulates apoptosis in response to energy stress. Proceedings of the National Academy of Sciences of the United States of America 101:3329–35.

Shibue, T., S. Suzuki, H. Okamoto, H. Yoshida, Y. Ohba, A. Takaoka, and T. Taniguchi. 2006. Differential contribution of Puma and Noxa in dual regulation of p53-mediated apoptotic pathways. The EMBO journal 25:4952–62.

Shindiapina, P., J. R. Brown, and A. V Danilov. 2014. A new hope: novel therapeutic approaches to treatment of chronic lymphocytic leukaemia with defects in TP53. British journal of haematology 167:149–61.

Sievers, C., G. Billig, K. Gottschalk, and T. Rudel. 2010. Prohibitins are required for cancer cell proliferation and adhesion. PloS one 5:e12735.

Smith, S. W. 2009. Chiral toxicology: it's the same thing...only different. Toxicological sciences : an official journal of the Society of Toxicology 110:4–30.

Souers, A. J., J. D. Leverson, E. R. Boghaert, S. L. Ackler, N. D. Catron, J. Chen, B. D. Dayton, H. Ding, S. H. Enschede, W. J. Fairbrother, D. C. S. Huang, S. G. Hymowitz, S. Jin, S. L. Khaw, P. J. Kovar, L. T. Lam, J. Lee, H. L. Maecker, K. C. Marsh, K. D. Mason, et al. 2013. ABT-199, a

potent and selective BCL-2 inhibitor, achieves antitumor activity while sparing platelets. Nature medicine 19:202–8.

Sripathi, S. R., W. He, C. L. Atkinson, J. J. Smith, Z. Liu, B. M. Elledge, and W. J. Jahng. 2011. Mitochondrial-nuclear communication by prohibitin shuttling under oxidative stress. Biochemistry 50:8342–51.

Strasser, A. 2005. The role of BH3-only proteins in the immune system. Nature reviews. Immunology 5:189–200.

Supale, S., F. Thorel, C. Merkwirth, A. Gjinovci, P. L. Herrera, L. Scorrano, P. Meda, T. Langer, and P. Maechler. 2013. Loss of prohibitin induces mitochondrial damages altering β-cell function and survival and is responsible for gradual diabetes development. Diabetes 62:3488–99.

Suter, M., U. Riek, R. Tuerk, U. Schlattner, T. Wallimann, and D. Neumann. 2006. Dissecting the role of 5'-AMP for allosteric stimulation, activation, and deactivation of AMP-activated protein kinase. The Journal of biological chemistry 281:32207–16.

T

Tait, S. W. G., and D. R. Green. 2010. Mitochondria and cell death: outer membrane permeabilization and beyond. Nature reviews. Molecular cell biology 11:621–32.

Tait, S. W. G., G. Ichim, and D. R. Green. 2014. Die another way--non-apoptotic mechanisms of cell death. Journal of cell science 127:2135–44.

Tang, Y.-C., B. R. Williams, J. J. Siegel, and A. Amon. 2011. Identification of aneuploidy-selective antiproliferation compounds. Cell 144:499–512.

Taylor, R. C., S. P. Cullen, and S. J. Martin. 2008. Apoptosis: controlled demolition at the cellular level. Nature reviews. Molecular cell biology 9:231–41.

Theiss, A. L., and S. V Sitaraman. 2011. The role and therapeutic potential of prohibitin in disease. Biochimica et biophysica acta 1813:1137–43.

Thuaud, F., N. Ribeiro, C. G. Nebigil, and L. Désaubry. 2013. Prohibitin ligands in cell death and survival: mode of action and therapeutic potential. Chemistry & biology 20:316–31.

V

Vaux, D. L., and A. Strasser. 1996. The molecular biology of apoptosis. Proceedings of the National Academy of Sciences of the United States of America 93:2239–44.

Viana, R., C. Aguado, I. Esteban, D. Moreno, B. Viollet, E. Knecht, and P. Sanz. 2008. Role of AMP-activated protein kinase in autophagy and proteasome function. Biochemical and Biophysical Research Communications 369:964–968.

Vincent, E. E., P. P. Coelho, J. Blagih, T. Griss, B. Viollet, and R. G. Jones. 2014. Differential effects of AMPK agonists on cell growth and metabolism. Oncogene.

Vousden, K. H., and D. P. Lane. 2007. p53 in health and disease. Nature reviews. Molecular cell biology 8:275–83.

W

Walensky, L. D. 2006. BCL-2 in the crosshairs: tipping the balance of life and death. Cell death and differentiation 13:1339–50.

Wang, K., C.-Y. Liu, X.-J. Zhang, C. Feng, L.-Y. Zhou, Y. Zhao, and P.-F. Li. 2014. miR-361-regulated prohibitin inhibits mitochondrial fission and apoptosis and protects heart from ischemia injury. Cell death and differentiation.

Wang, S., N. Nath, M. Adlam, and S. Chellappan. 1999a. Prohibitin, a potential tumor suppressor, interacts with RB and regulates E2F function. Oncogene 18:3501–10.

Wang, S., N. Nath, G. Fusaro, and S. Chellappan. 1999b. Rb and prohibitin target distinct regions of E2F1 for repression and respond to different upstream signals. Molecular and cellular biology 19:7447–60.

Wang, S., P. Song, and M.-H. Zou. 2012. Inhibition of AMP-activated protein kinase α (AMPKα) by doxorubicin accentuates genotoxic stress and cell death in mouse embryonic fibroblasts and cardiomyocytes: role of p53 and SIRT1. The Journal of biological chemistry 287:8001–12.

Wang, S., B. Zhang, and D. V Faller. 2002. Prohibitin requires Brg-1 and Brm for the repression of E2F and cell growth. The EMBO journal 21:3019–28.

Wei, M. C., W. X. Zong, E. H. Cheng, T. Lindsten, V. Panoutsakopoulou, A. J. Ross, K. A. Roth, G. R. MacGregor, C. B. Thompson, and S. J. Korsmeyer. 2001. Proapoptotic BAX and BAK: a requisite gateway to mitochondrial dysfunction and death. Science (New York, N.Y.) 292:727–30.

Westphal, D., R. M. Kluck, and G. Dewson. 2014. Building blocks of the apoptotic pore: how Bax and Bak are activated and oligomerize during apoptosis. Cell death and differentiation 21:196–205.

Wilson, P. M., P. V. Danenberg, P. G. Johnston, H.-J. Lenz, and R. D. Ladner. 2014. Standing the test of time: targeting thymidylate biosynthesis in cancer therapy. Nature Reviews Clinical Oncology 11:282–298.

Y

Yamaguchi, R., L. Lartigue, G. Perkins, R. T. Scott, A. Dixit, Y. Kushnareva, T. Kuwana, M. H. Ellisman, and D. D. Newmeyer. 2008. Opa1-mediated cristae opening is Bax/Bak and BH3 dependent, required for apoptosis, and independent of Bak oligomerization. Molecular cell 31:557–69.

Yoshimaru, T., M. Komatsu, E. Tashiro, M. Imoto, H. Osada, Y. Miyoshi, J. Honda, M. Sasa, and T. Katagiri. 2014. Xanthohumol suppresses oestrogen-signalling in breast cancer through the inhibition of BIG3-PHB2 interactions. Scientific reports 4:7355.

Youle, R. J., and A. Strasser. 2008. The BCL-2 protein family: opposing activities that mediate cell death. Nature reviews. Molecular cell biology 9:47–59.

Young, J. D., S. Y. M. Yao, J. M. Baldwin, C. E. Cass, and S. A. Baldwin. 2013. The human concentrative and equilibrative nucleoside transporter families, SLC28 and SLC29. Molecular aspects of medicine 34:529–47.

Young, L., J. Sung, G. Stacey, and J. R. Masters. 2010. Detection of Mycoplasma in cell cultures. Nature protocols 5:929–34.

Z

Zenz, T., D. Mertens, R. Küppers, H. Döhner, and S. Stilgenbauer. 2010. From pathogenesis to treatment of chronic lymphocytic leukaemia. Nature reviews. Cancer 10:37–50.

Zhang, K., H. Li, and Z. Song. 2014. Membrane depolarization activates the mitochondrial protease OMA1 by stimulating self-cleavage. EMBO reports 15:576–85.

Zhou, T.-B., Y.-H. Qin, F.-Y. Lei, W.-F. Huang, and G. P. C. Drummen. 2013a. Prohibitin is associated with antioxidative protection in hypoxia/reoxygenation-induced renal tubular epithelial cell injury. Scientific reports 3:3123.

Zhou, T.-B., Y.-H. Qin, F.-Y. Lei, W.-F. Huang, and G. P. C. Drummen. 2013b. Prohibitin attenuates oxidative stress and extracellular matrix accumulation in renal interstitial fibrosis disease. PloS one 8:e77187.

JOURNAL ARTICLES

The journal articles derived from this thesis are:

*D. M. González-Gironès, *C. Moncunill-Massaguer, D. Iglesias-Serret, A. M. Cosialls, A. Pérez-Perarnau, C. M. Palmeri, C. Rubio-Patiño, A. Villunger, G. Pons, and J. Gil. 2013. **AICAR induces Bax/Bak-dependent apoptosis through upregulation of the BH3-only proteins Bim and Noxa in mouse embryonic fibroblasts.** Apoptosis : an international journal on programmed cell death 18:1008–1016. Imapct Factor: 4.788.

*These authors contributed equally to this study.

A. Pérez-Perarnau, S. Preciado, C. M. Palmeri, C. Moncunill-Massaguer, D. Iglesias-Serret, D. M. González-Gironès, M. Miguel, S. Karasawa, S. Sakamoto, A. M. Cosialls, C. Rubio-Patiño, J. Saura-Esteller, R. Ramón, L. Caja, I. Fabregat, G. Pons, H. Handa, F. Albericio, J. Gil, and R. Lavilla. 2014. **A Trifluorinated Thiazoline Scaffold Leading to Pro-apoptotic Agents Targeting Prohibitins.** Angewandte Chemie International Edition 53:10150–10154. Impact factor: 13.734.